Clinical Utility of Proposed Gait Stability Measures: Selection, Application and Evaluation of the Extrapolated Centre of Mass

by

Jeremy C. Hall

A thesis submitted in partial fulfillment of the requirements for the degree of

Master of Science

Department of Biomedical Engineering
University of Alberta

Abstract

Gait stability is the ability to maintain a state of equilibrium during locomotion. In humans, this includes the need to maintain a stable walking pattern while regularly positioning the body in a state of imbalance. Thus, it is not surprising that gait is accompanied by an increased risk of falling, particularly among the elderly and individuals with physical impairments, such as stroke, spinal cord injury, amputation, or hemophilic arthropathy. In addition, the precarious nature of gait makes it difficult to establish an exact definition of stability, leading to the development of a variety of different measures, each based on its own set of unique principles and assumptions. As a result, these measures have varying characteristics and experimental requirements, often limiting their feasibility for clinical implementation. In light of these considerations, the objectives of this thesis research were to: (1) conduct a literature review to identify the characteristics of proposed gait stability measures and select those that are clinically feasible based on pre-defined criteria; (2) demonstrate the practical feasibility of obtaining the selected measures and assess their robustness for a non-disabled sample; (3) evaluate the between-session reliability of the measures, as a key requirement for clinical implementation; and (4) demonstrate the clinical utility of the measures using three clinical case studies. Proposed gait stability measures were identified, reviewed, and scrutinized based on their expected burden on the patient, in terms of the required walking distance; the time required for assessment, including setup and trial time; the versatility of being applied to multiple walking conditions; and the mechanistic link between gait and the theoretical basis for stability. In total, three gait stability measures were identified as being clinically-feasible: the extrapolated centre of mass (XCoM), the gait sensitivity norm, and the stabilizing and destabilizing forces. For the purpose of this study, only the XCoM was used for further investigation as per the preceding objectives. To quantify stability, the XCoM, a quantity that accounts for both the

position and velocity of the center of mass, must remain within the limits of the base of support. The degree of stability at a given instant in time is then given by the margin of stability (MoS): the minimum distance between the XCoM and the base of support. Fifteen non-disabled participants were asked to walk in the Computer-Assisted Rehabilitation Environment at self-selected speed on a level, treadmill-driven surface. All participants returned for a repeat session several weeks following initial testing. Three case study participants with hemophilic arthropathy, unilateral transtibial amputation, and mild traumatic brain injury were also included, each completing one session. Careful attention was given to choose data collection and analysis techniques that would overcome common barriers to clinical implementation and support its feasibility in that respect. Acquired kinematic and kinetic data were used to compute the XCoM and corresponding MoS. To quantify stability in the mediolateral and anteroposterior directions, mean MoS values were taken at heel strike (MoS-HS) and mid-stance (MoS-MS). In addition, the minimum MoS value between heel strike and contralateral toe off (MoS-HScTO) was used to quantify stability in the ML direction. The protocol was designed to minimize the burden on the patient, as well as the time required for setup and overall trial length. Gait stability results suggest that MoS-HS is best suited to quantifying stability in both the mediolateral and anteroposterior directions. Not only does MoS-HS demonstrate reasonable within- and across-participant variability, it also showed good repeatability between sessions. Although the identified repeatability is not sufficient to support clinical implementation at this point, it is sufficient for continued use of the MoS in research. Furthermore, MoS-HS provided promising results towards highlighting differences between right and left body sides in the case study participants. Despite recommendation of the MoS-HS, further investigation is warranted before dismissing any of the MoS measures in either the mediolateral or anteroposterior direction. This work represents a significant step towards demonstrating that the

MoS is a robust measure that can be reliably used in fundamental research to quantify human gait stability. Further work is necessary to achieve the repeatability necessary for clinical purposes and investigate the ability of the MoS measures to detect difference in a larger sample of impaired participants.

Preface

Some of the research conducted for this thesis forms part of a research collaboration, led by Jacqueline S. Hebert and Albert H. Vette at the University of Alberta and Glenrose Rehabilitation Hospital. The experimental protocol described in Chapter 4 was developed through the design of a Performance Assessment Tool (PAT) for the Computer-Assisted Rehabilitation Environment (CAREN), with that portion of the work performed under Contract with Canada and Queen's University / Canadian Institute for Military and Veterans Health Research, through the Surgeon General's Health Research Program, Canadian Forces Health Services Group. These design efforts were led by Jacqueline S. Hebert, Albert H. Vette, and Juan Forero, and supported by Brendan Kelly and myself. The analysis in Chapter 4 is my original work, along with the literature review in Chapter 2 and the subsequent selection of clinically feasible gait stability measures in Chapter 3. The human research described in Chapter 4 received human research ethics approval from the Health Research Ethics Board of the University of Alberta, Project Name "Development of a Performance Assessment Tool for the Computer-Assisted Rehabilitation Environment", HREB Pro00066076 (June 27,2016).

Acknowledgments

I would like to express my sincere appreciation and utmost gratitude to my supervisor, Dr. Albert Vette. Over the last two years, he has acted as an incredible mentor, continuously challenging me to pursue and achieve the highest quality of work. His invaluable guidance in my research and career ambitions allowed me to develop a passion for research and grow as a research scientist. I am incredibly fortunate to have had the opportunity to complete my Master of Science under Albert's mentorship.

I am also grateful to my co-supervisor, Dr. Jacqueline Hebert, for providing thoughtful insight and professional support. A special thanks is deserved by Dr. Juan Forero, whom I assisted with the design of the Performance Assessment Tool for the CAREN system. Juan provided tremendous support on a daily basis, sharing his mindful intelligence and shrewd feedback whenever necessary. Many thanks go to Darrell Goertzen for his help with the CAREN system, along with all members of the Glenrose Rehabilitation Hospital. I would also like to thank my colleagues who were instrumental in my research efforts and personal development: Hosein Bahari, Brendan Kelly, Aïda Valevicius, McNiel Keri, Brad Roberts, Kshitij Agarwal, Sarah-Beth Riske, Andrew Williams, Alireza Noamani, and Milad Nazarahari.

Finally, I would like to thank all my family and friends for their continuous support throughout my studies. A very special thank you is expressed to my parents, Glen and Gisele, along with my brother, Darren, and his beautiful fiancée, Megan, for their unrelenting care and patience.

I am grateful to the Faculty of Engineering, University of Alberta; Faculty of Medicine and Dentistry, University of Alberta; the Glenrose Rehabilitation Hospital Foundation, Alberta Health Services; and the Canadian Institute for Military and Veteran Health Research.

Table of Contents

List of Tables

List of Figures

1 Introduction

1.1 Motivation

Simply defined, dynamic stability is the ability to maintain a state of equilibrium during movement [1]. With respect to human gait, this involves the capacity to integrate a stable upright posture with a rhythmic stepping pattern [2]. Meanwhile, forward progression requires that the human body be repeatedly placed in a position of imbalance [3]. This has led to bipedal walking being described as controlled falling, with each successive step preventing a person from falling over [4]. The inherent need to maintain a stable walking pattern while regularly positioning the body in a state of imbalance highlights the precarious nature of gait.

Control of stable gait relies on proprioceptive and visual feedback [5] to estimate the body's current kinematic and kinetic state, to evaluate possible future states and select the best option, and to determine the optimal means to execute the step-to-step transition [6]. Due to this demanding coordination process, it comes as no surprise that the majority of falls occur during walking [7]. Among the elderly population, falls during gait account for up to 70% of the total number of falls [1]. Oftentimes, these falls result in physical affliction in the form of fractures [1], [8]–[10], chronic pain [9], and other non-fatal injuries [5], [11], with the most extreme consequence being death [9], [10]. At the same time, an elderly individual suffering a fracture is known to be at a greater risk of mortality [12]. Falls can also lead to psychological consequences, referred to as post-fall syndrome [9]. Symptoms of this ailment include the fear of falling again [10], [11], [13], depression and confusion [9], [10], loss of limb function [8], [11], and reduced mobility and independence [9], [10]. Although it is obvious that falls can have a devastating effect on the affected person's quality of life, it can also place a considerable burden on their family, friends, and the healthcare system. On average, the duration of fall-related hospitalizations for seniors is 15.1 days [9], nine more than those admitted for any other cause [10]. This translates to an estimated financial cost to the healthcare system of $2 billion annually in Canada alone [9].

By 2036, the number of Canadian seniors who experience a fall is expected to more than double to 3.3 million, from 1.4 million in 2005 [9]. It is estimated that roughly 115,000 of falls that occur will result in hospitalization [9]. These increases are projected to drive healthcare spending for

fall-related injuries to $4.4 billion by 2031 [9]. Based on these numbers, a drastic increase in pressure on the healthcare system cannot be denied. Many of the personal and economic consequences associated with fall-related injuries can be mediated with targeted interventions (e.g., gait training, assistive devices); however, in light of the rapidly aging population, these efforts will need to be doubled to stay on pace [9]. This includes not only implementing optimized interventions to improve walking performance, but also improving our efforts in identifying individuals at risk of falling during gait and assessing their functional mobility. In addition, follow-up assessments are necessary to evaluate the effectiveness of a prescribed intervention. Unfortunately, knowledge on the mechanisms of stability in gait is scarce [7], [14]–[19], resulting in poor targeting efficiency of health care resources to those that would benefit most [8].

1.2 Dynamic Gait Stability

The commonly accepted general definition of stability proposed by Leipholz [20] involves perturbing a system and analyzing the ensuing behavior [21]. If, after a finite period of noticeable disturbance, the system gradually returns to its original state, it is deemed stable. At the same time, if differences from the initial state persist, the system is unstable. In a more gait-specific context, Bruijn et al. [15] used a pragmatic definition of gait stability by assessing various measures, describing it simply as 'gait that does not lead to falls in spite of perturbations'. This certainly presents a more conceivable interpretation of the term; however, it is problematic when applied to real-life applications as it cannot be used to predict future falls without observing a fall in the first place. Knowing that falls have the potential to result in serious injury, instigating falls is an incredibly risky procedure in experimental settings. In various other contexts, attempts have been made to diagnose fall risk in terms of suspected injury mechanisms, clinical history, walking speed, and kinematic or kinetic variables. However, none of these provide an actual measure of stability, and are thus speculative at best [18].

Together, the collection of definitions and attempts by several research and clinical groups to interpret gait stability expose the ambiguity of the term. Despite the lack of a clear definition, the clinical need to address stability has motivated the development of a number of gait stability measures [15]. Though the measures are well-defined mathematically [22], they are derived from

a variety of principles and are based on different assumptions. Thus, without an exact definition of stability, the measures must be validated in simulated models, as well as experimental studies with human participants.

Ideally, one or a combination of the measures would emerge as a valid means to quantify gait stability and differentiate between stable and unstable individuals. However, since the end goal is to use this as diagnostic tool, the chosen measures must also be clinically feasible. This implies that it is not sufficient to simply demonstrate that a measure can reliably quantify stability. As all of the proposed gait stability measures rely on their own unique set of principles and assumptions, there will be notable differences between their methods for assessment. Therefore, it is important to consider how the respective assessment techniques align with clinical standards, the feasibility of clinical implementation, and the needs of both the patient and treating clinician. In addition, when evaluating measures that generate quantitative data, it is important to ensure that repeated measurements are consistent and, thus, reliable. This is vital to help determine whether or not a potential measure is of any value in a clinical setting [23].

1.3 Thesis Objective

Based on the above considerations, the objectives of this thesis research were to: (1) conduct a literature review to identify the characteristics of proposed gait stability measures and select those that are clinically feasible based on pre-defined criteria; (2) demonstrate the practical feasibility of obtaining the selected measures and assess their robustness for a non-disabled sample; (3) evaluate the between-session reliability of the measures, as a key requirement for clinical implementation; and (4) demonstrate the clinical utility of the measures using three clinical case studies.

1.4 Thesis Outline

Chapter 2 presents a detailed review of the literature surrounding human gait stability assessment, including an overview of conventional gait assessment and the proposed measures of gait stability. In addition, topics related to kinetic and kinematic data acquisition and processing, and the estimation of reliability using the intraclass correlation coefficient are provided. In Chapter 3,

development of the criteria for clinical feasibility of a measure are described. These criteria are then used to evaluate each of the proposed gait stability measures and select those most suitable to implementation in a clinical setting. In Chapter 4, the practical utility of the selected measures are evaluated in a sample of non-disabled participants. An experiment was conducted to obtain the selected measures for participants walking on a level-surface at self-selected speed. Variability of the measures are assessed, along with the between-session reliability. Measurements are also compared to those obtained from 3 impaired participants who underwent the same protocol. The results and implications of this study are discussed. Chapter 5 provides concluding remarks on the contributions of this thesis to the domain of human gait stability assessment. A proposition of future work is included.

2 Literature Review

2.1 Human Gait Stability Assessment

2.1.1 Introduction

In order for any system to function properly and achieve its objectives, it is absolutely imperative that the system remain stable [21]. The human body and its execution of bipedal locomotion are no exception, as one of the basic requirements for walking is the maintenance of a stable upright posture [2]. Without the ability to keep the body upright, falls are inevitable, which means locomotion is impossible. Thus, the characterization of stability – and specifically gait stability in this context – is critical for the understanding of any system (e.g., the moving human body) [21]. However, a precise definition of stability does not exist [20], [21], [24], [25], and a consensus is yet to be reached regarding what constitutes stability in gait [7], [17], [26]–[28].

Unsurprisingly, searching for a helpful definition of stability proves futile, as descriptions such as ‘firmness in position’, ‘continuance without change’, or ‘resistance to change’ reveal no more than is already known. A physics-based interpretation, meanwhile, does provide a bit more utility; however, it is still insufficient for the purpose of human gait [27]. In this case, the stability of a system is linked to its response to a perturbation [20], [21], [25], [27]. To classify a system as stable, a perturbation cannot lead to an unbounded change in the variables that describe the system [27]. At first thought, it seems like this might provide a plausible means to interpret stability in gait: every day, humans encounter disturbances that alter the gait cycle and compromise balance. The problem is that, for human walking, a fall implies a bounded response [27]. When such fall occurs, gait ceases to continue, without further change once the individual is lying on the ground [27]. If this definition were to be accurately applied to gait, modifications are necessary.

The issues with the mechanical definition of stability for gait reveal that stability is context dependent [21]; as such, it is necessary to make modifications depending on the system to which it is applied. In recent literature, stable gait has been described as gait that does not result in falls, despite the presence of perturbations [7], [15], [22]. From a practical standpoint, this definition appears quite useful as characterizing stability, or instability, would simply involve perturbing a

participant multiple times at progressively higher magnitudes and comparing body mechanics between instances with and without a fall. Experimentally, this is not so easily accomplished as provoking falls has the potential to result in injury, posing a serious ethical dilemma.

With the inability to characterize the mechanics leading to a fall, gait stability research has shifted towards the assessment of walking performance using objective biomechanical data [6], [8], [15], [18], [29]–[33]. Though it remains unknown whether or not this is an effective way to evaluate fall risk, data-based measures certainly have clear advantages over the typical methods involving questionnaires and functional tests that are often qualitative and subjective [13]. Objective methods have the potential to offer greater sensitivity and specificity for assessing gait stability on an individual basis. It is important to note, however, that performance alone cannot be used to quantify stability and, thus, fall risk [34]. In an environment with varying conditions and a multitude of potential disturbances, it is not sufficient to focus strictly on repeating the same cycle step after step. Rather, some flexibility is necessary to successfully recover from different perturbations. Systems with the ability to alter their parameters while maintaining stability are deemed robust [21]. Therefore, in order to assess gait stability, attention must be given to investigating both the performance and robustness of gait [27].

The most common biomechanical data-based gait assessment techniques include temporal and spatial parameters [35], [36] which describe time and distance characteristics of the gait cycle, respectively. With dozens of possible parameters available, a breadth of valuable individualized gait information may be gained from their measurement. Temporal and spatial gait parameters – or temporo-spatial gait parameters – are a valid means to evaluate and compare gait characteristics across populations and, as such, have evolved to become a conventional means of clinical gait assessment.

Recently, a number of new measures to assess gait and its stability have been proposed, each based on its own set of unique assumptions and principles. These include: the largest Lyapunov exponent [18], [37], [38], the maximum Floquet multiplier [29], the extrapolated centre of mass (XCoM) [30], [39], stabilizing and destabilizing forces [40], the gait sensitivity norm (GSN) [32], [41], [42], variability measures [8], [43], long-range correlations [33], [44], the foot placement estimator

(FPE) [6], [45], [46], and the largest recoverable perturbation [15]. It is worthwhile to note that, while some of these measures have been used extensively in human gait, others have either never been used or only to a limited extent [15].

2.1.2 Conventional Gait Assessment

2.1.2.1 Temporo-Spatial Gait Parameters

Temporo-spatial parameters are a common quantitative measurement for assessing gait. Since first defined, they have been used extensively to make comparisons across a variety of populations and conditions. Their relative simplicity has led them to be one of the most widely used assessment measures to date. In many gait studies, researchers will often report a number of temporo-spatial quantities, potentially alongside values of a primary stability measure [18], [47]–[50]. The reason being is that many of the parameters are well documented and help to explain why one population may be deemed more stable than another. Furthermore, normative values exist [35], [36], [51] for the sake of comparison to a sample population.

The term ‘temporo-spatial’ is a blend of the words ‘temporal’ (relating to time) and ‘spatial’ (relating to space). Therefore, temporo-spatial parameters are quantities that are defined by time and space (i.e., displacement/position). Some of the most commonly reported temporo-spatial parameters are:

- velocity – the walking speed
- stride length – the distance covered between two consecutive footfalls for the same foot, in the direction of travel
- stride time – the time elapsed between two consecutive footfalls for the same foot
- step length – the distance covered from footfall for one foot to the next footfall of the opposite foot, in the direction of travel
- step width – the lateral distance between the feet, from footfall for one foot to the next footfall for the opposite foot
- cadence – the rate at which a person walks, expressed in terms of steps per minute
- swing time – the time spent in swing phase over the course of one stride
- stance time – the time spent in stance phase over the course of one stride
- swing to stance ratio – the ratio of swing time to stance time

Countless more options are available, depending on the application and intent of a particular gait assessment or study. A few other parameters that have been used in the past, though less frequently, are toe clearance [52]–[55] and foot velocity [55]. Given the broad definition of temporo-spatial parameters, the range of possibilities is seemingly limited only by the imagination of the clinician or researcher.

Over the years, values of these most popular parameters have been shown to vary between populations and conditions, oftentimes providing an indication of the level of stability. For example, a larger step width is often seen in populations at greater risk of falling (i.e., more unstable), such as prosthetic users [56]. Since a larger step width means a larger base of support (BoS) in the mediolateral (ML) direction [47], this makes sense: the wider the BoS, the more room for displacement of the centre of pressure (CoP), and the better chance of maintaining stable gait. Meanwhile, cadence (i.e., step frequency) has been shown to increase in the presence of continuous perturbations, a destabilizing environment [56].

From a data collection perspective, the requirements will vary depending on the parameters of interest. The majority of the parameters listed above can be determined through force plate data or kinematic marker data from motion capture. However, quantities such as joint angles, toe clearance, or upper limb movements would certainly require the use of motion capture. Though there is no stipulation on the length of the time series required for calculation of spatiotemporal parameters, it is customary to take the mean value over a number of steps or strides. It is important to keep that in mind when planning assessments or experiments, to ensure that a reliable estimate is attained.

Going forward in the investigation of gait and dynamic stability, temporo-spatial parameters are best suited to be complementary assessment measures, adding further insight into the conclusions obtained from the proposed stability measures. At this point, these quantities are well established and provide known distinctions between different populations, however, there remains a gap in using them to obtain relevant and reliable estimates of stability. Thus, rather than relying on these measures to quantify stability themselves, temporo-spatial parameters could help to clarify the distinction between multiple populations who present with different levels of stability. This is

particularly important in the search for a comprehensive means to quantify stability during gait. If a certain measure correlates well with typical gait characteristics, in terms of temporo-spatial parameters, then it may be validated as a viable candidate for the assessment of walking stability.

2.1.2.2 Compensatory Strategies

Compensatory strategies describe body movement techniques used to preserve a steady-state gait pattern. However, of most interest is the analysis of the recovery responses to perturbed gait, or the nominal gait pattern of patient populations (e.g., post-stroke, amputees). In this case, the motion of body segments is tracked to determine the body's primary strategies to maintain stability. In gait, these strategies can be further broken down into three subcategories, differentiated by the governing body segment: (1) stepping strategies; (2) ankle strategies; and (3) hip strategies.

Stepping strategies relate to the trajectory of the foot during a step, as well as the relative placement of the foot on the walking surface [57], [58]. Since proper foot placement is vital to gait stability, these are some of the most commonly investigated strategies, particularly in perturbed walking environments. One situation that has received great attention is the response to an unexpected trip. Schillings et al. [59] induced trip-like perturbations while participants walked on a treadmill and identified two main recovery reactions, the elevating strategy and the lowering strategy. The decision of which to employ depends on the timing of the perturbation. The elevating strategy, which involves elevating the swing limb to overcome a trip, is typically exercised during perturbations applied during the early stages of the swing phase [58]. This effectively lengthens the step and increases toe clearance [58]. In exercising such a technique, an individual is able to complete the disturbed step without having to slow down. Meanwhile, the lowering strategy requires a deceleration of the body as the perturbed step is aborted [58]. This strategy involves dropping the foot to the walking surface as fast as possible and occurs for mid to late swing perturbations. Further work by Schillings et al. [60] uncovered another strategy that applies the elevating and lowering strategies in succession, the delayed lowering strategy. After elevating the foot in attempt to overcome the trip and maintain speed, the foot is instead lowered to the ground. Originally, this technique was observed to occur during the transition between early to late swing (i.e., mid-swing); however, Forner Cordero et al. [58] concluded that it is also elicited by prolonged

perturbations in early swing. Since then, most of the work surrounding trip responses has focused on the transition between strategies [61], along with investigating other factors that may affect strategy selection [58], [62].

Though important, trips present just one condition for which stepping strategies need to be understood. Other studies have examined not only stepping strategies, but also ankle strategies, which consist of three-dimensional (3D) rotations about the ankle joint [47], [57], [63]. The consensus among the studies conducted by Hof [47], [57] and Reimann [63] is that, although both strategies are critical to maintaining stable gait, their contributions are significantly different. On the one hand, the ankle strategy offers a quick response, but can only be used to accomplish minor corrections. On the other hand, the stepping strategy has the capacity to make much larger corrections; however, response is slower because it requires the execution of a step. Under the stepping strategy, a decision on where to place the foot must be made well in advance. Once that decision is made and a walker enters the swing phase of gait, the opportunity to correct foot placement is very limited [47]. The ankle strategy helps to mediate incorrect foot placement by making minor adjustments through the stance phase [47], [57].

Hip strategies focus, as expected, on motion about the hip joints. Beginning with the work of Horak and Nashner [64], these movements have been studied extensively in human standing. The process is slightly more complicated in gait as forward locomotion requires continuous movement through the hip. Flexion and extension of the hip are certainly vital components, although, in terms of stability, most of the interest lies in circumduction and pelvic tilt. Circumduction is characterized by excessive hip abduction of the swing leg, whereas pelvic tilt refers to a frontal plane elevation of the pelvis on the side of the swing leg [65]. These strategies are typically observed in patient populations with loss of lower limb function [65], [66], or in response to inclined walking surfaces [67].

Compensatory strategies during walking have already been investigated in a variety of conditions, including normal walking [47] or in the presence of pushes and pulls at the trunk [57] and leg [68], translations of the walking surface [69], sinusoidal oscillations of the walking surface [48], [56], [70], [71], a rocky walking surface [53], galvanic vestibular stimulation [63], and induced trips

[58]–[62], [72]. With this extensive work, compensatory strategies may be better suited as secondary assessment measures, similar to the temporo-spatial parameters, as they provide a more detailed insight into the mechanics of gait. Applied in combination with stability measures, they may assist in explaining observations and validating results.

2.1.3 Proposed Gait Stability Measures

2.1.3.1 Largest Lyapunov Exponent

The Lyapunov exponent is a measure that arises from dynamical systems theory which, in short, attempts to describe the time dependence of points in geometric space. In particular, the Lyapunov exponents quantify the average exponential rates of divergence or convergence of nearby orbits in space, over time [37]. For an n-dimensional dynamical system, there exist n Lyapunov exponents, each describing the linear expansion or contraction along a particular direction. To help visualize the concept, imagine a 3D sphere. As time progresses, suppose this sphere evolves into an ellipsoid. The rate of expansion or contraction of the 3 principal axes are described by 3 Lyapunov exponents which, taken together, are known as the Lyapunov spectrum [37], [38]. Positive and negative exponents indicate expansion and contraction, respectively. Adding the first two Lyapunov exponents together provides the growth rate of the area defined by their respective principal axes. Furthermore, adding all three Lyapunov exponents together gives the growth rate of the system's volume [37]. Oftentimes, rather than the dynamical system simply expanding or contracting, as is the case in a sphere evolving into an ellipsoid, the system will fluctuate around an attractor, a region of space towards which trajectories converge over time. Here, both positive and negative exponents will be present as the system both diverges from (i.e., small fluctuations), and converges towards, the steady-state path. The presence of one or more positive exponents indicates a chaotic system as these are directions undergoing repeated, yet unpredictable, expansion and contraction [37], [38]. This is the case in human gait as a person tends to move along the same general path throughout the gait cycle; however, there are slight deviations in the cycle from stride to stride. With all of this in mind, an estimate of the largest positive Lyapunov exponent will reveal the greatest rate of divergence from the steady-state trajectory [15]. In terms of gait, this may be interpreted as the degree of stability: an individual's capacity to dampen small inertial disturbances that cause fluctuations in the gait cycle and remain on a steady path.

For continuous dynamical systems, the equations of motion are usually known explicitly, and there is a straightforward technique to determine the complete Lyapunov spectrum. However, for discrete time series of finite length, as is the case with gait data, the equations are unknown and this technique cannot be applied [37], [38]. Two algorithms have been developed to compute the Lyapunov exponents from an experimental time series. In the first, Wolf et al. [37] developed a method to determine the entire Lyapunov spectrum from a time series. Meanwhile, the approach of Rosenstein et al. [38] is used to calculate only the largest Lyapunov exponent. Both techniques compute the largest Lyapunov in a similar manner [15]; however, the algorithm by Rosenstein et al. is more often used as it takes advantage of all the available data and requires less computation [38].

To apply the algorithm by Rosenstein et al. [38] to human gait, system dynamics must first be approximated by reconstructing an *n*-dimensional state-space from a single time series of experimental kinematic data. This is accomplished using the method of delays [37], [38], [49], [73]. The general form of the state-space is:

$$\mathbf{X} = \begin{bmatrix} X_1 \\ X_2 \\ \vdots \\ X_M \end{bmatrix} \tag{1}$$

where X_i is the state of the system at point i:

$$X_i = \left[x_i, x_{i+J}, x_{i+2J} \cdots x_{i+(d_e-1)J}\right] \tag{2}$$

where each x_i is a data point from the original time series of length N, J is the lag, and d_e is the embedding dimension. Therefore, $\mathbf{X}$ is an M x d_e matrix where $M = N-(d_e-1)J$.

The lag, J, is estimated, in number of samples, by the first minimum of the average mutual information function [7], [15], [22], [28], [74], [75]. This method provides an estimate of the delay that is neither too small, resulting in a delay-embedded time series very similar to the original time series, nor too large, which could result in a delay-embedded time series that is completely independent of the original time series. The first minimum of the average mutual information

function provides the most suitable estimate of delay to reconstruct a delay-embedded state space that best represents the dynamics of the system.

The embedding dimension, d_e, is estimated using a false nearest neighbors analysis [7], [15], [22], [28], [75], [76]. As d_e increases, subsequent computation increases; however, using a d_e that is too small increases the number of false nearest neighbors (i.e., neighbors that appear close in a low-dimensional space but far in a higher-dimensional space) [76]. Therefore, a false nearest neighbors analysis seeks to identify the minimum embedding dimension that minimizes the number of false nearest neighbors. Ideally, the minimum embedding dimension would be one that eliminates all false neighbors and thereby identifies only the true neighbors. However, this often leads to large estimates of the embedding dimension. A more realistic approach is to set a threshold for the allowable number of false nearest neighbors (e.g., less than 1%) and determine an embedding dimension that meets that criteria.

With a properly reconstructed state space, the next step of the algorithm by Rosenstein et al. [38] is to identify the initial nearest neighbor for each data point. Iterating through each point (i.e., reference point) in the state space, first the Euclidean distance between that reference point, X_j, and all other points in the state space is determined (i.e., M-1 distances). The initial nearest neighbor, $X_{j,}$, is then identified by searching through all successive points in the vector of calculated distances to identify the data point that minimizes the Euclidean distance to the reference point:

$$d_j(0) = \min_{X_{\hat{j}}} \left\| X_j - X_{\hat{j}} \right\| \tag{3}$$

where $d_j(0)$ is the initial distance from the j^{th} point to its nearest neighbor.

To ensure nearest neighbors are not selected from the same period, an additional restriction is imposed in which nearest neighbors must have a temporal separation greater than the mean period of the time series. In terms of human gait, this means that nearest neighbors must be separated by at least one period of the gait cycle.

Then iterating through each pair of nearest neighbors, j, the separation distance, d_{j+k}, between them is calculated for each successive step in the state-space. Separation distances are calculated at successively larger step sizes, k, from the reference point:

$$d_{j+k} = \left\| X_{j+k} - X_{\hat{j}+k} \right\| \tag{4}$$

Theoretically, the distances can be calculated step-by-step from the reference point until the end of the time series. However, in iterating through the state space, each pair of nearest neighbors will be one step closer to the end, thus eliminating the largest step size and the corresponding distance that can be calculated at that point. As a result, the separation distance at the largest step sizes can only be calculated for the first few pairs of nearest neighbors. This is important for the next part of the algorithm as the separation distances for all nearest neighbors are grouped together, based on step size, and averaged to compute the mean separation of initial nearest neighbors at every step size. For the intervals spanning close to the entire time series, the mean separation distance will be calculated from a small subset of values. With that in mind, best practice is to specify a maximum step size and iterate only up to the pair of nearest neighbors that lies that length (i.e., maximum step size) away from the last element in the state space. In doing so, the mean separation distances at every step size will be averaged using the same number of values. Finally, the natural logarithm of each of the mean separation distances is calculated and plotted against the step sizes for which they were calculated. The largest Lyapunov exponents are then calculated as the slope of this mean divergence curve.

When applying the largest Lyapunov exponent to human gait, a few considerations and best practices should be followed. First, prior to state-space reconstruction, the time series should be normalized to an average number of data points per stride (i.e., 101 is typical) [22], [28], [49], [73], [75]. In addition, if the intent of an assessment or study is to compare results between participants and conditions, it is important that each time series collected contains the same number of strides. Meeting both these criteria ensures that each state space contains the same number of strides and data points [15]. The optimal number of strides necessary to reach precise estimates of the largest Lyapunov exponent, and thus draw conclusions, is not yet completely established. Bruijn et al. [73] suggest time series with at least 150 strides as they demonstrated a limited increase in statistical precision past that point. However, there are ample studies that have drawn

conclusions using less than the recommended 150 strides [2], [18], [49], [75], [77], [78]. In fact, Sloot et al. [77] showed that, at a group level, multiple episodes of 7 strides can be used to demonstrate the destabilizing effects of galvanic vestibular stimulation (GVS). However, a corresponding increase in the maximum Lyapunov exponent has been observed for increasing time series length [73]. It has been suggested that this may be due to a more densely populated state space, which increases the likelihood that nearest neighbors are initially closer together [73].

Another common practice is to express the Lyapunov exponent as divergence per stride; therefore, step sizes along the horizontal axis of the mean divergence curve should be rescaled in terms of strides, rather than data points. So long as the original time series was normalized to an average number of data points per stride, rescaling simply requires dividing the axis values by that number.

Over time, two separate largest Lyapunov exponents have been considered, differentiated by the region over which the slope of the mean divergence is calculated. The short-term Lyapunov exponent, λ_S, is calculated from 0 to 1 strides, whereas the long-term Lyapunov exponent, λ_L, is calculated from 4 to 10 strides. Thus, the maximum step size can be defined using these criteria. If only calculating λ_S, the maximum step size need only be set to 1 stride, which has the benefit of reducing the computation time. However, if only λ_L is desired, the step sizes can be specified as a range from 4 to 10 strides. In the event that both exponents are needed, specifying a maximum step size of 10 strides allows both to be calculated. Though both λ_S and λ_L are often reported, many studies have shown that λ_S, and not λ_L, is correlated to decreased stability during gait, which in consequence has led to the assumption that only λ_S needs to be reported in human gait studies [15].

As an alternative to reconstructing a state space using the method of delays, recent studies have constructed biomechanical state spaces [17], [79]. Rather than using multiple time-delayed copies of an individual time series, a combination of the 3D position, velocity and acceleration time series is used to characterize the system. In their comparison of various state spaces, Gates et al. [80] recommended the use of biomechanical state spaces composed of positions and velocities, or delay-embedded state-spaces reconstructed from an individual time series. Note that the algorithm by Rosenstein et al. [38] is applied in the same manner, regardless of the method used to create the state space.

The main advantage of using the largest Lyapunov exponent to quantify gait stability is the ability to use any source of kinematic data, irrespective of the reference frame [15]. The major stipulation, however, is that the data must be free of non-stationarities: any noise or induced deviations from the typical path will affect the estimate. To reduce noise, filtering is possible, but that runs the risk of also eliminating some of the inherent temporo-spatial fluctuations in the data. Though the requirement of stationarity prevents the study of mechanically perturbed gait (i.e., induced slips or trips), it is possible to analyze gait at fixed inclines or under continuous pseudo-random oscillations [22], [28], [75], [81].

Despite the proven ability of the largest Lyapunov exponent to distinguish between groups with varying levels of stability, it may not be an appropriate measure for individual-level assessment. As mentioned, the most precise estimates of the largest Lyapunov exponent are attained with a time series length of 150 strides or more. For many individuals with reduced stability during gait, this is not practical as mobility impairments often prevent them from walking long distances. Therefore, use of the largest Lyapunov exponent may be more appropriate for performing group-level analyses in an experimental setting where multiple walking trials of shorter duration can be used.

2.1.3.2 Maximum Floquet Multiplier

Like Lyapunov exponents, Floquet multipliers are also used in the assessment of dynamical systems. However, rather than quantify the rate of divergence (or convergence) of the system over time, as is accomplished with Lyapunov exponents, Floquet multipliers quantify the rate at which all trajectories diverge (or converge) from the limit cycle trajectory (i.e., closed orbit) [15], [29]. In Floquet theory, the system is assumed to be strictly periodic [15], [22]: each cycle is independent from the next and presumed to follow the same general path, the limit cycle. In the presence of finite perturbations, every consecutive orbit will differ slightly as it either diverges from, or converges towards, the closed orbit. The rate of divergence or convergence between successive orbits is quantified by the Floquet multipliers. In essence, the Floquet multipliers act as scaling factors for the next orbit. Just as with Lyapunov exponents, there exist n Floquet multipliers for an n-dimensional dynamical system, with each multiplier describing the rate of divergence or

convergence towards the closed orbit along one of the principal axes. Any fluctuation from the closed orbit along a particular direction is multiplied by its respective Floquet multiplier by the subsequent cycle [7]. Multiplier values greater than 1 indicate divergence from the limit cycle (i.e., small perturbations grow by the subsequent cycle), whereas values less than 1 indicate convergence towards the limit cycle (i.e., small perturbations diminish by the subsequent cycle). With that in mind, the limit cycle can be deemed stable if and only if all of the Floquet multipliers are less than 1. Therefore, all that is needed to classify a limit cycle as unstable is the presence of one multiplier greater than 1. This justifies the calculation of only the largest Floquet multiplier: if the largest multiplier is less than 1, all are less than 1, and the limit cycle is orbitally stable.

Again, similar to the Lyapunov exponents, calculation of Floquet multipliers is relatively straightforward when the equations of motion are known. In this case, the limit cycle trajectory is given by the equations themselves. However, in experimental gait data, the equations of motion are unknown, and the closed orbit must be determined by other means. In addition, another issue arises in conceptualizing how finite perturbations may be applied to the state variables (i.e., kinematic time series) during gait [15]. Hurmuzlu et al. [29] addressed both of these issues in introducing a method to estimate gait stability using the maximum Floquet multiplier. First, the closed orbit is taken as the mean trajectory of all the independent orbits, with each orbit being one stride (i.e., one iteration of the gait cycle). Second, they assumed that the natural variability in human gait eliminates the need to apply actual, physical perturbations.

Prior to applying the algorithm outlined by Hurmuzlu et al. [29] to calculate the largest Floquet multiplier, the system dynamics need to be characterized by creating a state space using either of the two options discussed in the previous section: biomechanical or delay-embedding. With an appropriate state space, the next step is to segment the data into individual strides and time-normalize each stride into 101 samples, with each sample representing the state of the system at a certain percent of the gait cycle (0-100%). Using the normalized data, a Poincaré section can be defined for every percent of the stride. Briefly, a Poincaré section is a plane that intersects an orbit perpendicular to the line of trajectory. In this context, each percent of the gait cycle can be interpreted as a plane and, thus, a Poincaré section. Creating each Poincaré section is accomplished by reorganizing the data according to the points in the gait cycle on a per stride basis. In matrix

form, this results in 101 matrices (one for each percent of the gait cycle), all with a size K x n, where K is the total number of strides and n is the dimensionality of the state space. In turn, these Poincaré sections are used to create 101 Poincaré maps, otherwise known as first-recurrence maps, that describe the state of the system after one cycle (S_{k+1}) as a function of its current state (S_k), where k refers to the stride of interest:

$$S_{k+1} = F(S_k) \tag{5}$$

This relationship illustrates the major underlying assumption of Floquet theory – periodicity. In other words, each cycle is expected to closely follow the limit cycle trajectory. It is important to note that there is no general method to construct a Poincaré map, particularly for higher dimensional systems. Rather, the theory behind a Poincaré map provides the basis to define the limit cycle trajectory. Knowing that the limit cycle trajectory is a closed orbit, every point will be the same for each successive cycle. These are assumed to be the fixed points of the trajectory, defined as:

$$S^* = F(S^*) \tag{6}$$

Figure 2.1 provides a visual aid for understanding the relationship between the Poincaré section, the Poincaré map, and the limit cycle trajectory.

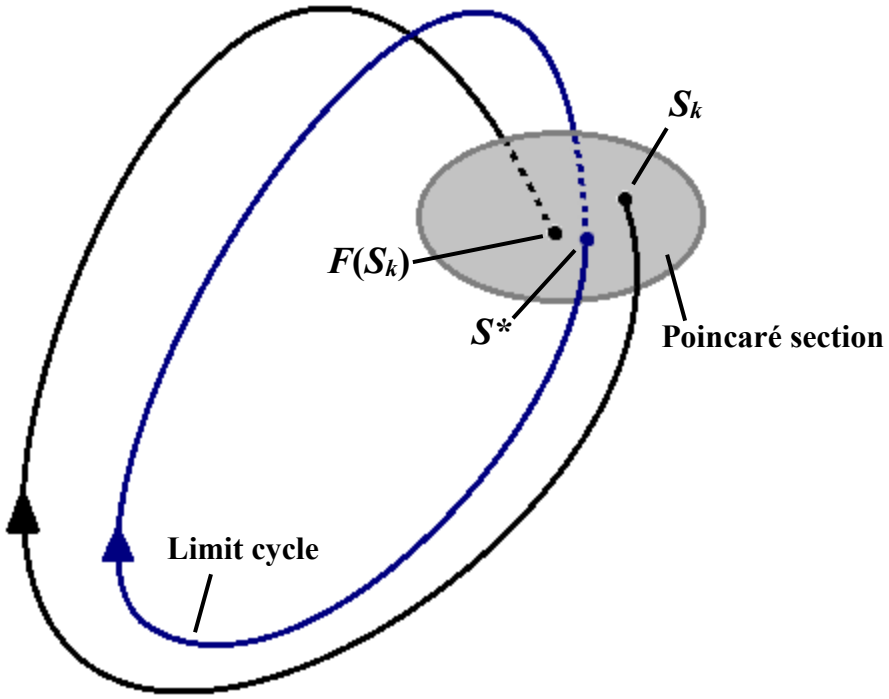

Figure 2.1: Illustration of the Poincaré section, the Poincaré map, and the limit cycle trajectory. The Poincaré section intersects the trajectory at a plane perpendicular to the direction of flow. The Poincaré map projects the point S_k onto point F(S_k), both on the Poincaré section. The limit cycle returns to the fixed point, S^*, on the Poincaré section.

To determine the closed orbit from experimental gait data, each of the fixed points along the limit cycle are determined by averaging the points across all strides, for each percent of the gait cycle (i.e., Poincaré section). Once the limit cycle is known, the Poincaré map can be linearized:

$$[S_{k+1} - S^*] \approx J(S^*)[S_k - S^*] \tag{7}$$

where $J(S^*)$ is the Jacobian matrix for each Poincaré section (i.e., percent of the gait cycle). Performing a few matrix operations will then provide $J(S^*)$:

$$J(S^*) \approx [S_{k+1} - S^*] \cdot [S_k - S^*]^{-1} \tag{8}$$

Note that the matrix $[S_k - S^*]$ is of size K x n and, thus, not square. Therefore, the pseudoinverse is determined using a least-squares algorithm.

Finally, the magnitudes of the first n (i.e., dimension of state space) eigenvalues of each Jacobian matrix are the Floquet multipliers for each percent of the gait cycle. To visualize the progression

of orbital stability throughout the gait cycle, the maximum of the *n* multipliers is taken at each section. Averaging these 101 values will provide the maximum Floquet multiplier, and the mean level of stability, over the entire gait cycle. In some cases, instead of taking the single maximum of the *n* Floquet multipliers for each percent of the gait cycle, the mean value is calculated. Thus, each of the values is a mean Floquet multiplier rather than a maximum. This method is thought to provide a better overall measure of stability [15].

Another important remark is that the sampling point for each Poincaré section is arbitrary as, in theory, Floquet multipliers should remain constant throughout the gait cycle [29]. Therefore, the phase of the gait cycle used to segment the successive strides (e.g., heel strike or toe-off) is also arbitrary. Though relatively intuitive, it is vital that each segment stride begins and ends at the same instant of the gait cycle as segments will be normalized and compared against each other to compute the Floquet multipliers.

Since Lyapunov exponents and Floquet multipliers are both derived from dynamical systems theory, they share a number of common features when applied to experimental gait data. Arguably, one of the most important commonalities is the requirement of relatively long time series of kinematic data. As mentioned, time series containing at least 150 strides are needed to detect the variations in human walking [73]. In addition, the data must be free of non-stationarities, which limits its applicability to various forms of gait (i.e., perturbed gait). Again, similar to the Lyapunov exponents, the number of strides must be identical between participants and conditions to perform an acceptable comparison [73].

One of the most obvious differences from the Lyapunov exponents is the observation that the Floquet multipliers appear to decrease with increasing time series length [73]. Bruijn et al. [73] speculated that this may be a result of estimating the closed orbit as the mean trajectory: a greater number of strides leads to a better estimate which, in turn, leads to greater convergence towards the limit cycle. Due to the requirement for long series of data, Floquet multipliers may be another measure better suited to research, rather than clinical applications. However, there is still speculation as to whether or not it is a valid measure for quantifying stability in human walking

[15]. Further investigation is necessary before this statement can be made with certainty, and the Floquet multiplier is abandoned as a means to quantify gait stability.

2.1.3.3 Extrapolated Centre of Mass

The XCoM is a quantity derived from biomechanics to describe the stability of human locomotion. In particular, it is an extension of the inverted pendulum model that is typically used to describe stability in static conditions (i.e., human standing or sitting) [30], [39], [47], [57]. In the classic inverted pendulum model, the body is modelled as a single mass balancing on a stick of known length [39]. This model uses three quantities to describe stability in human standing: the centre of mass (CoM), the CoP, and the BoS. The CoM is the 3D location of the gravity vector acting on the body (i.e., centre of gravity), with the body's mass being modelled as the single mass of the inverted pendulum. Therefore, the mass acts at a known height above the ground. Meanwhile, the CoP is the location of the resultant ground reaction vector at the ground surface. With the ground surface defined as the vertical reference, the CoP is, thus, a two-dimensional (2D) position in the horizontal plane. Finally, the BoS represents the possible range of the CoP which, in two-legged standing, is the area beneath and between the feet [39], [47], [57]. An illustration of these quantities is shown in Figure 2.2.

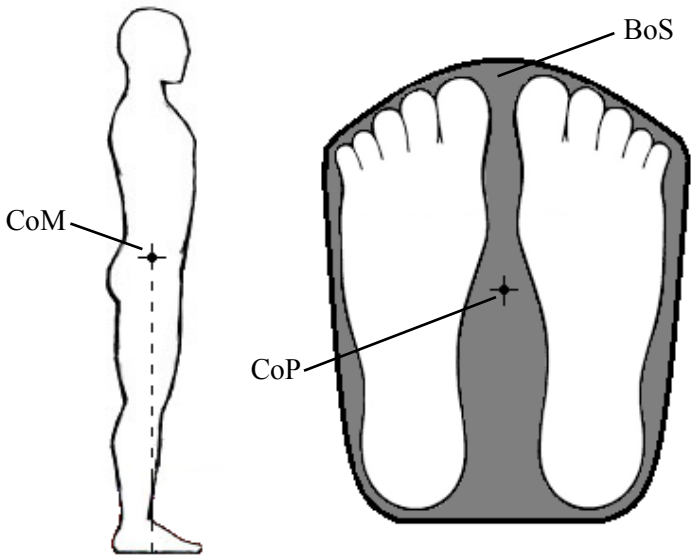

Figure 2.2: Illustration of the centre of mass (CoM), centre of pressure (CoP), and base of support (BoS) in human standing.

From these quantities, the general condition for static stability is that the vertical projection of the CoM on the ground must stay within the area defined by the BoS [30], [39], [47], [57]. In other words, the 2D coordinates of the CoM position on the horizontal plane (i.e., ground surface) must stay inside the limits set by the BoS. Mechanically, this can be explained in a clear manner using the inverted pendulum model. When the CoP and the vertical projection of the CoM coincide, the person is in perfect balance, however, as the CoM drifts away from the CoP location, by means of a rotation about the ankle joint, a horizontal separation distance is created, and a destabilizing moment ensues. In order to counteract the destabilizing moment and regain balance, the CoP needs to be repositioned beyond the CoM, with respect to the centre of rotation (i.e., the ankle). If the CoP is not adequately repositioned, the CoM will continue to drift further away until it reaches a position beyond the boundary of the BoS. Because the CoP location is bounded by the limits of the BoS, if the CoM is already beyond the BoS, the CoP can no longer be repositioned to a position that allows balance to be regained. In this case, two options are available: (1) do nothing and experience a fall; or (2) expand the BoS to allow the CoP to relocate to a position that allows the person to regain balance. The latter of these two options is accomplished by taking a step in the direction of travel of the CoM.

Though the classic condition for stability, defined above, is reasonable for static cases (i.e., standing), it is insufficient to quantify stability in dynamic situations as shown by Pai et al. [82]. In performing tasks such as walking, the CoM position moves at a much higher rate, dictated by the motion of the walker. As a result, the velocity of the CoM needs to be accounted for [39], [47], [57], [82]. If the CoM velocity is directed outward, away from the CoP, the CoP would have to be relocated to a position in which it can create a sufficient counteracting moment to first stop the outward progression of the CoM, and then move it back to a stable position that coincides with the CoP. Due to the added need to accommodate for velocity, balance may be impossible despite the fact that the instantaneous position of the CoM is still within the limits of the BoS [39].

The formula for the XCoM combining both CoM position and velocity was derived from the inverted pendulum model by Hof et al. [39] and is expressed as:

$$\mathrm{XCoM} = \mathrm{CoM} + \frac{V_{\mathrm{CoM}}}{\omega_0} \tag{9}$$

with CoM being the instantaneous position of the CoM, V_{CoM} being the velocity vector of the CoM, and ω_0 being the inverted pendulum's eigenfrequency. The eigenfrequency is calculated as:

$$\omega_0 = \sqrt{\frac{g}{l}} \tag{10}$$

where g is the acceleration due to gravity (9.81 m/s^2) and l is the equivalent pendulum length. Thus, in the case of dynamic stability, not only the CoM, but rather the XCoM must remain within the area defined by the BoS. This condition can be used to specify the margin of stability, MoS, the distance between the XCoM and the boundary of the BoS:

$$\mathrm{MoS} = \mathrm{BoS} - \mathrm{XCoM} \tag{11}$$

Furthermore, the temporal margin of stability, b_τ, quantifies the time available to reposition the CoP before the XCoM crosses the BoS:

$$\mathrm{MoS}_\tau = \frac{b}{V_{\mathrm{CoM}}} \tag{12}$$

Given equations 9 to 12, four quantities must be determined before computing the XCoM and using it to quantify stability in human walking: The CoM position and velocity, the area encompassed by the BoS, and the equivalent pendulum length. For each of these quantities, a number of proven experimental techniques exist to estimate its value.

First, and typically the most cumbersome to determine is the CoM; however, three different options are available [83], each presenting its own trade-off between complexity and limitations. The most complex, yet highly regarded, of these methods is the kinematic method. Despite being a time-consuming process, it is considered by many to be the gold standard in CoM estimation [84]. The application of this method combines anthropometric data with skin markers placed on essential body segments [83]–[85]. The position of the markers is tracked by a motion capture system. Obtained body orientation data, along with standardized anthropometric measurements are then used to compute the 3D position of the whole-body CoM by a weighted-sum of the body

segments' centres of mass [85]. With this technique, the degree of precision relies heavily on correct placement of the markers and accurate anthropometric data, the latter of which was evidenced by a study of Lenzi et al. [86].

Both the zero-point-to-zero-point [87]–[89] and low-pass filter [90] techniques for CoM estimation are based on the CoM's relationship to the CoP. They present a much simpler approach, relying only on force plate data; however, neither is able to predict the height of the CoM. Therefore, these options only allow for the vertical projection of the CoM to be determined [83]. Fortunately, only the 2D coordinates of the CoM on the walking surface are necessary as the margin of stability is a measure of the distance between the limits of the BoS and the XCoM on the horizontal walking plane. Thus, this major limitation does not inhibit the accurate prediction of the XCoM and the margin of stability, leaving them to be the preferred CoM estimation options due to their simplicity.

It is important to note that stability assessment should be performed separately for the ML and anteroposterior (AP) directions as the mechanics of each differ significantly in gait. With respect to the ML direction, stability analysis is completely warranted and produces expected results. However, forward progression requires that the CoM repeatedly passes beyond the BoS. Therefore, when gait stability is assessed in the AP direction, negative values for MoS and MoS_{τ} are found [15]. From theory, these results indicate instability and the need for voluntary action to extend the BoS. This is exactly what occurs during gait: the CoM extends beyond the BoS, resulting in a negative margin of stability value, and a step is taken to extend the BoS beyond the CoM to maintain stability. Despite the evidence of instability, stable gait is maintained which leads to questions about the pertinence of stability assessment in the AP direction [15]. Based on this outcome, the margin of stability may not be a valid tool to assess stability in the sagittal plane, in the traditional sense. However, it is certainly possible that it still provides relevant information for gait assessment. In agreement with this line of thought, Bruijn et al. [15] suggest that it may reveal information on foot placement and stepping strategies.

Since its introduction, the XCoM has been used extensively in a variety of gait studies: with non-disabled participants [3], [19], [95]–[100], [39], [47], [56], [57], [91]–[94] and prosthetic users [47], [95], [100], to quantify stability in the ML [3], [19], [39], [47], [56], [57], [91]–[93], [95],

[96]–[98], [100] and AP [3], [17], [102], [19], [39], [56], [93], [94], [98], [99], [101] directions, and in normal [3], [39], [47], [56], [91]–[93], [96] and perturbed [17], [19], [57], [94], [95], [97]–[99], [101] walking. Based on this information, one of the major advantages of the XCoM is its applicability to both normal and perturbed gait [15]. Moreover, it can be implemented on a sample-by-sample basis, meaning there is no restriction on the length of time series required. These elements are incredibly attractive for both clinical and experimental applications.

2.1.3.4 Stabilizing and Destabilizing Forces

Another measure derived from biomechanics is the concept of stabilizing and destabilizing forces [40]. Although these quantities were first applied to gait by Duclos et al. [40], the destabilizing force was originally introduced by Delisle et al. [103] to quantify stability during a lifting task. As with the XCoM, both forces are explained by the inverted pendulum model. First, the stabilizing force is the force necessary to stop the CoM from moving past the limits of the BoS [40]. To understand this quantity, recall the case in which the inverted pendulum is drifting away from equilibrium, the point at which the CoP and vertical projection of the CoM coincide. As the horizontal distance between the CoP and CoM increases, there is a proportional increase in the velocity of the CoM. Accordingly, the system as a whole gains mechanical energy. In order to regain equilibrium, that mechanical energy must be canceled out by the stabilizing force [31]. To find a mathematical description for the stabilizing force, begin with an expression for the work required to bring the CoM to a standstill:

$$W = \Delta E = E_{\mathrm{f}} - E_{\mathrm{i}} \tag{13}$$

where ΔE is the change in energy between the limit of the BoS (E_{f}) and the current position of the participant (E_{i}). Note that calculation of the stabilizing force is completed at a given instant in time; therefore, there is no displacement of the CoM and, thus, no change in gravitational potential energy. Consequently, the work is due solely to the change in kinetic energy; however, since the overarching goal is to cancel out mechanical energy and stop the CoM, the participant will be at rest in the final state. The expression for work is then:

$$W = 0 - E_{\mathrm{i}} = -\frac{m \cdot V_{\mathrm{CoM}}^2}{2} \tag{14}$$

where m is the mass of the participant. This is simply the kinetic energy of the CoM at the current position of the participant and, thus, the work needed to bring it to a standstill at the BoS limit. At the same time, the work required to bring the CoM to a standstill can be achieved by the stabilizing force (F_S) acting over the minimum distance between the CoP and the boundary of the BoS:

$$W = F_S \cdot d_{CoP} \tag{15}$$

where d_{CoP} is the minimum horizontal distance between the CoP and the vertical projection of the limit of the BoS, in the direction of V_{CoM}. Combining equations 19 and 20, and isolating F_S yields:

$$F_S = -\frac{m \cdot V_{CoM}^2}{2 \cdot d_{CoP}} \tag{16}$$

which can be used to calculate the stabilizing force in either the AP or ML direction. Expressed in vector notation, the stabilizing force is:

$$\vec{F}_S = -\frac{m \cdot \left(\vec{V}_{CoM} \cdot \vec{V}_{CoM}\right)}{2 \cdot d_{CoP}^2} \vec{d}_{CoP} \tag{17}$$

which can be used to calculate an overall stabilizing force in the direction of V_{CoM}.

Next, the destabilizing force is the force necessary to tip the participant (i.e., the inverted pendulum) over [15]. Formally, it is the theoretical force necessary to bring the CoP to the limit of the BoS [40]. To understand the relationship between these definitions, recall that the BoS represents the potential range of the CoP. Movement of the CoP within the BoS occurs in an attempt to counteract the destabilizing moment caused by a deviation of the vertical projection of the CoM from the CoP. Clearly, the more the CoP moves away from equilibrium, the larger the counteracting moment it enduces. The limit of the BoS acts as the endpoint for extension of the CoP, therefore, it defines the point at which the maximum counteracting moment may occur. This is the tipping point as any destabilizing moment larger than this value will cause the participant to fall. This concept provides the theoretical background for the destabilizing force. Mathematically, this can be expressed as:

$$M_D = F_D \cdot h_{CoM} \tag{18}$$

where M_D is the torque necessary to tip the participant over, and F_D is the destabilizing force applied at the height of the CoM, h_{CoM}. The torque can also be quantified by:

$$M_D = R_Z \cdot d_{CoP} \tag{19}$$

where R_Z is the vertical component of the ground reaction force. Combining equations 23 and 24 and isolating for $F_{D,}$ an expression for the destabilizing force is attained:

$$F_D = \frac{R_Z \cdot d_{CoP}}{h_{CoM}} \tag{20}$$

which can be used to calculate the destabilizing force in either the AP or ML direction. Expressed in vector notation, the stabilizing force is:

$$\vec{F}_D = \frac{\vec{R}_Z \cdot \vec{n}}{h_{CoM}} \vec{d}_{CoP} \tag{21}$$

where $\vec{n}$ is the unitary vector normal to the contact surface. This expression can be used to calculate an overall destabilizing force in the direction of V_{CoM}.

In terms of stability, theory dictates that the lower the stabilizing force, the easier it is for the participant to maintain stability by keeping the CoM within the BoS. In comparison, the lower the destabilizing force, the easier it is to move the CoP to the limit of the BoS, indicating reduced stability.

Finally, Duclos et al. [40] proposed a ratio of the forces, deemed the index of stability:

$$\text{Index of stability} = \frac{F_D}{F_S} \tag{22}$$

The thought here is that the higher the ratio, the lower the cost to maintain stability and, thus, the higher the level of overall stability [40]. Concerning each quantity, this would mean a high destabilizing force and low stabilizing force are required to achieve superior stability.

It is worth noting that both the stabilizing and destabilizing forces may be calculated per sample, so there is no need for excessively long time series. In theory, the index of stability could then be calculated on a per sample basis as well. The problem with that approach is that it may not provide any useful information. Rather, a mean stability index over a step, or consecutive steps, may be of more use.

Looking a little closer at both the stabilizing and destabilizing forces, it is apparent that each relies on entirely different sets of assumptions. The destabilizing force, based on static assumptions, appears to be a measure of postural balance [104]. For this reason, some regard it as being too simplistic for gait applications [15]. In contrast, the stabilizing force takes into account movement speed, thereby quantifying dynamic balance [104]. Because of these distinctions, Bruijn et al. [15] suggested that the index of stability is an unsuitable means to evaluate stability. Further, the criticism of the index and destabilizing force led to the belief that the stabilizing force, by itself, may be sufficient to quantify dynamic stability [15]. Similar to the XCoM, if the stabilizing force were to be combined with a theoretical maximum force, it may provide its own margin of stability to predict when an extension of the BoS is needed [15]. More than likely, this would only be practical for the ML direction since an extension of BoS will require the stabilizing force to exceed the theoretical maximum in the AP direction. An investigation into whether or not this is the case, and if so, by how much the stabilizing force needs to exceed the maximum to meet certain conditions (e.g., speed, step length, etc.) presents a great opportunity for future research.

Judging by some of the most recent studies that have applied both the stabilizing and destabilizing forces while leaving out the index of stability [104]–[107], it seems there may be mixed opinions concerning the suggestions of Bruijn et al. [15]. On the one hand, leaving out the index of stability may suggest the belief that it is inappropriate to use a ratio of forces derived from completely separate assumptions. On the other hand, inclusion of the destabilizing force indicates that it may provide some indication of stability, despite its simplicity. To reinforce the latter point, Lemay et al. [106] stated that analysis of both components of balance, i.e., postural (via destabilizing force) and dynamic (via stabilizing force) balance, are necessary to characterize walking performance in individuals with incomplete spinal cord injury. Still, there is opportunity to develop an improved form of the destabilizing force that takes into account movement speeds and accelerations.

Since their introduction to gait applications [40], stabilizing and destabilizing forces have only been used to quantify gait stability a handful of times [40], [104]–[109]. In all cases, overall stabilizing and destabilizing forces were computed in the direction of CoM velocity, rather than in the ML and AP directions separately. This seems inappropriate given that the characteristics of gait are very different between these directions. An investigation into the different force values, and the factors that influence those values, in either direction is surely warranted.

Although Bruijn et al. [15] did not include the stabilizing and destabilizing forces as a measure that can be used to assess stability in response to perturbations, the general nature of the measure should certainly permit it to be applicable to walking in perturbed environments. At the time of publication, no studies had been conducted in which the stabilizing and destabilizing forces were used to evaluate stability in response to perturbations. However, Ilmane et al. [109] recently investigated dynamic and postural balance of non-disabled participants in response to slip-like perturbations on a split-belt treadmill. Though they admit further study is necessary, it was indicated that stabilizing and destabilizing forces may be useful to gauge balance difficulty in perturbed environments [109]. Interestingly, they also pointed out that the stabilizing and destabilizing forces could present a valuable means to detect the most suitable magnitude of perturbation for gait balance training [109]. This is an intriguing opportunity that deserves further attention, potentially using different types of mechanical perturbations (e.g., platform translation) and in fall-prone populations (e.g., prosthetic users). In addition, it would be interesting to see the effect of walking at various slopes or on an irregular surface on the stabilizing and destabilizing forces.

2.1.3.5 Gait Sensitivity Norm

The GSN [41] is a measure that owes its roots to robotics research. In short, it aims at quantifying the ability of a walker to resist falling over in the presence of relatively large disturbances. Of course, the key element to that statement, the ability to resist falling, is the overall goal of gait stability research. The GSN aims to accomplish that goal by applying a specific perturbation (i.e., disturbance) to the walker and analyzing the dynamic response of a specific gait indicator [41]. In this case, the term ‘specific’ entails that the quantity (i.e., perturbation or gait indicator) must be

measurable and related to the objective of the study. Individually, the chosen perturbation (e.g., push, pull, change in floor height) needs to be able to provoke the meaningful ways to fall (i.e., failure modes), while the gait indicators (e.g., step time, step width, margin of stability) should reflect the gait characteristics directly related to those failure modes [41]. With the perturbations and gait indicators acting as the input and output, respectively, the dynamic response of the system is given by the variability of the gait indicator as a result of the perturbation [41]. The greater the variability, the higher the dynamic response (i.e., GSN) and, thus, the greater the instability. A walker who is able to limit gait variability and swiftly return to the nominal gait pattern after being subject to a perturbation will exhibit a lower GSN value and be deemed more stable. Therefore, another interpretation of the GSN is that it quantifies how fast the walker returns to its nominal, steady-state gait pattern.

When introducing the GSN measure for stability, Hobbelen et al. [41] described two methods of computation: the direct input-output identification method and the state-space description method. The direct input-output identification method is better suited for real-life applications such as robot prototypes, whereas the state-space system description is preferred for simulation purposes [41]. Going forward, only the direct input-output identification method will be described as the intent of this review is to identify measures able to quantify stability in human walking, a real-life application.

Calculation of the GSN for physical prototypes is as follows:

1. choose a perturbation (e_0) based on the failure modes to be investigated;
2. choose gait indicators (g_k) that are most related to the expected failure modes. Note that multiple gait indicators, denoted by k, may be included in the GSN calculation, if desired;
3. estimate the steady-state value of each of the gait indicators (g_k*). This is accomplished by performing a steady-state walking trial (i.e., no perturbations) and taking the nominal value of the gait indicator as the mean value over multiple strides;
4. perform a perturbed walking trial in which the gait indicators are measured during consecutive strides, $g_k(i)$, following the disturbance. Note that consecutive strides are denoted by i; and

5. assuming a linear relationship between perturbation size and response of the gait indicator, compute the dynamic response to a perturbation using the H_2-norm:

$$\left\|\frac{\partial \mathrm{g}}{\partial \mathrm{e}}\right\|_2 = \frac{1}{|e_0|}\sqrt{\sum_{k=1}^{q}\sum_{i=0}^{\infty}(\mathrm{g}_k(i) - \mathrm{g}_k^*)^2} \tag{23}$$

where q is the number of gait indicators.

Since the method outlined above was originally intended to assess gait stability in robots, a few remarks should be made concerning its applicability to human gait. Primarily, two major concerns exist. First, by observation of equation 28, it can be seen that the gait indicators need to be tracked for an infinite number of steps, an impossible feat in physical applications [15]. Assuming an individual does not fall immediately following a perturbation, it may be assumed that they will return to their nominal gait pattern after a certain number of recovery steps. Fortunately, there is evidence to support this assumption, such as the work of Cordero et al. [58] who recommended incorporating at least three strides in any study investigating gait recovery following a perturbation.

The second concern with the application of GSN to human gait is a consequence of the natural variability of human gait. Bruijn et al. [15] contended that the natural variability of a gait indicator might overestimate the GSN and provide an erroneous measure of stability. To solve this issue, they proposed normalizing the transient variability in the GSN calculation by removing the steady-state variability of the gait indicator [15]. Thangal et al. [110] applied this scheme while using the GSN to assess stability in a neuromusculoskeletal (NMS) model. The modified form of the GSN formula, accounting for natural variability is given by:

$$\left\|\frac{\partial \mathrm{g}}{\partial \mathrm{e}}\right\|_2 = \frac{1}{|e_0|}\sqrt{\sum_{k=1}^{q}\sum_{i=0}^{\infty}\left(\mathrm{g}_k(i) - \mathrm{g}_k^* - \mathrm{g}_{k\,SSvar}\right)^2} \tag{24}$$

where $\mathrm{g}_{k\,SSvar}$ is the steady-state variability of the gait indicator.

In the assessment of the NMS model, a sensitivity analysis demonstrated that the steady-state variability was negligible in comparison to that induced by the perturbation [110]. Notably, the study focused on a simulated model; therefore, it is possible that steady-state variability would be larger in physical studies with human participants. This would certainly have to be investigated.

According to the step-by-step procedure, two trials are necessary to compute GSN values in physical studies: steady-state and perturbed. Alternatively, these may be combined into one trial so long as the participant is allowed to walk at steady-state for a sufficient number of strides prior to, or just after the perturbation. Nominal values of the gait indicators can be estimated by taking the mean across the steady-state walking strides over the desired period (i.e., before or after perturbation). In either case, it is important that the first few strides be omitted from the mean calculation as these are transient strides. In the event that nominal gait occurs prior to the perturbation, gait initiation will create the added variability to the first few strides. Meanwhile, when nominal values are estimated from steady-state walking that occurs after the perturbation, variability will be a result of the perturbation. After a few transient recovery strides, an individual will return to the nominal gait pattern [58], at which point steady-state values of the gait indicators can be estimated. Therefore, when employing a combined method (i.e., single trial) for data collection, it is imperative that the first few strides be omitted. The exact number should be determined experimentally or from literature.

To date, the majority of literature surrounding the GSN deals with its application to actual robots [41], [111], [112] or simulated models [41], [110]–[115]. In these contexts, the GSN has been shown to correlate well with actual disturbance rejection (ADR), thereby proving it to be a useful measure in robotics research. Use of the GSN in human walking is limited to two instances in which data was presented at a conference [32], [42]. Both times, the assumption of a linear relationship between the perturbation and gait indicators was investigated and proven to be valid. The most recent study [42] also reached the conclusion that higher perturbation magnitudes appear to provide better statistical precision.

2.1.3.6 Variability Measures

In the context of gait, variability refers to the amount of fluctuation of a particular parameter over successive walking strides. The use of variability as a measure of gait stability is based on the belief that an increase in variability is indicative of reduced stability [15]. In certain simple dynamical systems, this rationale holds true; however, as the complexity of the system grows, the argument changes. In complex dynamical systems, such as human gait, it is possible that a large portion of the variability is an element of the control strategy [15], [116], [117] or due to the multiple degrees of freedom available to the system [15]. This view is supported by experimental evidence that, for example, has demonstrated decreased variability in participants with anterior cruciate ligament deficiency in comparison to non-disabled controls [118]. Thus, reduced variability can also be indicative of impairment [116]–[118]. Regardless of these concerns, variability measures have been shown to indicate instability, by means of fall prediction in older adults [8], [119].

Conveniently, the calculation of a variability measure is remarkably straightforward – it merely requires computing the standard deviation of the chosen gait variables [119]. First, the investigator must decide on which walking parameters to analyze for a certain walking trial. Note that these may include discrete (e.g., step width, stride length) or continuous (e.g., joint angle time series) quantities; however, some data processing differences do exist between the two. Discrete variables are already specific to each stride; therefore, the variability can be determined by calculating the standard deviation of the values from all strides. Meanwhile, variables given by a time series (i.e., continuous) must be cut into strides and time-normalized. Typically, each stride is normalized to 101 data points (0-100% of gait cycle) to enable successive strides to be aligned. The standard deviation is then computed at each of the aligned points, leaving 101 variability values. These may be interpreted graphically to identify the points of the gait cycle that exhibit the greatest variability, or they may be used to find a single mean or summed value.

The clear advantage of the variability measures is the ease of their calculation as it simply requires choosing gait variables and finding the standard deviation for a number of strides. Despite this, there are a number of disadvantages that may hinder its utility as a measure of gait stability. First and foremost is the question of whether or not variability is indicative of instability. Though there

is evidence on either side of the argument, one certainty is that it cannot be used to characterize stability in all cases. To understand why, take Bruijn's example [15] of comparing two individuals walking with different step widths, but equivalent step width variability. By variability alone, both participants demonstrate an identical level of stability. However, based on knowledge of the margin of stability, the individual with a larger step width would be deemed more stable. From this, it is apparent that an understanding of the constraints (e.g., margin of stability) and control strategy (e.g., step width) must accompany variability to make a valid assessment of gait stability [15].

Since the variability measures attempt to quantify gait stability by measuring the fluctuations around a nominal value, any non-stationarities in the data will lead to an overestimate of variability, affecting the interpretation of stability. Thus, it is imperative that the data are stationary [15]. The real-life implication of this is that variability can only be used to assess normal gait on a level or inclined walking surface, or in the presence of pseudo-random oscillations of the support surface. Visual oscillations and vestibular stimulation are also possible, but any technique that introduces non-stationarities by displacing the body (i.e., mechanical perturbations) is not permitted.

In their 2001 study, Grabiner et al. [120] discussed the issue of inadequate statistical power caused by the failure to record an adequate number of strides. In this study, analysis included 20 strides from which to compute the standard deviation. Though significant differences between non-disabled younger and older adults were obtained for certain gait parameters, a number of results conflicted with what had been previously published in the literature. In addition, there were noticeable differences in the coefficients of variation reported between studies, with the smaller coefficients corresponding to those studies that included a greater number of strides. Grabiner [120] attributed these discrepancies to the unequal number of strides collected in the studies. In turn, this discussion led to an investigation by Owings and Grabiner [43] to pinpoint the number of strides for which the maximum precision of variability estimates is obtained. They determined that precision did not increase for data sets that included 200 strides or more. As with the Lyapunov exponents and Floquet multipliers, this represents a substantial number of strides. This is a difficult feat for many patient populations, thereby diminishing the usefulness of the variability measures

for clinical applications. When using discrete gait variables, there is the possibility that the stride requirement can be reached over multiple trials with a rest period in between, but even then, 200 strides is challenging.

2.1.3.7 Long-Range Correlations

A second statistics-based measure of gait stability – the other being variability measures – are long-range correlations. Motivation for this form of walking assessment stems from evidence supporting the notion that future variations in gait depend on past variations [15]. Intuitively, this makes sense: when an individual exhibits a misstep (e.g., due to incorrect foot placement) and stability is compromised, recovery is made in the subsequent strides. When dependence occurs, a power law relationship exists, with the degree of correlation given by the scaling exponent (α). With respect to long-range correlations, the scaling exponent measures the rate of decay of statistical dependence between two points in a time series separated by an increasing time interval. Though this definition appears similar to exponential decay, there is a distinction between the two. The power-like decay of long-range correlations results in a much slower decay in dependence than that exhibited by exponential decay.

Calculating the strength of long-range correlations begins with the collection of gait data during a steady-state walking trial. With the help of post-processing, these data can be used to create a discrete time series for the gait parameter of interest (e.g., stride with, stride length, peak force). Each data point of the time series should represent the value for a specific stride. The exact protocol for data collection will depend on the gait variables to be investigated, but may include kinematic and/or kinetic data. Once a time series for the discrete gait variable is obtained, detrended fluctuation analysis (DFA) [121] is used to calculate α. Though there are other techniques that accomplish the same task, DFA has become the standard for gait data since it is robust to the effects of non-stationarities [33]. A thorough step-by-step description of the procedure is given by Damouras et al. [33]. An outline of the algorithm is given below, along with a graphical illustration (Figure 2.3) to assist in understanding.

1. integrate the stride interval time series after removing its mean to obtain a stationary time series. Note that stationarity is important to completing correlation analysis [121]:

$$y(i) = \sum_{j=1}^{i} |x(j) - \bar{x}| \tag{25}$$

where i = [1,N], with N being the number of strides, $x(j)$ is the parameter value for the j^{th} stride, and $\bar{x}$ is the mean value of the gait parameter;

2. divide the integrated series into $\lfloor N/n \rfloor$ non-overlapping boxes of equal length, where n is the size of the box and $\lfloor \cdot \rfloor$ is the greatest integer function;
3. in each box, fit a least-squares line to the data. The sequence of these fitted lines represents the trend series, whereas the total number of strides falling within all boxes is $N_n = n\lfloor N/n \rfloor$;
4. calculate the average fluctuation, $F(n)$, of the integrated series (y) about the straight-line segment (i.e., line of best fit) in each window:

$$F(n) = \sqrt{\frac{1}{N_n} \sum_{i=1}^{N_n} |y(i) - y_n(i)|^2} \tag{26}$$

where y_n is the trend series, the sequence of fitted lines;

5. given a range of box sizes $[n_1, n_m]$, repeat steps 2 to 4 for each box size. In doing so, a range of fluctuations, one for each box size, is obtained; and
6. create a log-log plot of $F(n_k)$ versus n_k, where k = [1,m]. A linear relationship between $\log F(n)$ and $\log(n)$ reveals that scaling occurs; therefore, the scaling exponent (α) can be estimated by the slope of a linear line of best fit.

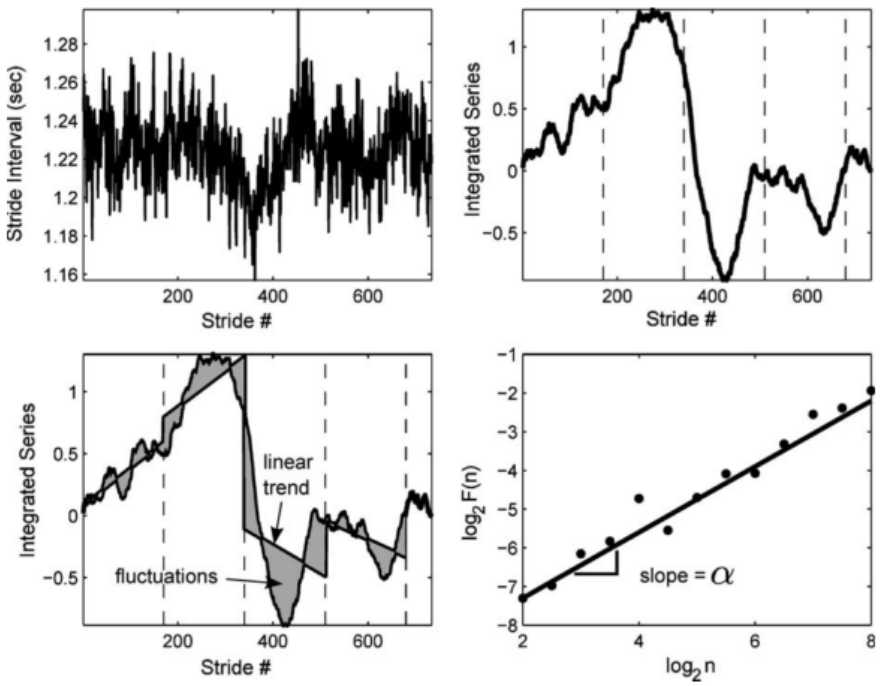

Figure 2.3: Illustration of DFA procedure. Raw walking data (top left), integrated series divided into boxes (top right), least-squares line fit to each box (bottom left), and log-log plot of $F(n)$ versus n (bottom right). Reprinted from [33], with permission from Elsevier (© 2009 Elsevier)

As with any statistical measure, more data yields more accurate results, and long-range correlations are no different. Obtaining more precise estimates requires longer time series, which in gait experiments, entails longer periods of continuous walking. No matter the person, the longer they are required to walk, the more likely fatigue is to set in. Therefore, there is trade-off between precision and the length of a walking trial. Realizing this, Damouras et al. [33] investigated the number of strides required to reach the most precise estimate of the scaling exponent. In addition, they determined the optimal range of box-sizes for DFA applied to gait. Based on their results, walking trials should contain at least 600 strides of continuous walking, while a size-adjusted range of box sizes of $\left[16, \frac{N}{9}\right]$ is recommended for analysis.

Generally, systems with a scaling exponent near 0.5 are uncorrelated, with smaller values (i.e., $\alpha < 0.5$) and larger values ($\alpha > 0.5$) indicating anti-persistance of fluctuations and positive correlations, respectively [15]. In human walking, values greater than 0.5 are expected (specifically $0.5 < \alpha < 1.0$), indicating that large (or small) values are more likely to be followed by another larger (or smaller) one [15]. Although, in practice, that is not always the case. Despite

the evidence that variations in past strides have an effect on the execution of future strides, this notion is not always supported by long-range correlations. For example, Jordan et al. [122] observed α values of 0.5 at a preferred walking speed, thus, implying weak long-range correlations between successive strides. Regardless of the fact that preferred walking speed is perceived as the most stable, small inertial forces and mechanical noise are present nonetheless. These will create perturbations that will require a reaction from the walker in subsequent strides [15]. Therefore, it makes little sense to conclude that there is no relationship between strides, even at preferred walking speed. Furthermore, several studies found α values near 0.5 for patient groups [15]. These are groups that are known to have a reduced ability to accommodate natural perturbations (i.e., inertia and noise), displaying greater variability that must be corrected by reactive movements.

The relationship between long-range correlations and gait stability is, so far, quite weak. Further work needs to focus on developing a stronger theoretical foundation [15] and identifying which values of the scaling exponent are indicative of instability, or if a connection between the two exists at all. Still, if the preceding objectives are met, there is still the requirement for long time series of data. Since 600 strides of continuous walking may be challenging, even for non-disabled walkers, the question remains as to whether long-range correlations are a viable option for clinical use.

2.1.3.8 Foot Placement Estimator

The FPE [45] is another gait stability measure that came to light through robotics research. Drawing inspiration from the stepping strategies that humans use to maintain balance in response to disturbances [64], it was introduced by Wight et al. [45] as a method for bipedal gait control. Rather than take the traditional approach, in which the control strategy attempts to maintain balance at all times, the FPE focuses on restoring balance through proper foot placement [45].

To derive the FPE, an inverted pendulum representation was employed to model the simple bipedal walker in 2D [45].This depiction assumes a mass (m) with two massless legs of constant length (L), separated by the leg separation angle (β). The location of m in 2D space is given by the CoM, which also acts as the origin of both legs. Furthermore, the moment of inertia about the CoM is given by I_{CoM}. An illustration of the model can be seen in Figure 2.4 below.

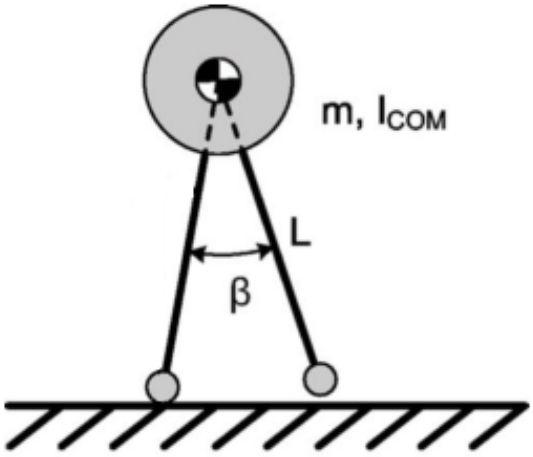

Figure 2.4: Inverted pendulum representation of a simple biped walker with mass *m*, moment of inertia about the centre of mass I_{CoM}, constant leg length *L*, and leg separation angle β. Reprinted from [45], with permission from ASME (© 2008 ASME).

With respect to gait, the inverted pendulum model goes through alternating phases of single- and double-support [123] (i.e., one or two legs in contact with the ground, respectively). In single-support, the point of contact of the leg with the ground defines the CoP. Meanwhile, in double-support, when both legs are in contact with the ground, the CoP is located between the two points of contact. The stability of the biped is then defined by the relationship between the CoP and the CoM, which forms the basis for the FPE. Essentially, the FPE calculates the correct placement of the CoP, in relation to the CoM, to ensure the biped is able to transition to a statically stable pose [124]. Note that the term 'statically stable pose' is basically a standing position, so the FPE is the location of the CoP that allows the walker to stop gait in a single stride, without falling over [45].

An alternative, yet complementary, approach to understanding the foundation for the FPE is in terms of energy. In bipedal walking, there is a continuous exchange of gravitational potential and kinetic energy that results in the two being out of phase [125]. In other words, when kinetic energy is at its peak, potential energy is at a minimum, and vice versa [125]. This energy exchange is cyclic in nature, repeating on a step-by-step basis. To gain insight into this energy cycle, refer again to the inverted pendulum, particularly the trajectory of the CoM [126]. At mid-swing, the CoM is at its greatest height above ground, therefore, peak potential energy occurs. As forward movement continues, the CoM rotates about the point of contact between the stance leg and the ground, gradually lowering the CoM. The change in height results in a conversion of energy from

potential to kinetic, which occurs until the swing leg comes into contact with the ground. At that point, maximum kinetic energy is reached. That kinetic energy is then converted to potential energy up until midstance is reached. Here, the CoM is once again at its maximum height (i.e., peak potential energy) and the cycle repeats. This continues onwards until gait termination. During this special case, the walker needs to come to a standstill while remaining in the upright standing position. This position is similar to midpoint of stance (or swing) in that it is the point of peak CoM height. In order to come to a stop at this location in the cycle, the kinetic energy at impact must be just enough to reach peak potential energy and reach the standing position [6]. This is the definition of the FPE in terms of energy.

In introducing the FPE, Wight et al. [45] presented three cases to demonstrate the consequences of stepping relative to the FPE (Figure 2.5). In the first case (Figure 2.5a), the biped takes a shorter step than is required to meet the FPE. Upon impact, the kinetic energy exceeds the peak potential energy and the biped falls forward. In the second situation (Figure 2.5b), the biped takes a longer step than required, so the post-impact kinetic energy is lower than the peak potential energy and the biped falls back onto the swing foot, a stable position. The third and final case occurs when the biped steps at the exact location of the FPE (Figure 2.5c). When this happens, the kinetic energy upon impact is exactly equal to the peak potential energy and the biped comes to a standstill in the balanced, upright position.

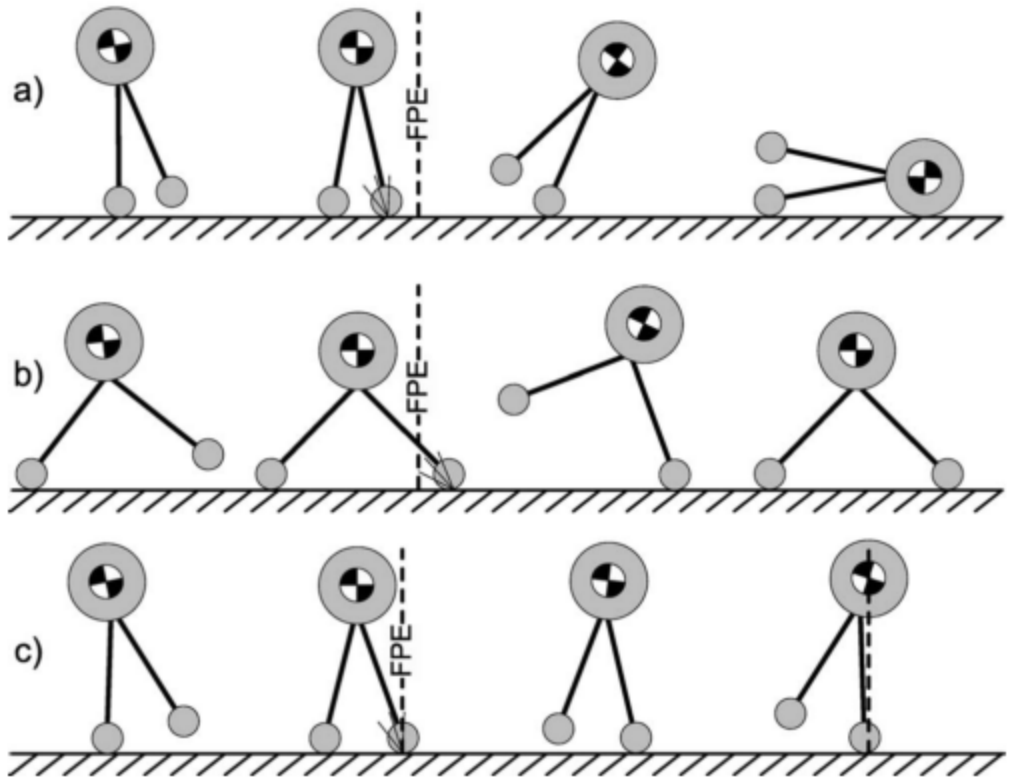

Figure 2.5: A depiction of simple biped stepping relative to the FPE. (a) Too short a step causes a forward fall. (b) Too far a step causes the biped to fall back onto the swing leg. (c) Stepping at the FPE balances the CoM above the CoP. Reprinted from [45], with permission from ASME (© 2008 ASME)**.**

Referring to Figure 2.6, derivation of the FPE [45] begins with the conservation of angular momentum between pre- and post-impact conditions:

$$H_1 = H_2 \tag{27}$$

$$mL(v_x \cos\phi + v_y \sin\phi) + I_{\mathrm{CoM}}\dot{\theta}_1 = (mL^2 + I_{\mathrm{CoM}})\dot{\theta}_2 \tag{28}$$

where H_1 is the pre-impact momentum, H_2 is the post-impact momentum, v_x is the *x*-component of the pre-impact linear velocity, v_y is the *y*-component of the pre-impact linear velocity, $\dot{\theta}_1$ is the pre-impact angular velocity, and $\dot{\theta}_2$ is the post-impact angular velocity. Angle ϕ is the angle between the swing leg and a line perpendicular to the ground up to the CoM. The leg length can also be expressed in terms of the current height of the CoM (h):

$$L = \frac{h}{\cos\phi} \tag{29}$$

This eliminates the need to know L exclusively and allows for variable leg lengths to be used. Substituting into equation 33, and solving for $\dot{\theta}_2$, the post-impact rotational velocity can be calculated from pre-impact conditions:

$$\dot{\theta}_2 = \frac{mh\left(v_x \cos\phi + v_y \sin\phi\right)\cos\phi + I_{\mathrm{CoM}}\dot{\theta}_1 \cos^2\phi}{mh^2 + I_{\mathrm{CoM}}\cos^2\phi} \tag{30}$$

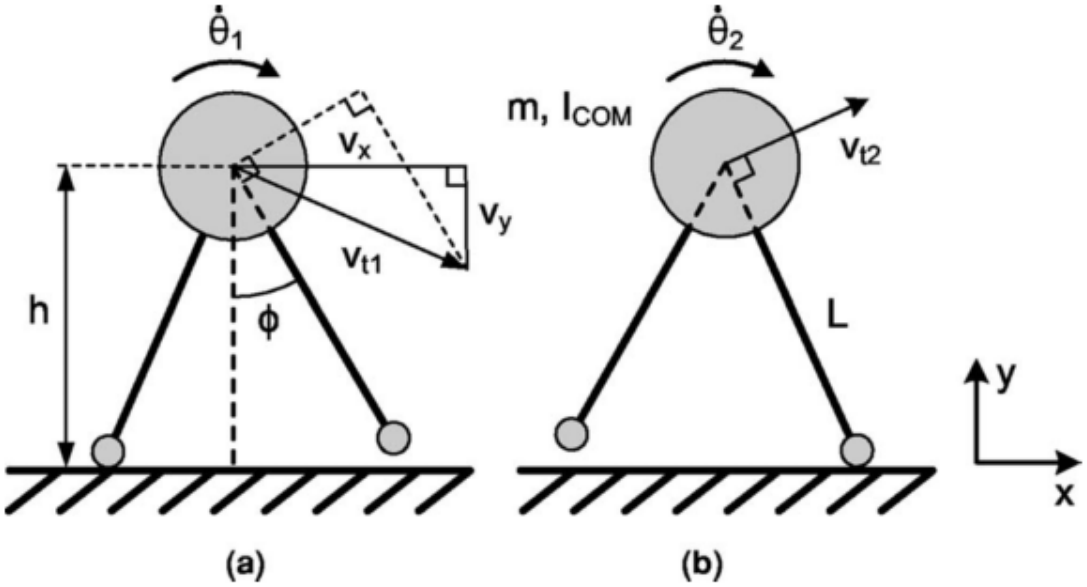

Figure 2.6: Schematic of the simple biped illustrating the parameters for (a) pre-impact, and (b) post-impact conditions. Reprinted from [45], with permission from ASME (© 2008 ASME).

Applying the conditions for energy described earlier, the FPE location is given by ϕ when the total system energy post-impact $(T_2 + V_2)$ is equivalent to the peak potential energy (mgh_{peak}):

$$T_2 + V_2 = mgh_{\mathrm{peak}} \tag{31}$$

$$\frac{1}{2}(I_{\mathrm{CoM}} + mL^2)\dot{\theta}_2 + mgL\cos\phi = mgL \tag{32}$$

$$(I_{\mathrm{CoM}}\cos^2\phi + mh^2)\dot{\theta}_2^2 + 2mgh\cos\phi\,(\cos\phi - 1) = 0 \tag{33}$$

Substituting the expression for $\dot{\theta}_2$ (equation 35) into equation 38 gives:

$$\frac{\left[mh\left(v_x \cos\phi + v_y \sin\phi\right)\cos\phi + I_{\mathrm{CoM}}\dot{\theta}_1 \cos^2\phi\right]^2}{mh^2 + I_{\mathrm{CoM}}\cos^2\phi} + 2mgh\cos\phi\,(\cos\phi - 1) = 0 \tag{34}$$

Finally, solving equation 39 for ϕ using numerical methods for nonlinear equations and then applying simple trigonometry, the location of the FPE is determined. Figure 2.7 illustrates the relationship between the FPE and angle ϕ.

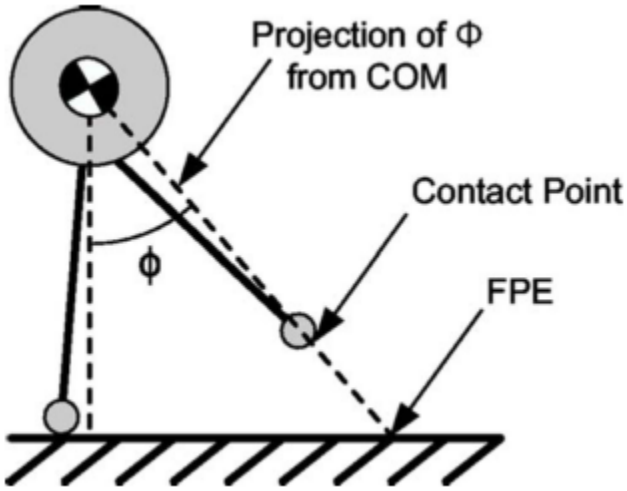

Figure 2.7: The location of the FPE is given by the projection of ϕ from the CoM to the ground. Reprinted from [45], with permission from ASME (© 2008 ASME).

The trigonometric relationship used to find the location of the FPE, $X(\phi)$, is given by:

$$X(\phi) = h\tan\phi \tag{35}$$

Note that the above equations only pertain to 2D movement in the sagittal plane. To implement the FPE in 3D (3DFPE) [46], assessment is completed separately for the AP (i.e., sagittal plane) and ML (i.e., frontal plane) directions. Depending on direction, the respective plane is taken as the 'plane of progression' and all quantities are projected onto that plane. The 2D equations described above can then be applied to each plane individually, prior to translating the FPE results back into the 3D world.

Although the FPE was first described as a means to control bipedal gait in robots, recent work has been done to see if it can be used to predict human foot placement (HFP) and provide insight into

gait stability [6], [46], [124], [127]. In the application to human gait, however, a number of the parameters necessary to apply equation 39 are not explicitly known (h, I_{CoM}, v_x, v_y, $\dot{\theta}_1$) and must be measured using experimental techniques:

- the height of the CoM (h) can be approximated as a certain percentage of total body height [84], or through kinematic methods [83]–[85]. For the latter method, a few options exist that differ with respect to the number of markers used. The simplest option is to approximate the height of the CoM as the height of the second sacral vertebrae [84], which involves a single sacral marker along with a predetermined offset. The other option is a full-body marker set to predict the 3D position of the CoM [83], [85], but this will also require the use of anthropometric data;
- the total body moment of inertia about the CoM (I_{CoM}) is estimated using a combination of kinematic measurements and anthropometric data [128]. This involves a segmental analysis in which movement of every segment is tracked using a full-body marker set. To determine the contribution of each segment about the CoM, the parallel axis theorem is applied to each individual segment, and the results are summed;
- the linear velocity of the CoM (v_x, v_y) is also determined using kinematic means. This may be accomplished by tracking the 3D displacement of the CoM using either a single sacral marker [84] or a full-body marker set [83], [85]; and
- the angular velocity ($\dot{\theta}_1$) is calculated using the following formula:

$$\dot{\theta}_1 = \frac{H_{\mathrm{tot}}}{I_{\mathrm{CoM}}} \tag{36}$$

  where H_{tot} is the total body angular momentum. Experimentally, it is calculated as the sum of each segment's angular momentum about the CoM [129]. As with the other parameters, this requires full-body kinematics.

To summarize the above list, estimation of each parameter is dependent on kinematic data. Since the techniques involved in obtaining such data are time-consuming and cumbersome relative to other collection methods, this presents a disadvantage to human applications of the FPE. Furthermore, Millard et al. [6] reinforced the need for accurate measurements in segmental analyses by stating that a 10% error in the mass of the head, arms, and trunk (HAT) could change the FPE calculation by 2 to 3 cm.

Despite the disadvantages, the nature of the FPE does reveal a number of distinct benefits. First, the FPE does not require long data series with hundreds of successive strides. Instead, calculation can be completed on a stride-by-stride basis, meaning a minimum number of strides is required [124]. The ability for the FPE to be applied to perturbation experiments [15] presents another important advantage as it opens to the door to investigations on recovery. Lastly, the FPE appears to demonstrate a logical means to measure stability in human gait. The relative distances between the horizontal projection of an individual's CoM, actual foot placement, and the FPE may be used to quantify the effectiveness of a step in restoring overall balance [6].

In the development of the FPE, the following four assumptions are necessary to apply a simplified model of walking dynamics and reach the solution:

1) the leg length remains constant through impact;
2) the total body moment of inertia remains constant through impact;
3) the total body energy (i.e., kinetic and potential) is conserved through impact; and
4) the total body angular momentum about the contact point is conserved through impact.

Sensitivity analyses [6], [124] were conducted to determine the effect of deviations from the assumptions that occur during human walking. In both cases, the authors observed that the errors were usually smaller than the effects of walking speed. These results led Millard et al. [6] to conclude that FPE-HFP errors are likely due to decisions made by the participant rather than systematic violations of the assumptions.

2.1.3.9 Largest Recoverable Perturbation

The largest recoverable perturbation is a measure first discussed by Bruijn et al. [15] in their review of dynamic stability measures. In contrast to the other measures discussed, the largest recoverable perturbation does not require a detailed theoretical background. Instead, as the name would suggest, this measure seeks to identify the largest magnitude of perturbation that a participant can tolerate without falling [15]. This would certainly differ depending on the type of perturbation (e.g., change in dual-belt treadmill speed, pushes at the trunk, moving support surface), the direction at which it is delivered, and the phase of the gait cycle at which it is delivered. In each

case (i.e., type, direction, phase), identifying the largest recoverable perturbation would require a continuous spectrum of magnitudes, which brings into question the practicality of this measure. Determining the largest recoverable perturbation would require an extensive and time-consuming experimental procedure [15].

Though the ideal experiment may not be realistic, a case may be made to perform an adapted version or slight variation that significantly increases the feasibility. First, rather than apply a continuous scale in an attempt to identify the perturbation magnitude at which each participant will fall, it may be more suitable to choose a finite number of equal perturbation magnitudes to apply and measure how many times each participant falls [15]. Another option may be to, again, choose a finite number of equal perturbation magnitudes but apply each of them over a relatively long distance (or time). Here, the thought is that the distance (or time) will form somewhat of a continuous spectrum and participants may lose stability at different points.

It is likely that a great deal of slight variations exist to assess an adapted measure of the largest recoverable perturbation; however, it is important that the chosen approach reflects the intention of the study.

2.2 Motion Capture

2.2.1 Introduction

Regardless of the setting – rehabilitation, ergonomics, or high performance sport – grading the performance of any movement skill requires an accurate biomechanical analysis of the human musculoskeletal system [128]. Oftentimes, this includes characterizing relative movement patterns between adjacent body parts, or segments [128]. The term used for these measurements is *kinematics* where a full kinematic description includes the 3D linear and angular components of displacement, velocity, and acceleration [128]. The position of all body segments or a particular subset of body segments is first recorded during the activity or movement of interest. These collected data are then used to compute the kinematic variables necessary to evaluate the movement [128].

A number of techniques exist to measure 3D movements: electromagnetic tracking systems [130]–[134], wearable inertial measurement units (IMUs) [135]–[143], markerless motion capture systems [144]–[150], optoelectronic stereophotogrammetry [151]–[156], and stereoradiography [157], [158]. Despite the selection of choices, stereophotogrammetry is considered the best available option and is commonly used in fundamental scientific research [151]. Furthermore, 3D position data reconstructed from video images are preferred over radiographs or photographs as they require a reduced investment of both time and money [159]. These video-based systems, otherwise known as motion capture systems, are the gold standard in human movement research and commonly used as a reference to validate emerging techniques such as IMU-based and markerless systems [135], [141], [148], [149].

2.2.2 Kinematic Data Acquisition and Processing

The acquisition of kinematic data using a motion capture system is accomplished by recording the instantaneous positions of markers in 3D space with a set of specialized cameras [128], [151], [160], [161]. For human movement analysis, markers may be placed on assumed joint centres between body segments (i.e., anatomical markers) or in clusters of multiple markers (e.g., cluster plates) [151], [161]. To define joint centres and segmental coordinate systems for each body segment, at least three markers are necessary to be placed on the segment of interest [160]. To ensure that three markers are visible at all times, a fourth marker is added in the event that marker occlusion leads to missing data for a particular marker [160].

The markers used by a video-based motion capture system may be either passive or active in nature [162]. Retroreflective passive markers are used in conjunction with light-emitting diodes (LEDs) that illuminate the markers via infrared light [156], [162]. Because all markers appear identical when using a passive system, identifying individual markers and preventing marker swapping is performed using pattern recognition software or dedicated hardware circuits [162]. In contrast, active markers emit LED light themselves according to a sequential pulse timing [162]. This active light emission eliminates the need for additional software or circuitry as the system is able to automatically detect each marker by the timing of its pulsating LED light [162]. Although active markers require additional hardware (e.g., batteries, wires) on the body of the participant, they do provide greater accuracies and sampling rates than passive marker systems [162].

No matter the type, 2D marker coordinates from every camera are passed to a computer where they are combined together with calibration data and a set of reconstruction parameters to triangulate each marker's 3D position. So long as the marker is visible to at least two cameras, the 3D position data can be obtained through simple triangulation [162], [163]. Mounting a greater number of cameras within a system increases the likelihood of at least 2 cameras being able to view each marker at all times, improving the robustness of the acquired position data.

2.2.3 Limitations

Given the complexity of motion capture analysis – specialized equipment, key assumptions – it comes as no surprise that there exist multiple sources of error which include instrumental errors [162], soft tissue artifacts [164], and anatomical landmark displacement errors [165]. Instrumental errors include random errors from electronic noise, marker flickering, or marker image distortion; and systematic errors due to improper camera and lens set-up or photogrammetric calibration inaccuracies [162]. A camera calibration aims to determine the geometric and optical characteristics of the cameras, as well as the position and orientation of the camera relative to the laboratory environment [162]. It is crucial that these parameters be as accurate as possible to reliably estimate 3D marker positions from the combined 2D images of multiple cameras.

Errors originating from markers moving relative to a body segment or improper marker location on the body segment are classified as soft tissue artifacts [164] and anatomical landmark displacement errors [165], respectively. Soft tissue artifacts are often a result of skin movement or deformation of a body segment due to muscle contraction during movement [164]. In comparison, anatomical landmark displacement error is a direct result of incorrect placement of a marker with respect to the segment of interest [165]. Proper identification of anatomical landmarks depends on the expertise of the researcher or clinician, the palpation procedure, and the shape of the anatomical landmark[161], [166].

2.3 Force Plates

2.3.1 Introduction

Kinematic measurements are used to describe relative movements between adjacent body parts; however, they are unable to describe the forces causing those movements [167]. Knowledge of the forces involved is necessary for understanding the cause of any movement [128]. As a person moves, they apply a proportional amount of force to the floor which is matched by the reaction of the floor in an equal and opposite direction. The forces exerted on the body by the floor are termed *ground reaction forces* (GRFs) and represent the algebraic summation of the mass-acceleration products of all body segments [168]. These GRFs are measured by carefully constructed devices called force platforms, or force plates, that may be mounted into the floor [66], [153], [155], [169]–[175] or embedded within a treadmill [39], [43], [107], [108], [122], [176]–[178]. Regardless of the configuration, the GRFs as measured by a force plate depict the resultant vertical and shear forces acting on the surface of the platform [168].

Early force plates used pneumatics and mechanical springs as force-sensing elements; however, these devices came with significant limitations [167]. Nowadays, most force plates used in human movement analysis are equipped with one of two types of transducers: strain gauge or piezoelectric [179]. Both function using the same basic principle whereby a deformation of the transducer due to an applied load (e.g., GRF) creates an output voltage proportional to the load. The difference between the two transducers lies in their respective mechanisms used to generate the output voltage. A strain gauge transducer contains four individual strain gauges arranged in a Wheatstone bridge circuit where each strain gauge consists of a resistive metallic foil mounted onto an insulated, flexible backing. Such a configuration allows for measurement of the change in resistance across the transducer. As a load is applied, the metal elements are distorted and a change in resistance is observed which, in turn, affects the resulting output voltage. Meanwhile, a piezoelectric transducer takes advantage of the piezoelectric effect common to many crystal-type materials. An applied load excites the particles within the material, causing them to become distorted and thereby displacing the electrical charges that accumulate on opposing planes. This creates an output voltage proportional to the force characteristics of the load.

2.3.2 Kinetic Data Acquisition and Processing

Independent of the transducer used, a conventional force plate is constructed with four 3-component sensors, with each sensor measuring force in the vertical (VT), ML, and AP directions [180]. In order to determine the resultant force (i.e., the GRF) in each direction, the components of each individual sensor are summed. Furthermore, the four individual sensors are typically located in each corner of the force plate which enables calculation of the 3D moments, as well as of the CoP [180].

It is worthwhile noting that the output voltages from the transducer are so small that they are essentially unsuitable for acquisition purposes [180]. Therefore, the analog voltage signals are amplified prior to digital sampling by an analog-to-digital (A/D) converter. After A/D conversion, the digitized output signals are passed through calibration matrices and multiplied by their scaling factors to produce the six GRF components for each sample, in their respective units (N and Nm for forces and moments, respectively). The 2D location of the CoP is then determined using these measured forces and moments. Oftentimes, the voltage signal is filtered and smoothed during the amplification process; however, depending on the analysis to be performed, it may be desired to further filter the kinetic output with post-processing techniques [180].

Once the final output is attained, the components may be analyzed directly or used in subsequent calculations. For example, Prieto et al. [181] outline multiple CoP-based measures used to characterize postural control and stability. In another context, the horizontal forces (i.e., AP and ML) along with the position of the CoP can be used to estimate the 2D projection of the CoM on the ground [87], [89], [169], [182]. Finally, in combination with body kinematics and accurate anthropometric data, the kinetic data measured by a force plate can be used to calculate joint reaction forces and moments [128].

2.3.3 Limitations

Common to every force plate are a set of important technical characteristics that have the capability to significantly affect the validity and reliability of kinetic measurement [183]. These include linearity, hysteresis, range, crosstalk, and natural frequency of vibration [180], [184], all of which depend on the design and setup of a particular force plate. With respect to force plates, linearity is

defined as the maximum deviation of measured kinetic data from a straight line [183]. It is a measure of how closely the input and output force (applied and measured, respectively) follow a relationship of direct proportionality. Although perfect linearity is ideal, it is not required to obtain accurate data as the calibration parameters can be determined with a higher order polynomial [183], [184]. Hysteresis is the difference in output values observed during loading and unloading of a mass on the force plate [180]. The cause of this discrepancy may be attributed to the mechanical lag that occurs as a transducer material returns to its original shape during unloading [180]. The range of a force plate specifies the upper and lower limits within which an applied force can be accurately measured [183]. If the range is too small for the forces being measured, the output will saturate, meaning it will reach a constant value at the maximum or minimum limit [183]. The range shares an inverse relationship with sensitivity, which is described as the change in the measured signal for a unit change in the applied force [183]. Therefore, to attain optimal sensitivity, it is essential to choose a range that just avoids saturation. When measuring forces in multiple directions, crosstalk defines the tendency for an applied force in one direction to affect the measurement of the other components [184]. Though interference between component channels will always exist to at least a minor extent, it is important to minimize this quantity as much as possible and prevent measurement errors [180]. Finally, every force plate has a natural frequency of vibration when in use [180], [183], [184]. This natural frequency must be kept as high as possible so as not to overlap with the frequency of movements being measured by the force plate [180], [183], [184].

Even with an optimal force plate design, there exist many external sources of error from thermal, chemical, and electrical noise [180]. As can be assumed, thermal noise deals with the temperature of the device [180]. Particularly in strain gauge transducers, temperature can affect the resistance in the metallic material, thus, skewing the recorded output. Fluctuations in atmospheric conditions such as temperature, pressure, and humidity result in chemical noise [180], whereas electrical noise is incurred by other electrical devices in the area around the force plate [180]. The latter exists at 60 Hz and its harmonics (e.g., 120 Hz, 180 Hz); however, it is progressively weaker at each successive harmonic [180].

As demonstrated with the temperature sensitivity of the strain gauge transducer, there are sources of error specific to each type of transducer. With piezoelectric sensors, a drift can develop over longer periods of time [185], due to the tendency for piezoelectric materials to leak an electrical current that will be perceived as an applied force [184]. In addition, it has been found that piezoelectric force plates tend to incorrectly estimate the moments and location of the CoP [185]–[188]. The cause of this error is due to asymmetric deformation of the piezoelectric material caused by a moment introduced by the bending of the force plate itself [186]. Though bending of the plate occurs regardless of the type of transducer, a strain gauge transducer's Wheatstone bridge circuit configuration allows these errors, among others such as temperature, to be compensated for [185]. In the case of a piezoelectric force plate, it is imperative that the platform be made from a material with high stiffness to avoid any errors in the measured moments and CoP [184].

2.4 Reliability

2.4.1 Introduction

In clinical settings, therapists regularly perform various measurements as part of a patient assessment [23]. Oftentimes, these assessments include the use of specialized equipment (e.g., goniometers) to determine specific metrics of interest [189]. If any of the equipment or metrics produce inconsistent readings, or if there are discrepancies in measurements taken either by different therapists or the same therapist at different times, serious problems can arise [190]. Consistent and accurate readings are essential in order to avoid errors in measurement that could lead to inappropriate referrals, incorrect assumption of extent of disease progression or prescribed response to interventions, and under- and over-diagnosis [190]; it is therefore absolutely critical to ensure consistent and accurate readings are obtained. Thus, in order to use any equipment and/or metrics for clinical applications, their reliability must be established beforehand [189].

Reliability refers to the consistency of a measurement [191] and thereby defines the extent to which the measurement in question can be replicated [189]. Mathematically, reliability represents a ratio of the true score variance, the variance resulting from true differences between measurements, to the total variance, a combination of true score variance and measurement error [23], [189]. The greater the ratio, the greater the amount of total variance attributable to true differences [23], and

the better the reliability. Despite best efforts of the therapist, nearly all clinical measurements will contain some degree of measurement error which includes both systematic and random error [23], [191]. As an example, a systematic error may occur as a result of a learning effect where a retest value may be higher than the initial measurement [23]. As such, systematic errors are predictable, unidirectional (e.g., retest value leads to improved score, is constant and biased [23], [191]). In contrast, random errors are due to chance and unpredictable [23]. As might be assumed, they have the tendency to both increase and decrease measurements in a random manner [191], making them the primary concern for reliability [23].

Historically, there are number of statistics that have been used to quantify reliability: Pearson correlation coefficient, paired *t*-test, Bland-Altman plots, coefficient of variation, and the repeatability coefficient [189]. However, many of these are now regarded as either inappropriate for reliability estimation or unable to provide a complete picture of reliability [23], [189], [191]. The intraclass correlation coefficient (ICC) provides a more desirable estimate of reliability [189] as it reflects both the degree of consistency and agreement between measurements [23], [189].

2.4.2 Intraclass Correlation Coefficient

Modern ICCs are widely used to assess reliability of measurements taken by different raters (inter-rater), the same rater at different points in time (intra-rater), or an instrument or variable under repeated conditions (test-retest). No matter the application, computing the ICC begins with a repeated-measures analysis of variance (ANOVA) [191] to estimate the distinct variances (e.g., across and within participants) as mean squares values [23]. Depending on the context, a selection of these variances is used in the true to total variance ratio. One item of note is whether to include both systematic and random error, or only random error in the total variance [191], the denominator. This is especially important in test-retest situations where there is a known learning effect. Here, systematic error may be regarded as a natural phenomenon [191] and, thus, may unnecessarily deflate the reliability estimate. Fortunately, multiple options for ICC calculation exist, some of which reflect inclusion of all or a portion of the error.

Typically, ICC formulas refer to the conventions defined by Shrout and Fleiss [192], and McGraw and Wong [193]. First, Shrout and Fleiss [192] defined six forms of ICC, each presented as two

numbers between parentheses. The first number designates one of three *Models* (1, 2, or 3) while the second number refers to the *Type* which uses 1 to designate a single rater/measurement, or *k* to designate the mean of *k* raters/measurements [189]. In their definition, McGraw and Wong [193] defined a third concept, the *Definition*, describing the relationship considered to be important (consistency or absolute agreement) [189]. Note that in the Shrout and Fleiss [192] convention, the *Definition* is defined implicitly within the three models.

Given the number of different formulas for calculating ICCs, it is important that researchers understand the distinct assumptions in order to select the correct form for their application. Each of the forms will provide a different result where only one is appropriate for the given situation [189]. Furthermore, it is imperative that, within the text of their publications, authors clearly indicate which ICC formula was used as it has been found that only 5% of reviewed studies contained adequate information about ICC selection [190].

2.4.3 Intraclass Correlation Coefficient Selection

When describing the various forms of ICC, it is simpler to begin with the McGraw and Wong [193] convention as they include the six forms defined by Shrout and Fleiss [192], along with four additional options. Beginning with the *Model*, the three forms are one-way random effects, two-way random effects, and two-way mixed effects. Each of these may then be evaluated using a single or average measure approach which use either single measurements or average measurements, respectively, per participant as the basis for analysis. Finally, both two-way models – random and mixed – may be used to assess either the consistency or absolute agreement of the measurements. Based on the nature of the model, to be described below, only the absolute agreement of measurements may be evaluated with the one-way random effects model.

Models 1, 2, and 3 in the Shrout and Fleiss [192] convention refer to the one-way random, absolute agreement; two-way random, absolute agreement; and two-way mixed, consistency forms of the McGraw and Wong [193] convention. All three may also be evaluated using either single or average measurements as the basis for analysis. The six forms along with their McGraw and Wong [193] equivalents are listed in Table 2.1 below.

Table 2.1: ICC Forms According to McGraw and Wong [193], and Shrout and Fleiss [192].

McGraw and Wong [193] Convention	Shrout and Fleiss [192] Convention
1-way random, single measurement, absolute agreement	ICC(1,1)
2-way random, single measurement, consistency	-
2-way random, single measurement, absolute agreement	ICC(2,1)
2-way mixed, single measurement, consistency	ICC(3,1)
2-way mixed, single measurement, absolute agreement	-
1-way random, multiple measurements, absolute agreement	ICC(1,*k*)
2-way random, multiple measurements, consistency	-
2-way random, multiple measurements, absolute agreement	ICC(2,*k*)
2-way mixed, multiple measurements, consistency	ICC(3,*k*)
2-way mixed, multiple measurements, absolute agreement	-

Noting the differences between the various forms of ICC, it becomes apparent that an appropriate selection relies on the choice of model, number of measurements, and relationship of interest. Though all are crucial components, choosing the proper model may be the most confusing. Essentially, the model is selected according to where the sources of statistical variability are believed to lie [190]. With respect to the one-way random model, separate groups of participants are evaluated by a different set of raters, both of which are assumed to be randomly selected [190], [191]. In this case, the inconsistencies created by using a different set of raters per group of participants make it impossible to distinguish where the variation in measurements lie [190]. As a result, all sources of variation are lumped together and, thus, deemed as coming from one single direction (i.e., one-way) [190]. In addition, because both raters and participants are randomly sampled, it is regarded as a random effect [190], [191], leading to the definition of the one-way random model. For the two-way models, variation from participants and raters can be partitioned, meaning each source of variation comes a different direction (i.e., two-way) [190]. Similar to the one-way model, the two-way random effect model assumes both participants and raters are randomly sampled [190], [191]. In comparison, the two-way mixed effect model assumes participants are randomly sampled while the raters are fixed (i.e., only raters of interest), leading to a mixed nature [190], [191].

As already mentioned, the one-way random effect model is appropriate when there are multiple groups of raters, each of which performs measurements on a separate group of participants [190], [191]. An example of such a situation may be a cross-institutional study. When all participants are evaluated by the same group of raters, and both are believed to be representative of their respective populations, the two-way random effect model is appropriate [191]. In this case, the raters are thought to be typical of other raters, who would produce similar results [190]. Therefore, the two-way random effects model allows a researcher to generalize their reliability results [190]. This generalizability is the major distinction between the two-way random and mixed effect models. In the mixed model, all participants are again evaluated by the same group of raters, however, those raters are specific to the study [190] and not representative of a larger population. Rather than claim that other raters are likely to produce similar results, researchers typically use this model to assess the consistency of raters within their study [190].

Each of the three ICC models – one-way random, two-way random, and two-way mixed – can be calculated in one of two ways: If a single measurement from each participant is used in the analysis, then a single measure ICC is used to assess reliability. On the other hand, if k measurements are collected from each participant and the mean of all or a portion of those measurements are used in the subsequent analysis, an average measure ICC is applied [190]. It is crucial to note that k always represents the number of measurements, not the number of raters. For example, if for each participant, a single rater takes five measurements, which are then averaged, and five measurements on another occasion, which are also averaged, and the two mean values are used in the ICC calculation, k would be 5 and not 1 (the number of raters).

Lastly, the terms *consistency* and *absolute agreement* reflect the nature of the relationship that is deemed important and, thus, being investigated. The consistency option evaluates the extent to which multiple sets of scores have a similar sequence when arranged in ascending order [190], whereas absolute agreement gauges how well the actual values match each other [190]. From a mathematical standpoint, the difference between the two lies in the inclusion or exclusion of systematic error [191]. Absolute agreement considers both systematic and random error while consistency considers only random error [191]. Therefore, the decision on which definition to use may come down to the effect of systematic error (e.g., learning effects in test-retest situations).

2.4.4 Intraclass Correlation Coefficient Interpretation

To a certain degree, a calculated ICC value is relatively simple to interpret [191]. Based on the definition, it represents the proportion of variance in a set of measurements that is attributable to the true score variance [191]. For example, an ICC of 0.70 indicates that 70% of the observed score variance is attributable to the true score variance. Given that the value can, in theory, only vary between 0 and 1.0, it is tempting to try and define standardized ranges that represent acceptable levels of reliability. Despite repeated efforts from multiple sources, there is yet to be any consensus as to what represents a good (or poor) ICC [191]. It is very unlikely that such a standard will ever exist as the issue is complicated by two main elements: (1) the ICC varies depending on the version used; and (2) the magnitude of the ICC is related to the variability in the measurements [191]. The first was already highlighted while discussing the importance of proper selection and, thus, comes as no surprise. With respect to the latter concept, there is a direct relationship between the magnitude of the ICC and the level of heterogeneity between participants [191]. The greater the across-participant variability, the higher the ICC value. Therefore, due to the population-dependence, proper ICC interpretation may require an investigation of the across-participant variability. The simplest way to do this is with the *standard error of measurement* (SEM) which can be calculated, using the ICC value, via:

$$SEM = SD\sqrt{1 - \text{ICC}} \tag{37}$$

where *SD* is the standard deviation of measurements from all participants. The SEM estimates how repeated measurements tend to be distributed around the true score and, thus, quantifies the precision of the measurements [191]. While the ICC is unitless and a relative measure of reliability, the SEM has the same units as the measurement of interest and thought to be an absolute index of reliability [191]. Furthermore, the SEM can be used to compute the smallest difference required between separate measurements in order for the difference to be considered 'real'. This is known as the *minimum detectable change* (MDC) and may be calculated via:

$$MDC = SEM \times 1.96 \times \sqrt{2} \tag{38}$$

where 1.96 is the *z*-score for a 95% confidence interval (CI). Should a different confidence interval be desired, it is necessary to use the associated *z*-score.

3 Clinical Application of Gait Stability Measures

3.1 Definition of Clinical Feasibility Criteria

Generally speaking, the proposed gait stability measures have all been developed with the main focus of quantifying human gait stability. However, a clinical motivation also exists to find a diagnostic tool that will aid in identifying individuals at risk of falling and to measure rehabilitation progress of impaired individuals. Based on the review in Chapter 2, each of the proposed measures carries its own unique set of limitations, some of which create significant obstacles towards their clinical feasibility. This highlights the importance of carefully scrutinizing each measure to evaluate whether it is appropriate for use in a clinical setting. Not only does this hold value in terms of selecting a single measure, or set of measures, for clinical use, but it may also help to refine future clinical research focusing on the most viable options.

When it comes to clinical application of the measures, the most important consideration is the expected burden on the patient. If a new tool, test, or protocol is to be adopted, it should not place excessive pressure on, or require unreasonable exertion from the participant. In regard to the gait stability measures, attention should be given to the recommended number of continuous strides required to achieve a precise estimate. For many individuals with impaired gait, the ability to walk over long distances is limited, which implies that a selected measure should necessitate a minimum number of strides and/or walking trials. This is also important when considering the time requirement, as typical clinical assessments are allotted a short amount of time for completion. Multiple publications have identified time as one of the barriers to implementation of standardized measures in health care and functional assessment [194]–[196]. Concerning gait stability measures, the more walking that is necessary, the more time it will take, and the less likely it is for the measure to be adopted in practice. Furthermore, when time is of concern, the setup protocol needs to be acknowledged. This is especially important in the collection of patient-specific kinematic and kinetic data as it is not unusual to employ equipment that requires considerable setup. All in all, in evaluating the time-feasibility of a measure, both the setup and overall trial time need to be considered.

Another important criterion in evaluating the use of a given gait stability measure is its capacity to be applied to multiple walking conditions, including over-ground, treadmill (fixed and self-paced), and perturbed gait. The belief here is that, if a certain measure can be used to quantify stability in a variety of environments, then it would be preferred over another that may only be suitable to analysis of one particular form of gait. Such versatility in a single measure allows for a modular design of assessment that may create benefits related to efficiency [197], and assist in overcoming barriers related to implementation [194]–[196]. With respect to efficiency, the ability for a single measure to quantify stability in a variety of conditions allows the transition between different protocols to be completed with reduced time and cost [197]. In addition, modularity of a single measure improves the likelihood of adoption in a clinical environment as it reduces the burden of training for its eventual use and interpretation [194]–[197].

Finally, it is worthy to note that, in some cases, thought needs to be given to the theoretical basis of a proposed measure. Because these measures are to be applied in a real-world clinical setting, it is imperative that there be a clear, mechanistic link between a particular measure and actual human gait, and the foundation by which gait stability is quantified. The need for a plausible connection between the theoretical basis of a measure and the biomechanical features of human stability is highlighted by several authors [6], [7], [15], [44], [198]–[202].

Summarizing the aforementioned criteria, the proposed gait stability measures will be evaluated based on: (1) the minimum length of walking trial required, in terms of consecutive strides or overall distance; (2) the time required for assessment, including setup and trial time; (3) the applicability to multiple walking conditions; and (4) the theoretical basis and vital assumptions. It should be noted that the following discussion is based on the present body of work surrounding each measure. Since there is limited information for some measures, and it is not yet known whether those measures relate to actual human gait stability and fall risk, no prioritization was given to measures with more progress towards validation. For clarity, this simply implies that one measure was not ranked above another when it lacked evidence-based results. In addition, cost was not a factor in the evaluation. All of the proposed measures use objective, quantitative data and require similar laboratory equipment.

3.2 Evaluation of Proposed Gait Stability Measures

Having completed a thorough literature review of each of the proposed stability measures in Chapter 2, it is possible to evaluate the measures in terms of the outlined criteria, with the goal of identifying those that may be viable options. Thus, the following paragraphs include a short characterization of the requirements of each of the measures, in the order they are presented in Chapter 2.

Beginning with the largest Lyapunov exponent and maximum Floquet multiplier, both have the ability to be calculated from any source of kinematic data. This presents a huge advantage because it opens the door to relatively simple methods of data collection [15], [203] (e.g., [18], [77], [204], [205]). For example, tracking trunk motion, as is suggested, requires only a few markers or an inertial sensor to be placed on the body, thereby requiring minimal setup time. The problem, however, is that there is yet to be a conclusive answer to which types of kinematic data are most sensitive to differences in stability. As a result, it is possible that a more extensive model is necessary that would necessitate additional setup time. Regardless of the discussion surrounding the correct parameters to use for creation of the state space behavior, the ability to use any form of kinematic data has led both the largest Lyapunov exponent and maximum Floquet multiplier to be quite popular in the attempt to quantify gait stability. Although each of them is built from a sound theoretical basis, there is some debate concerning the validity of their assumptions with respect to gait [15]: calculation of Lyapunov exponents assumes the system is aperiodic [22], whereas Floquet multipliers assume periodicity [22]. Since gait is neither aperiodic nor periodic [28], these assumptions provide grounds for argument. Furthermore, both measures rely on the data being stationary [15], which eliminates the possibility to study gait in the presence of any type of mechanical perturbations (e.g., slips, trips) – reflecting situations in which stability is most compromised. It is also possible that non-stationarities that are due to internal noise and that are present in human gait may lead to an overestimate of either the largest Lyapunov exponent or maximum Floquet multiplier [73]. The most compelling limitation in using either of these measures, especially in a clinical setting, is the need to obtain walking trials of 150 continuous strides or more for precise estimates for a given individual [73]. With an average stride length of roughly 1.5 m, 150 strides translate to a distance of nearly 250 m, which may be difficult, or altogether impossible, to achieve for certain clinical populations. Though there is evidence that

supports the possibility of using multiple trials of fewer strides, it is only applicable for group-level analyses [77]. This would entail making conclusions concerning entire populations and, in turn, using those conclusions to assess the level of stability for a given patient. This is certainly not a viable option since differences exist in the ability between individuals with similar impairments. In conclusion, due to the uncertainty surrounding the basic assumptions (aperiodic versus periodic), the limitations imposed by the need for stationary data, and the requirement that walking trials need to include 150 strides or more, neither the largest Lyapunov exponent or maximum Floquet multiplier appear to be viable candidates for a clinically applicable measure of gait stability.

Moving on, the extrapolated centre of mass (XCoM) appears to be a more practical option. Most importantly, the margin of stability presents a simple and intuitive way to gauge stability: anytime the XCoM moves outside the base of support (BoS), a fall is expected, unless an adjustment is made [39]. Since, in gait, forward motion naturally requires the XCoM to consistently move past the BoS, there is some skepticism on the applicability of the XCoM in the anteroposterior (AP) direction [15]. However, this is by no means a violation of the model or any of its assumptions. Next, the majority of the parameters needed for calculation can be attained through simple means that require a nominal setup time. The greatest hindrance is dependent on the chosen method for centre of mass (CoM) estimation: If, due to a potential lack of a force plate, the kinematic method [83], [85], [175], [206] is necessary, the setup time would increase drastically and likely push it to the threshold of feasibility. However, if a force plate is available, two options exist to determine the horizontal projection of the CoM – the double integration [87], [88], [182] and low-pass filter techniques [90], [207] – that do not require any additional setup time. In addition, the XCoM can be calculated on a sample-by-sample basis; therefore, there is no restriction on the minimum number of strides that need to be collected. That being said, analysis would likely still include multiple strides. Another advantage is the capability to assess gait under a vast array of conditions [15], including over-ground, treadmill, and perturbed walking. Therefore, the XCoM clearly satisfies the aforementioned criteria and appears to be a suitable option for dynamic gait assessment.

Derived from many of the same principles as the XCoM, the stabilizing and destabilizing forces present many of the same advantages (i.e., no minimum stride restriction, applicable to both normal and perturbed gait). The key differences between the two are (1) the extent to which each has been applied in practice; and (2) a few of the parameters from which they are calculated. Considering that the stabilizing and destabilizing forces are a newer concept in terms of quantifying stability, they have been used quite a bit less and, thus, need further development. Specifically, the concept needs to be expanded to include some form of stability criterion [15]. A likely candidate is a theoretical maximum for the stabilizing force [15]. Such a criterion can then be used to compare against the instantaneous measurements, similar to the margin of stability for the XCoM. This presents a definite gap that will certainly need to be addressed in future work. With respect to the parameters needed for calculation, the most meaningful addition in comparison to the XCoM is the height of the CoM, which may require a more elaborate experimental setup. Altogether, the stabilizing and destabilizing forces present another intriguing possibility for gait stability evaluation.

In terms of setup time, the gait sensitivity norm (GSN) is largely reliant on the choice of gait indicators. While information on the application of the GSN to actual human gait is extremely limited, temporo-spatial parameters seem to be the most appropriate variables to use [41], [42]. To date, no recommendations exist on which parameters are most suitable; however, since they must reflect characteristics related to the failure mode [41], [110], it is likely that the choices will depend on the type perturbation enacted. Nearly all temporo-spatial quantities can be estimated using a force plate or only a few kinematic markers on the lower limbs. Consequently, the time necessary for setup is not of large concern. In addition, the GSN does not place a significant restriction on the minimum number of strides. Instead, all that is necessary is sufficient time for the participant to recover their nominal gait pattern after a perturbation. Based on the work of Forner Cordero et al. [58] this typically takes three steps after the perturbed step. Even in a more conservative approach where a few more steps are included post-perturbation, the required number of strides still represents a reasonable expectation for clinical populations. Finally, the GSN seems to employ the mechanical definition of stability by perturbing the system and observing how the system responds in comparison to its nominal behavior [41]. Hence, the GSN is constrained to measuring

stability in perturbed environments relative to non-perturbed gait. Nevertheless, it is surely another measure to keep in consideration.

Variability measures quantify the degree of fluctuation by computing the standard deviation of gait variables [119], typically temporo-spatial parameters, over successive walking strides. Therefore, setup time is determined by the requirements for measuring temporo-spatial parameters which, as previously mentioned, do not imply a great burden. The primary concern in using variability measures to quantify gait stability is the minimum of 200 strides that are necessary to achieve precise estimates [43]. Since this translates to roughly 300 m of continuous walking, it definitely pushes many clinical populations past their limits. As such, variability measures may not be clinically feasible. Furthermore, there is also the debate of whether or not variability is indicative of instability. On the one hand, it has been demonstrated to predict instability [15]; on the other hand, it is believed that variability may be a means or consequence of intact control, or simply a result of exploiting multiple degrees of freedom [15].

Similar to variability measures, long-range correlations apply statistical means to temporo-spatial parameters of consecutive strides, in an attempt to quantify stability. Although temporo-spatial parameters do not entail unreasonable amounts of setup for their measurement, long-range correlations do possess a number of flaws when applied to gait. Most prominent is the stipulation that at least 600 strides be collected to obtain accurate results [33]. Besides that, there is little evidence to prove that long-range correlations have any relation to walking stability whatsoever [15]. It seems valid to assume that every walking stride has an effect on the next few that succeed it; however, this is not indicated by the long-range correlations. Given these deterrents, i.e., the need for long time series and a poor theoretical foundation, long-range correlations appear insufficient for stability measurement, clinically or not.

At first glance, the foot placement estimator (FPE) appears as a great candidate for clinical use: it has a strong theoretical background, does not have an excessive stride requirement, and is applicable to walking in a wide range of conditions. However, the one provision that hinders its use is the need for a full-body marker set to estimate full-body angular momentum and moment of inertia [6]. This requirement involves a great deal of setup time as each marker must be placed

with utmost accuracy. Should a simpler method to estimate momentum or the moment of inertia come to light, the FPE would be an excellent choice. Until then, it is likely too time-consuming to be applied in practice.

In regard to the largest recoverable perturbation, the need for a continuous spectrum of perturbations poses a major problem. Though the technology exists to accomplish such a task, the protocol would require too much time to complete. In addition, the largest recoverable perturbation can only be identified by having an individual fall, thus, risking injury. For these reasons, the largest recoverable perturbation is not a viable means to assess gait stability in practice.

3.3 Selection of Proposed Gait Stability Measures

A summary of the above discussion regarding the proposed gait stability measures, along with a verdict on their clinical feasibility, is provided in Table 3.1. Note that the XCoM, stabilizing and destabilizing forces, and GSN were the only three identified as clinically feasible. The reason for excluding the remaining measures is primarily due to excessive requirements from the participant (i.e., long walking trials), and impractical protocol requirements. Another important exclusion criterion was the inability to be applied to multiple gait conditions, particularly perturbations, as this is typically where stability is most compromised.

Table 3.1: Summary of the clinical feasibility of each gait stability measure.

Measure	Clinically feasible?	Reason
Largest Lyapunov exponent	NO	• requires >150 continuous strides • requires stationary data • assumes gait is aperiodic
Maximum Floquet multiplier	NO	• requires >150 continuous strides • requires stationary data • assumes gait is periodic
Extrapolated Center of Mass (XCoM)	YES	• no excessive stride requirement • reasonable setup time • applicable to all gait conditions
Stabilizing (F_S) & Destabilizing (F_D) Forces	YES	• no excessive stride requirement • reasonable setup time • applicable to all gait conditions
Gait Sensitivity Norm (GSN)	YES	• no excessive stride requirement • reasonable setup time • applies mechanical definition of stability
Variability measures	NO	• requires >200 continuous strides • requires stationary data
Long-range correlations	NO	• requires >600 continuous strides • requires stationary data • poor correlation with stability
Foot Placement Estimator (FPE)	NO	• requires full-body marker set
Largest recoverable perturbation	NO	• excessive protocol requirements • high risk of injury

4 Utility of the Extrapolated Centre of Mass for Gait Stability Assessment during Unperturbed Walking

4.1 Introduction

Based on the discussion of clinical feasibility in Chapter 3, three of the nine proposed gait stability measures were identified as having the practical characteristics to be applied in a clinical setting. The extrapolated centre of mass (XCoM), stabilizing and destabilizing forces, and gait sensitivity norm (GSN) all incur reasonable protocol requirements with respect to time, setup, and the burden on the patient, while demonstrating a sound theoretical link to gait. Given the lack of consensus on a valid stability criterion with the stabilizing and destabilizing forces [15], and that the use of the GSN in actual human gait is limited to pilot data [32], [42], it was decided to focus solely on the XCoM for the purpose of the present work. Based on these considerations, the utility of XCoM to quantify human gait stability via the margin of stability (MoS) in a clinical setting was evaluated in experiments involving human participants. This was accomplished by: (1) demonstrating the practical feasibility of obtaining the XCoM; (2) assessing its robustness for a non-disabled sample; (3) quantifying the between-session reliability; and (4) exploring the clinical application of the XCoM using three clinical case studies.

Participants were asked to walk at a self-selected speed on a level treadmill-driven surface while a motion capture system and force plates were used to collect kinematic and kinetic data, respectively. The XCoM was then calculated from the recorded walking data, and statistical methods were used to evaluate the variability and reliability of the obtained measures for both the normative sample and the clinical cases. In addition, common temporo-spatial gait parameters were determined to evaluate walking performance of the sample participants and provide further insight into the observed gait stability results.

4.2 Methods

4.2.1 Participants

A total of 15 non-disabled volunteers (Table 4.1) were invited to participate in this study. Each participant provided written informed consent (Appendix A) and had complete, pain-free active and passive range of motion of the lower extremities. Exclusion criteria included chronic pain conditions, pain on the day of testing, and medical contraindication to exercise. In addition to this normative sample, three individuals with (1) hemophilic arthropathy (HA); (2) unilateral transtibial amputation (TTA); and (3) mild traumatic brain injury (mTBI) were asked to participate in this study (Table 4.2). The individual with HA had limited range of motion (ROM) in both knees. The right knee was in permanent extension, while the left knee had roughly 20 degrees of flexion from full extension. The affected limb in the individual with TTA was the left leg, and the individual with mTBI also suffered from an amputation at the left elbow. This study and its experimental procedures were approved by the Health Research Ethics Board of the University of Alberta (HREB Pro00066076).

Table 4.1: Participant characteristics.

Gender	Age (years)	Weight (kg)	Height (cm)
F	33	75	164
F	23	77	173
M	23	70	180
F	19	65	166
M	31	93	186
M	23	90	180
F	28	55	164
M	25	73	170
M	37	69	170
M	31	59	171
M	25	112	196
M	29	87	184
M	38	97	176
F	40	54	152
M	41	92	181
Mean (Standard Deviation)	29.7 (6.9)	77.9 (16.9)	174 (11)

Table 4.2: Case study participant characteristics. Included are three individuals with: (1) hemophilic arthropathy (HA); (2) transtibial amputation (TTA); and (3) mild traumatic brain injury (mTBI).

	Gender	Age (years)	Weight (kg)	Height (cm)
HA	M	26	83	183
TTA	M	50	86	186
mTBI	M	31	109	185

4.2.2 Experimental Protocol

The present study was performed in conjunction with the development of a Performance Assessment Tool (PAT) for the Computer-Assisted Rehabilitation Environment (CAREN; Motek Medical, Amsterdam, Netherlands) at the Glenrose Rehabilitation Hospital, Edmonton, Alberta, Canada. The particular CAREN version installed at the Glenrose Rehabilitation Hospital is the CAREN-Extended virtual environment (Figure 4.1). This system consists of a 180-degree curved projection screen, a three-dimensional (3D) surround-sound audio system, a 12-camera motion capture system (Vicon Inc., Oxford, United Kingdom), and a 6-degree of freedom, actuated perturbation platform (Sarnicola Simulation Systems Inc., Conklin, NY, USA) with a dual-belt instrumented treadmill (Bertec Corp., Columbus, Ohio, USA). Functional integration of the hardware components and virtual scene is controlled using the D-Flow software (Motek Medical) [208]. D-Flow also provides an interface for synchronized data collection from multiple sources. In addition to acquiring motion and force plate data (from the motion capture system and the two treadmill-embedded force plates, respectively), the software may also be used to track treadmill speed and distance, as well as 3D perturbation platform displacements and rotations.

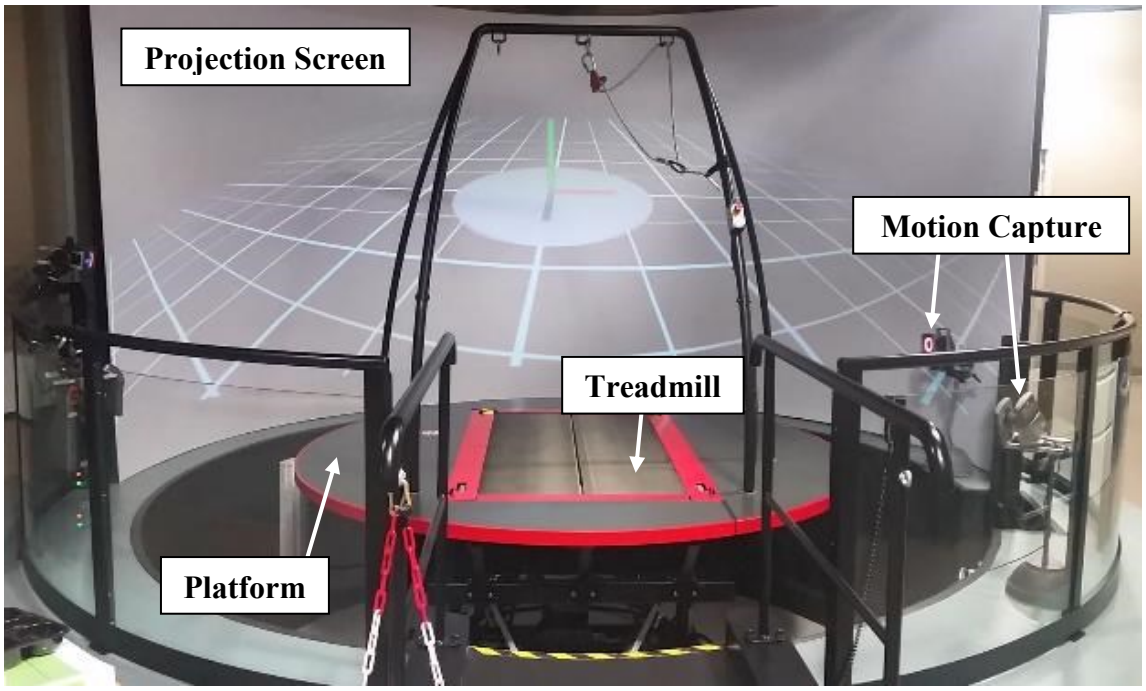

Figure 4.1: CAREN-Extended System at the Glenrose Rehabilitation Hospital. The CAREN includes a 180-degree curved projection screen, a three-dimensional surround sound audio system, a 12-camera motion capture system, and a 6-degree of freedom perturbation platform with dual-belt instrumented treadmill.

As part of the PAT protocol, every participant performed four standing-based tasks and three walking-based tasks. The standing-based tasks included: (1) single-leg balance; (2) step-to-target; (3) weight-shift; and (4) balance in response to horizontal perturbations. Further details on these tasks are provided in Appendix B. The standing-based tasks were preceded by a calibration routine (Figure 4.2) that included additional tasks such as sit-to-stand, heel-to-toe shift (eyes open and closed), and a staggered stance (left foot in front of right, and vice versa). The purpose of this calibration routine was to obtain accurate 3D joint angles that are not affected by the orientation of the marker cluster plates attached to the various body segments (*see Section 4.2.3: Experimental Data Collection*). Note that a stool was placed on the platform for the sit-to-stand task and removed upon completion.

Figure 4.2: Virtual environment for the calibration routine. Tasks included sit-to-stand, heel-to-toe shift (eyes open and closed), and a staggered stance (left foot in front of right, and vice versa). The purpose of this calibration routine was to obtain accurate three-dimensional joint angles that are not affected by marker cluster plate placement.

4.2.2.1 Walking-Based Tasks

A straight virtual pathway (Figure 4.3) was used to complete all walking procedures within the protocol. Minor variations (e.g., slopes) were programmed depending on the task to be performed;

however, the general configuration of the pathway and scenery remained unchanged. Prior to completing the walking-based tasks, a walking practice routine (Figure 4.3a) was completed to allow participants to familiarize themselves with walking in the virtual environment using the self-paced walking mode of the CAREN [5], [81], [178], [232], [233]. This mode measures the displacement of a marker attached to the participant's back from equilibrium, with the goal of adjusting the speed of the treadmill accordingly and enabling the participant to walk at their preferred, self-selected speed. During the walking practice routine, on-screen instructions prompted participants to speed up, slow down, return to normal pace, and walk in tandem (i.e., one foot in front of the other). The walking-based tasks that followed the walking practice included walking in the presence of: (1) sloped terrain [67], [78], [104], [178], [234]–[238]; (2) a simulated rocky environment [53], [100], [178], [239]; and (3) lateral perturbations of the support surface [5], [233], [240]–[243].

During the sloped terrain walking task (Figure 4.3b), participants walked at four different slopes: uphill [67], [78], [104], [178], [234], [235], [238], downhill [67], [78], [178], [234]–[236], [238], and both right and left cross-slopes [178], [234], [235] (i.e., lateral inclines). Between slopes, a 10 m interval of flat walking (0 degree incline) was used. Each slope consisted of a 5 m transition from flat, 20 m at the specified slope, and then a 5 m transition back to flat. One walk down the pathway consisted of a single iteration of each type of slope in the following order: uphill, downhill, left slope and right slope. The pathway was repeated three times, each with a different level of difficulty (easy, medium, hard) that depended on the degree of inclination. For the uphill and downhill slopes, the easy, medium, and hard levels of difficulty correspond to slopes of 4 degrees, 7 degrees, and 10 degrees [67], [78], [178], [235], [236], [238], respectively. Meanwhile, for the lateral inclines, these were 3 degrees (easy), 5 degrees (medium), and 7 degrees (hard) [178], [235].

The second walking-based task incorporated sections of a simulated rocky surface (Figure 4.3c), a function of the CAREN that creates random, scalable displacements ('vibrations') of the support surface. For a scaling factor of 1, the platform would be moved vertically to a maximum displacement of 1 cm and rotated in any direction to a maximum angle of 1 degree. Four iterations of the simulated rocky surface were included in one walk down the pathway. Each of these was 10

m in length and was preceded by 10 m segments of unperturbed walking (i.e., no vibrations). A schematic outlining the sequence of events for the walking-based task involving the simulated rocky surface is shown in Figure 4.4. Four repetitions of the pathway were completed, with vibrations scaled at 0.5, 1.0, 2.0, and 3.0.

The final task required that participants walk down the pathway and maintain balance in response to lateral translations (i.e., right and left 'perturbations') of the support surface (Figure 4.3d). Three different perturbation magnitudes were used, defined by the time for the platform to reach maximum displacement (see below). The magnitudes and their corresponding times to reach maximum displacement were: low (2.4 s), medium (1.6 s), and high (0.8 s). Perturbations were delivered at mid-stance based on foot marker measurements, with the first being delivered to the right at right mid-stance. Following the initial perturbation, an additional four perturbations were delivered in both the right and left directions (8 total), synchronized with either right or left mid-stance. For all perturbations, the platform was displaced 25 cm. The platform moved back to its original position at the same speed 7.5 s after reaching maximum displacement, and the time between consecutive perturbations was 6 to 8 s. The pathway was repeated for three levels of perturbation magnitude, differentiated by the time to reach maximum displacement.

Note that each level of the walking-based tasks began with a ramp up to a fixed treadmill speed. After 10 m at the fixed speed, self-paced control was activated, and the participant was given 20 m to achieve their preferred speed prior to the first incline, vibration, or perturbation. Furthermore, the first level of each walking-based task included an 8 to 10 s period of quiet standing (i.e., treadmill at rest). The purpose of this was to serve as a standing calibration to (1) ensure all motion capture markers were visible; and (2) locate them to define the initial conditions for the algorithm that would identify and label the markers and rigid cluster plates in real-time (*see Section 4.2.3: Experimental Data Collection*).

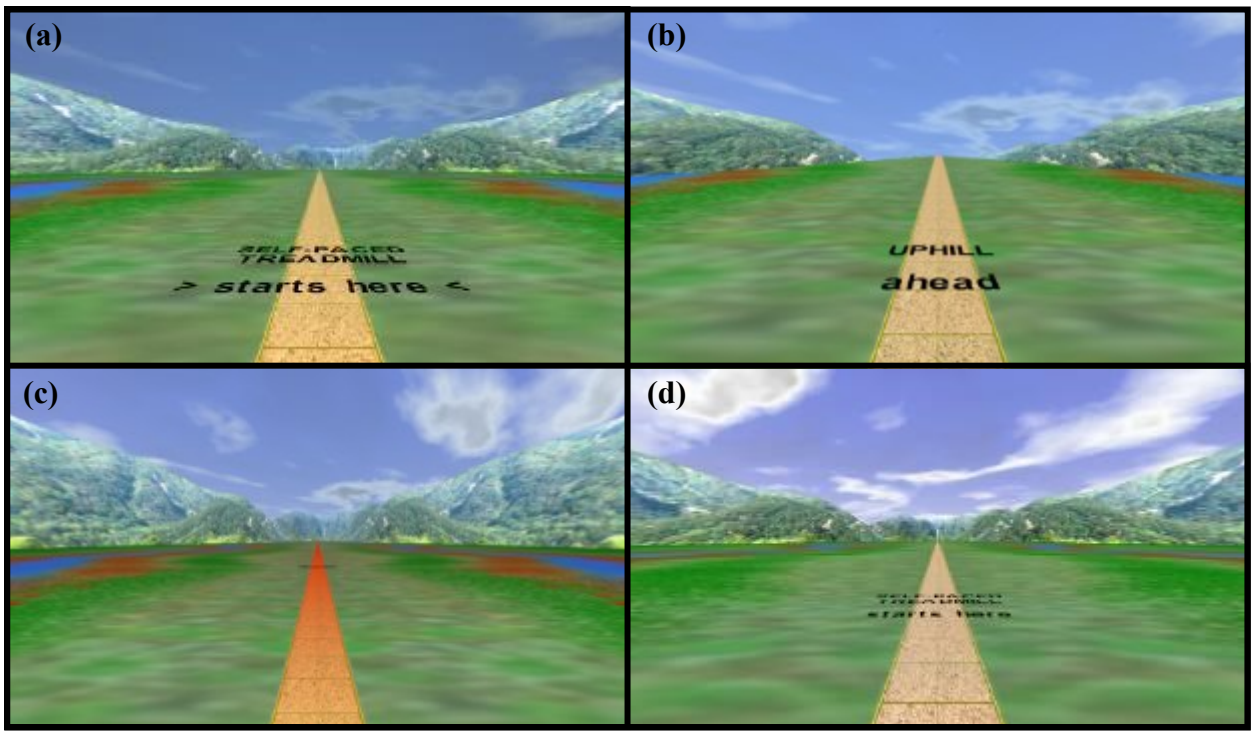

Figure 4.3: Walking-based tasks as part of the experimental protocol. (a) walking practice; (b) walking on sloped terrain; (c) walking in a simulated rocky environment; and (4) walking in the presence of lateral perturbations.

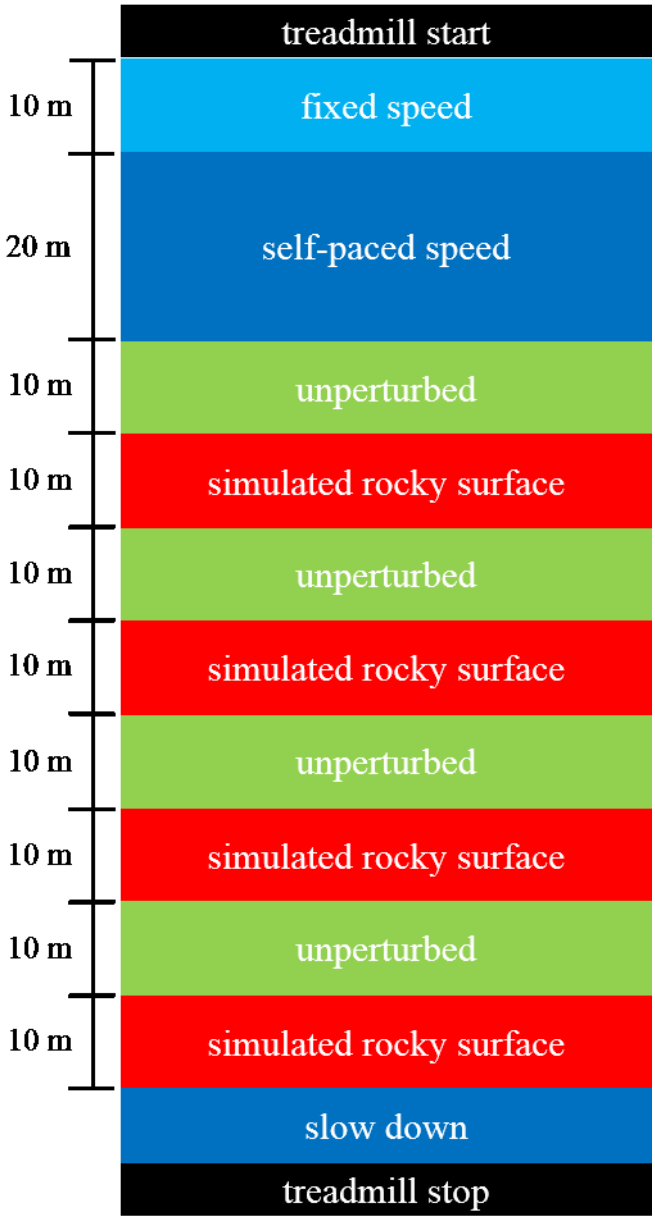

Figure 4.4: A schematic outlining the sequence of events within a single level (i.e., one walk down the pathway) walking-based task involving the simulated rocky surface. Each colored box represents a different segment, and the schematic flows from top (start of level) to bottom (end of level). At the start, the treadmill ramps up to a fixed treadmill speed, which is maintained for 10 m before self-paced treadmill control is activated. The participant is then given 20 m to achieve their self-selected walking speed. Once complete, four identical 20 m intervals take place, each with one 10 m segment of unperturbed walking followed by one 10 m segment of the simulated rocky surface. After the final simulated rocky surface segment, the treadmill slows to a stop. Note that this sequence of events is identical for all four levels of the walking-based task involving the simulated rocky surface.

4.2.2.2 Safety Measures

Before beginning the PAT protocol, participants were equipped with a full-body safety harness that was attached to the fixed frame on top of the CAREN platform. The safety harness attached to a participant can be seen in Figure 4.5 below. Note that the participant in the Figure 4.5, along with all subsequent figures, provided written consent to be photographed (Appendix A). The experimenter adjusted the length of the harness according to the requirements of each task being performed. For walking-based tasks, the length of the harness was limited to ensure participants could not place their forefoot beyond the frontmost portion of the treadmill belt [244], which would be likely to cause a fall. Both the CAREN operator and experimenters also closely monitored the participant for safety and any loss of balance events. In the case where a critical loss of balance or a fall could occur, the CAREN's emergency stop was in place to immediately cease all functions (e.g., treadmill and platform motion). At the end of each task, or level of a particular task, participants were asked whether they wanted to continue to the next task or level, respectively. Participants were allowed to take rests as long as needed between levels and tasks, and were offered water multiple times throughout the experimental protocol.

Figure 4.5: A participant on the CAREN prior to the simulated rocky surface walking task. Participants wore a full-body safety harness that was secured to the fixed, overhead frame. The length of the harness was adjusted separately according to the requirements of each task within the protocol. In case of a critical loss of balance or a fall, the CAREN's emergency stop was in place to immediately cease all functions.

4.2.3 Experimental Data Collection

4.2.3.1 Biomechanical Measurements

In order to collect the required kinematic data, a set of motion capture markers was attached to the participants to track the movement of the lower-body using the CAREN's motion capture system. The underlying kinematic model, defining the number and locations of the utilized markers, was evaluated in a previous study [245]. The model consisted of rigid plates of four retroreflective markers, with each being attached to the feet, shanks, and thighs. Another four-marker plate was placed on the back to track movement of the pelvis. Plates on the feet, shanks, and thighs were fixated to the body by elastic Velcro straps, while the back plate was secured by an elastic belt around the hips. The rigid plates belonging to both feet and the back were uniquely designed such that their orientation on the body was intuitive and clear to the experimenter. The plates on the feet included a pointed edge that was directed towards the front of the foot, whereas the back plate had two prongs facing downwards, resting along the participant's back. Meanwhile, the plates for the shanks and thighs incorporated a long and short axis, and were attached with the long axis running along the length of the leg. To differentiate between the rigid plates for the shank and thigh, the long axis was shorter for those designated to the shank. In addition, single markers were placed on the hands, shoulders, and sternum. Participants also wore an elastic headband with two markers around their forehead. The locations of all plates and markers on the body are shown in Figure 4.6. A separate four-marker plate was placed at the base of the fixed frame (Figure 4.7), on the left upright closest to the screen, in order to track movement of the platform. Note that this cluster was placed on the frame, rather than directly on the surface of the platform, to avoid the possibility of a participant stepping on it during the step-to-target task. Figure 4.8 provides the orientation of all plates, including the position of the platform cluster relative to the participant. 3D forces and moments as well as the CoP were collected for each force plate separately. Additional analog channels recorded 3D linear and angular displacement of the CAREN platform. All data were recorded at a sampling frequency of 100 Hz [43], [170], [178], [246]–[250].

4.2.3.2 Repeatability Testing

All 15 non-disabled participants returned on a separate day for repeatability testing after the initial testing session (4.3 ± 2 months), using the identical set up and experimental protocol. The same two experimenters executed the experimental protocol for all initial and repeat sessions.

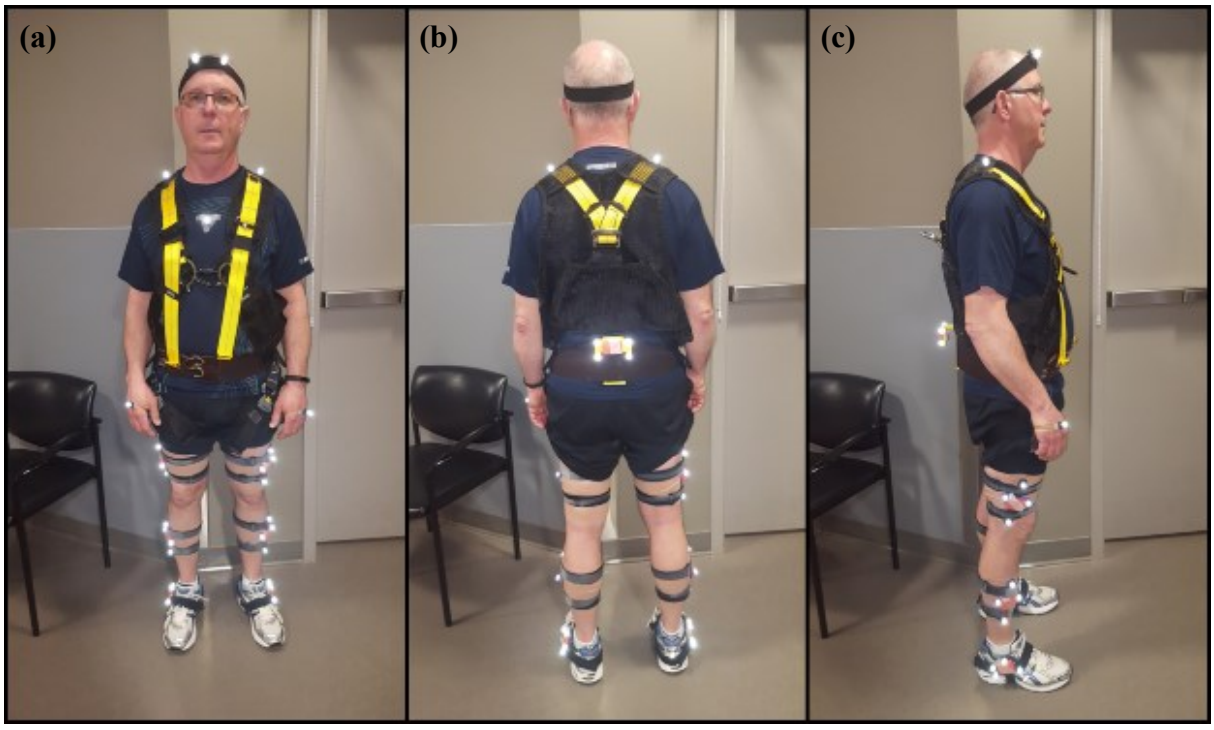

Figure 4.6: Location of cluster plates and single markers attached to the participant. (a) front; (b) back; and (c) side views. The kinematic model consisted of rigid plates of four retroreflective markers, with each being attached to the feet, shanks, thighs, and back (to track movement of the pelvis). Plates attached to the feet, shanks, and thighs were fixated to the body by Velcro straps, whereas the back plate was fastened by an elastic belt. Single markers were placed on the hands, shoulders, and sternum.

Figure 4.7: Location of the rigid plate and markers for tracking platform motion. This cluster was placed on the frame, rather than directly on the surface of the platform, to avoid the possibility of a participant stepping on it during the step-to-target task.

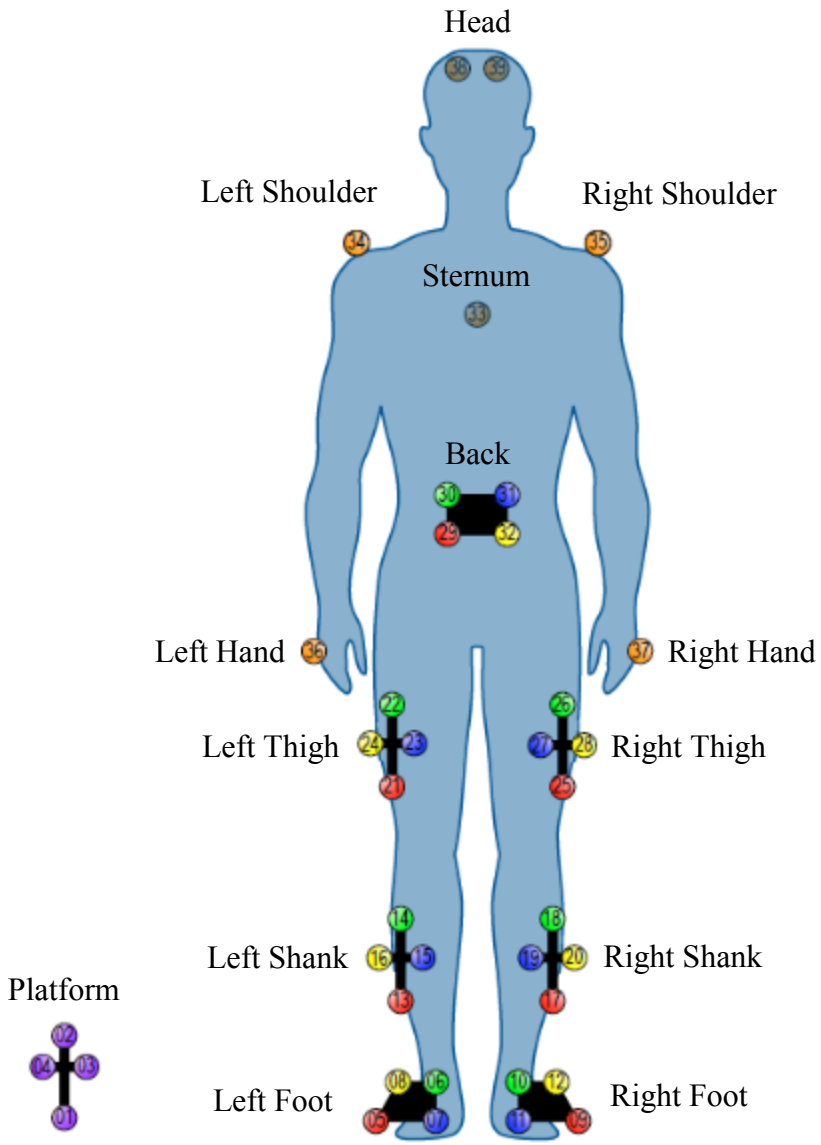

Figure 4.8: Position and orientation of all rigid plates and markers. The rigid plate tracking movement of the platform is to the left of the participant, with its long axis oriented vertically. For the plates on the feet, the red markers (5 and 9) point forward. All four plates on the shanks and thighs have their long axes oriented along the length of the leg. The back plate is oriented with the short edges running with the height of the participant. Hand markers were placed on the outside of the hand, while the head markers were positioned on the forehead.

4.2.4 Experimental Data Processing

The experimental data recorded from each participant were analyzed using Matlab R2016b (The MathWorks, Natick, MA, USA). Only data extracted from the first two levels of the simulated rocky surface task were used in the following analysis. No data from any of the standing-based tasks, nor any of the other walking-based tasks (inclines and lateral perturbations) were included

in this study. A standing segment, used to estimate the mass (m) and equivalent pendulum length (l) of each participant, was extracted from the period of quiet of standing that preceded the first level of the simulated rocky surface task. Three unperturbed walking segments were extracted from each of the first two levels of the simulated rocky surface task (Figure 4.4). Data from these walking segments were used to determine the centre of mass position (CoM) and velocity (v_{CoM}) to be used in the subsequent calculation of XCoM and margin of stability (MoS) for gait stability analysis. Kinematic data recorded only from the top two markers on the back plate (Figure 4.8, markers 30 and 31) and the top, front marker on either foot plate (Figure 4.8, markers 8 and 12) were used. Kinetic data measured by both force plates, as well as the D-Flow control output for platform movement were also used.

4.2.4.1 Extraction of Standing and Walking Segments

Standing segments were taken from the 8-10 s period of quiet standing at the beginning of the first level of the simulated rocky surface walking-based task. For each participant, a 3 s segment ending 1 s prior to treadmill start (end of standing period) was extracted. For example, if the period of quiet standing lasted 10 s, the interval from 6-9 s was used for further analysis.

Segments of unperturbed treadmill walking were extracted from the first two levels within the simulated rocky surface walking-based task. As mentioned in the description of the protocol (Figure 4.4), every iteration of the simulated rocky surface was preceded by a 10 m segment of unperturbed treadmill walking at self-selected speed ('self-paced'). Each level contained four repetitions of the simulated rocky surface and, thus, four segments of unperturbed walking. All but the first iteration in each of the first two levels was extracted for further analysis. The reason for excluding the first segment was that it was not bounded by successive intervals of the simulated rocky surface, as was the case for the second, third, and fourth segments of unperturbed walking. Therefore, the first segment was perceived to potentially be exposed to other influences than the second to fourth segments.

The D-Flow control output for platform rotations about the ML and AP axes were used to identify the unperturbed segments in the experimental data and, subsequently, extract those segments from the time series of either level. The start of an unperturbed segment was identified as the first frame

following a simulated rocky surface interval where platform rotation reached 0 degrees for 2 seconds, whereas the end of an unperturbed segment was identified as the last frame of 0 degree platform rotation prior to the next simulated rocky surface interval (with platform rotation ≠ 0 degrees). Note that the entire unperturbed segment was included at this point of processing to maximize the length of the time series prior to CoM estimation, which further cut down the time series (*see Section 4.2.4.5: Biomechanical Parameter Calculation*). Exclusion of data that may be affected by the previous perturbation was addressed prior to statistical analyses (*see Section 4.2.5.2: Extrapolated Centre of Mass and Margin of Stability*). In total, six 10 m segments of unperturbed walking were extracted for each participant.

4.2.4.2 Marker Sorting and Identification

In line with the kinematic model described above, a total of 39 markers were used to track movement of the participant and perturbation platform during the PAT experiments. However, for the purpose of the present study, only the markers on the feet and back were required. A custom algorithm (Appendix C) was used to identify and sort the markers, and to extract those belonging to the feet and back. Using the *cluster* function in Matlab, the algorithm first grouped the markers into one of two groups based on whether or not they belonged to a 4-marker cluster. From the group of 4-marker clusters, each cluster was then identified by the mean position of its respective markers. For example, to find the foot clusters, the algorithm identified the three clusters with the lowest values in the vertical (VT) direction (i.e., smallest height). Assuming upright standing and walking, two of these belonged to the feet, whereas the third belonged to the platform cluster. The platform cluster was located off the treadmill, approximately 2 m away from the origin (centre of treadmill), on the left body side of the participant. A comparison of the ML positions of the three clusters was, thus, used to differentiate the clusters on the feet from that on the platform. Similarly, right and left feet were identified by comparing the ML positions of the remaining two clusters. The back cluster was identified as the cluster with the largest value in the VT direction (i.e., greatest height). Finally, recall from the description of the kinematic model that the rigid plates for the back and feet were uniquely designed to be attached to the body in a specific orientation that was intuitive and clear to the experimenter. Furthermore, the individual markers on each plate remained fixed. These reasons, in combination with the observation that, during upright walking, the back cluster moved primarily through translation, allowed the individual markers on the rigid

plate of the back to be identified by their relative positions to each other. As for the foot clusters, considerable rotation of the foot does occur during walking, making it difficult to uniquely identify each marker. However, given the non-symmetric configuration of markers on the rigid plates for the feet, individual markers could be identified by their relative positions within the cluster.

4.2.4.3 Kinematic Data Reconstruction

During experimental data recording, there are often instances where a single marker is visible to less than two cameras. This can occur for variable lengths of time, thus, creating gaps in the position data for multiple consecutive frames. In order to mediate this issue, the values of the missing frames (i.e., location of the marker for those frames) can be estimated using interpolation. One method is to fit a cubic spline, constructed of a piecewise third-order polynomial, using the set of existing data points (i.e., frames) on both sides of the gap [251]. However, based on Nyquist's sampling theorem, a limit exists for the maximum number of consecutively missing frames that can be reconstructed without loss of accuracy in the information [252]. This theorem states that a signal must be sampled at a frequency that is at least twice as high as the maximum meaningful frequency component within that signal [128], [251]. Based on a frequency spectrum analysis (see Appendix D.1), it was found that the largest frequency component present in the motion capture signal was lower than 5 Hz. In theory, this means that the motion capture signal must be sampled at a minimum of 10 Hz. In the present study, motion capture data was sampled at 100 Hz, which is ten times larger than the theoretical sampling frequency. Therefore, a true representation of the signal can therefore be obtained, via interpolation, if ten or less consecutive samples are missing. This method was applied to each of the markers on the feet and back using the Matlab function *interp1*. Any intervals of missing data greater than ten consecutive frames were not reconstructed.

4.2.4.4 Removal of Force Plate Drift Offset and Data Filtering

In their evaluation of the CAREN's moveable platform and force-plate instrumented treadmill, Sinitski et al. [253] noted the baseline drift characteristics affecting the 3D ground reaction forces (GRFs) measured by the force plates. When a person is walking on the instrumented treadmill, AP and ML GRFs drifted less than 5 N over a 25-minute period, while VT GRFs drifted 5 N every 5 minutes. Likewise, all moments were determined to drift roughly 5 Nm every 5 minutes.

Considering that every level of the simulated rocky surface pathway takes less than two minutes to complete, the GRFs do not drift appreciably over the course of a single level. So long as the force plates are zeroed prior to each walk down the pathway, drift should not be of concern. However, due to the impracticality of having the participant repeatedly step on and off the platform, the force plates were only zeroed at the beginning of the PAT protocol. Thus, a drift will have accumulated in the GRF signals from the preceding standing and walking tasks, which adds an offset to the values measured during the simulated rocky surface levels. This offset will then affect any further calculations performed using the measured GRFs. Consequently, a procedure to remove the offset from the measured GRFs was needed. In other words, we required a means to re-zero the force plates during each level of the simulated rocky surface task through post-processing.

For this purpose, we applied a modified version of a post-processing technique typically used to estimate and remove baseline drift from 3D GRFs measured using dual-belt instrumented treadmills [254]. This technique involves estimating a mean drift during the swing phase of gait and removing that from the following stance phase [254]. However, a critical stipulation of this method is that it requires 'clean' gait cycles where only the left foot contacts the left force plate and only the right foot contacts the right force plate. For the unperturbed segments, 'clean' gait cycles could not be guaranteed as participants often shifted towards one side or another during the rocky surface perturbation. Although this did not affect the normal gait pattern during the unperturbed segment, it does imply that participants partially walked with both feet on the same treadmill belt. Recall, from the description of the experimental protocol, that every walking level began with a ramp up to a fixed treadmill speed, followed by 20 m at self-paced control, before encountering the first installment of the specified task (see Figure 4.4 for simulated rocky surface). Furthermore, each iteration of the simulated rocky surface was preceded by 10 m of unperturbed walking at self-selected speed. As a result, each level included more than 30 m of unperturbed walking prior to the first disturbance. From this interval, the longest segment of consecutive 'clean' gait cycles was found and used to predict a mean estimate of the offset in the 3D GRFs measured by each force plate. Heel strike (HS) and toe off (TO) were determined using the horizontal position of the foot relative to the pelvis [232], [255]. Due to the moving walking surface (i.e., treadmill), a graphical representation of the AP foot position (relative to the pelvis) versus time

results in a characteristic sinusoidal curve in which the peaks correspond to HS and the valleys correspond to TO. In the present study, AP foot position relative to the pelvis was given by the difference between the top, front marker on the foot plate (Figure 4.8, markers 8 and 12) and the mean position of the top two markers on the back plate (Figure 4.8, markers 30 and 31). For each step, a segment from five frames after TO to five frames before HS (i.e., swing phase) was extracted and appended to the end of the segment from the previous step. Performing this for each body side separately resulted in appended time series of 3D forces and moments measured from each of the force plates in their unloaded state. Mean values of the appended time series were calculated to determine estimates of the offset for an entire level. Finally, the mean values for a certain level were subtracted from the measured GRFs for all three unperturbed walking segments extracted from that level. The offset was removed from the standing segment by subtracting the mean estimates from the first level of the simulated rocky surface. Once the measured GRFs were re-zeroed, the components from both force plates were summed to obtain the resultant forces and moments in all three directions (i.e., ML, AP, and VT). This was done for both standing and walking segments.

All kinematic and kinetic time series were filtered using a zero-lag, fourth-order, low-pass Butterworth filter. Cut-off frequencies of 6 Hz [46], [53], [55], [94], [101], [256]–[260] and 10 Hz [66], [106], [108], [128], [177], [261], [262] were used for filtering of the kinematic and kinetic data, respectively. See Appendix D.2 for details on the filter design.

4.2.4.5 Biomechanical Parameter Calculation

From the quiet standing segment, m, was calculated by dividing the mean vertical force by the gravitational acceleration constant (9.81 m/s^2). Meanwhile, the equivalent pendulum length between the body's centre of mass (CoM) and ankle joint [19], [84], l, was approximated as the vertical distance between the mean location of the top two markers on the back plate (Figure 4.8, markers 30 and 31) and the mean location of the top, front marker on each foot plate (Figure 4.8, markers 8 and 12). Figure 4.9 provides a visual representation of this vertical distance.

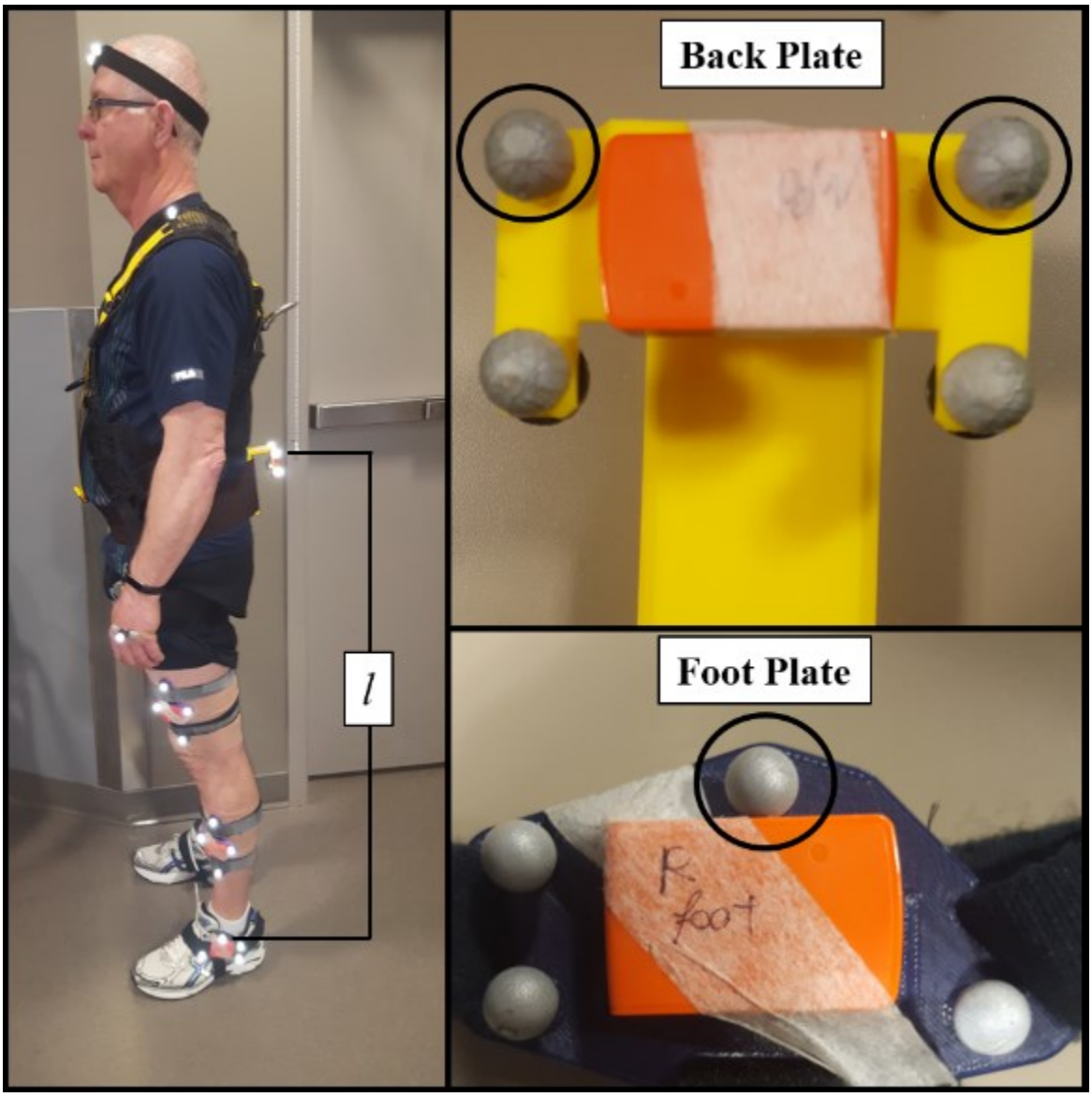

Figure 4.9: Illustration of how the length of the equivalent pendulum was calculated. (a) posture during standing segment and definition of the equivalent pendulum length; (b) back plate with top two markers circled in black; and (c) foot marker with top, front marker circled in black.

For all unperturbed walking segments, the centre of mass (CoM) position in the ML and AP directions was determined via the zero-point-to-zero-point (ZPZP) double integration technique [87]–[89]. In order to apply this method, however, accurate CoP data are required. Therefore, CoP trajectories for all segmented walking intervals were calculated using the de-drifted and filtered resultant GRFs.

The ZPZP technique is based on the assumption that, when the horizontal GRFs (ML and AP) are zero, the vertical projection of the CoM coincides with the CoP [83]. Thus, CoM position is found by twice integrating the horizontal acceleration of the CoM (horizontal GRFs divided by m) while using CoP position at successive points of zero force as the constant of integration. Note that, during human gait, the horizontal GRFs periodically cross the zero axis, meaning that multiple instances of zero force exist where the CoM and CoP theoretically coincide. To determine the CoM position across an entire walking trial, the ZPZP double integration technique was applied separately to each interval bounded by successive instants of zero force [83], [87], [89], and the results are then appended to each other to recreate the time series. Centre of mass velocity (v_{CoM}) was calculated using the same ZPZP technique; however, only a single integration was performed. It is worth noting that, because consecutive intervals are treated separately and appended to form the entire time series, discontinuities exist at the zero points (i.e., transition from end of one interval to beginning of next).

4.2.4.6 Calculation of Walking Speed

When using self-paced treadmill control, it is imperative that accurate walking speed is determined prior to calculating temporo-spatial parameters. Therefore, an algorithm using AP foot marker velocity during contralateral swing phase was applied to determine a mean value of walking speed for each step [178], [263]. Contralateral swing phase was identified as the interval five frames after TO to five frames before HS. During this interval, the stance foot and the treadmill moved at the same speed. Therefore, the top, front marker on the cluster plate of the stance foot (Figure 4.8, markers 8 and 12) was used to compute a velocity curve in the AP direction. From there, the mean value was computed from the eight consecutive frames with the smallest standard deviation of the AP velocity curve. Subsequently, it was ensured that all walking intervals contained only full steps, beginning and ending on either left or right HS.

4.2.5 Gait Stability Analysis

4.2.5.1 Temporo-Spatial Gait Parameters

To quantify and assess walking performance, average temporo-spatial parameters of walking speed, stride length, stride time, step length, step time, step width, swing per stride, and stance per stride were calculated for each participant [35], [36], [51], [178]. Both swing per stride and stance

per stride were expressed as a time percentage of the complete stride. Furthermore, based on previous evidence of a lack of significant differences between body sides [67], values from right and left body sides were combined in the mean calculation of all parameters for non-disabled participants [35], [36], [240], [264]. For the three case study participants, left and right body sides were treated independently, meaning separate values were obtained for all temporo-spatial parameters other than walking speed, stride length and stride time. For all participants, the mean and variability (across- and within-participant) of each parameter were calculated from steps within the unperturbed walking segments taken from the first level of the simulated rocky surface task. Values obtained from the first step (or stride) in a segment, or steps (or strides) containing missing marker data were excluded. Taking these exclusions into account, most unperturbed walking segments included 4 to 5 useable steps. Therefore, mean values for non-disabled participants were computed from 24 to 30 steps (12 to 15 strides) per participant. For case study participants, mean values of step length, step time, step width, swing per stride, and stance per stride were computed from 12 to 15 steps for each body side, while walking speed, stride length and stride time were computed from 12 to 15 strides.

4.2.5.2 Extrapolated Centre of Mass and Margin of Stability

The XCoM and margin of stability (MoS) were calculated using equations (9) and (11) (Chapter 2), respectively, with both quantities being determined separately for the ML and AP directions. The lateral and anterior bounds of the base of support (BoS) were provided by the instantaneous positions (in the ML and AP directions, respectively) of the top foot marker of the lead foot from ipsilateral HS to contralateral HS [48], [70], [98]. In other words, the boundaries of the BoS for MoS calculations in both the ML and AP directions were defined by the position of the top, front marker on the cluster plate of the stance phase foot (Figure 4.8, markers 8 and 12) from the instant it strikes the platform to the instant the contralateral foot strikes the platform. To quantify gait stability in the ML direction, MoS values were examined for three instances within each step: (1) HS; (2) mid-stance (MS); and (3) the minimum between HS and contralateral TO (HScTO). Similarly, MoS values in the AP direction were examined at two instances: (1) HS; and (2) MS. Previous studies [19], [91], [92], [97], [265]–[267] have investigated the MoS at these instances as they are believed to be the least stable points in the gait cycle. MS was defined as the point at which the CoM passes the foot marker [268]. Mean values of all five MoS measures were

calculated from 15 steps per body side. Exclusion criteria included the first step at the beginning of an unperturbed surface walking segment, or steps with missing data. Specific to the ML direction, steps with inordinate fluctuations of the ML force about zero were also excluded. Briefly, the ML force goes to zero only once over a typical step, shortly after HS. In some cases, however, minor fluctuations of the ML force created additional zero points through a step. This is problematic when applying the ZPZP algorithm as each zero point creates an additional discontinuity in the estimated CoM and v_{CoM}. See Appendix E for a full justification of these exclusions. To ensure that all mean values were calculated from a total of 15 steps, exclusions were replaced with values from the next appropriate step. In most cases, all values were taken from steps within the walking segments obtained from the first level; however, when insufficient steps were available, values were drawn from the segments of the second level.

4.2.6 Statistical Analysis

Non-parametric Friedman tests were applied to all MoS measures to test for significant differences between task levels (1 and 2) and body side (left and right). Only participants with at least 15 unexcluded steps on both body sides were included in these tests, and a significance level of $\alpha = 0.05$ was used. Across- and within-participant variability were used to assess the robustness of the MoS measures.

The between-session repeatability was assessed by calculating the intra-class correlation coefficient (ICC) for model (2,1), the standard error of measurement (SEM), and the minimal detectable change (MDC) [191] between the first and second session for all 15 participants. Equations (37) and (38) (Chapter 2) were used to compute SEM and MDC, respectively. ICC values of 0.75 or higher were considered excellent, 0.4-0.75 to be fair to good, and less than 0.4 to be poor, as used by [75], [264], [269]–[272] based on benchmarks suggested by [192], [273]–[275]. Further, based on recommendation from Chinn [276], good agreement was considered for ICC values greater than 0.6 [23], [277], [278].

4.3 Results

4.3.1 Temporo-Spatial Gait Parameters

Figure 4.10 provides a representative time series example of foot displacement for a single, non-disabled participant during an unperturbed walking segment from the first level of the simulated rocky surface walking task (Figure 4.4). The trajectory of either foot is provided by the position of the top, front marker on the outside of either foot (Figure 4.8, markers 8 and 12) for two complete walking strides (i.e., two steps per body side). Based on a visual inspection of Figure 4.10, the non-disabled participant appears to walk with a relatively consistent step-to-step gait pattern, demonstrating symmetry between left and right body sides. There seem to be some minor, expected fluctuations in the ML position of both feet; however, the participant does not appear to drift significantly from side-to-side.

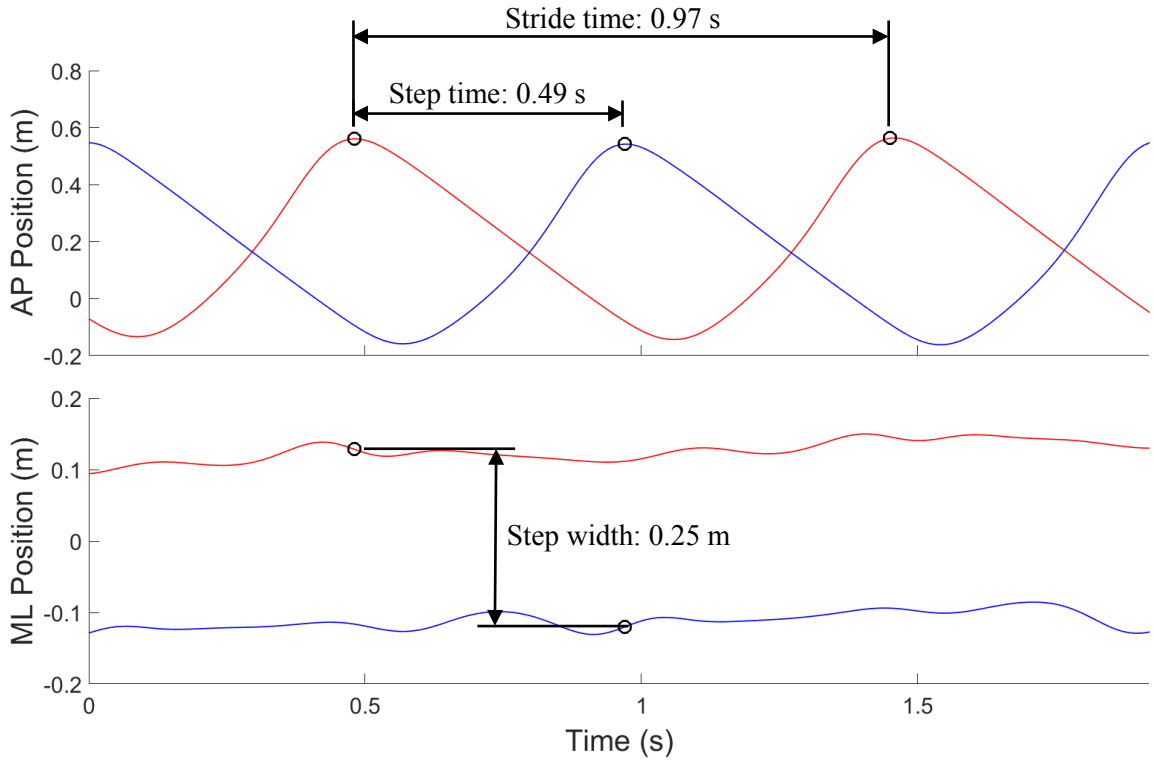

Figure 4.10: Displacement of the feet for two complete walking strides of a non-disabled participant in both the anteroposterior (AP) and mediolateral (ML) directions. Time series were obtained from an unperturbed walking segment within the first level of the simulated rocky surface walking task. Line color indicates body side: left (red) and blue (right). Circle markers indicate times of heel strike (HS). Values of stride time, step time and step width are shown, all beginning at left HS (right step).

Temporo-spatial parameters, including walking speed, stride length, stride time, step length, step time, step width, swing per stride, and stance per stride are provided in Table 4.3. Note that step width was calculated based on the lateral distance between the top, front markers on the rigid plates located on the outsides of the feet (Figure 4.8, markers 8 and 12), rather than markers located at the centre-line of either foot (e.g., heel markers). As suggested by Figure 4.10 and confirmed via the relatively low within-participant variability, non-disabled participants walked with a consistent gait pattern. While a higher across-participant standard deviation was found for walking speed due to the different self-selected speeds, the across-participant standard deviation for all other parameters remained relatively low (roughly 10% of the mean value).

Table 4.3: Temporo-spatial parameters of unperturbed walking on the CAREN. Data are presented as group means and across-participant standard deviations (SD). Average within-participant variability (WPV) is also presented for each parameter.

Parameter	*Mean ± SD*	*WPV*
Walking speed (m/s)	1.43 ± 0.23	0.07
Stride length (m)	1.48 ± 0.14	0.05
Stride time (s)	1.05 ± 0.11	0.02
Step length (m)	0.74 ± 0.07	0.03
Step time (s)	0.52 ± 0.06	0.02
Step width (m)	0.29 ± 0.04	0.03
Swing per stride (%)	39.12 ± 1.29	1.34
Stance per stride (%)	60.90 ± 1.29	1.02

4.3.2 Extrapolated Centre of Mass and Margin of Stability

Figure 4.11 provides a representative time series example of the relationship between the XCoM and BoS in the ML direction, along with the corresponding MoS for a non-disabled participant during an unperturbed walking segment from the first level of the simulated rocky surface walking task. The time series include two complete walking strides (i.e., two steps per body side). Recall that the BoS is defined by the top, front marker on the outside of the stance foot from ipsilateral HS to contralateral HS. Furthermore, the MoS is the distance between the XCoM and the BoS, in the ML direction. As seen in Figure 4.11, the participant's XCoM remained within the bounds of

the BoS, thus demonstrating a positive MoS throughout the representative time series. The MoS plot also indicates that slight variability in the trajectory of the MoS exists between body sides, as well as between separate steps on the same body side. Representative values of all three MoS measures in the ML direction (MoS-HS, MoS-MS, MoS-HScTO) are also provided in Figure 4.11, for a single step only. The MoS-MS is the largest, followed by MoS-HS and, finally, MoS-HScTO. Not surprisingly, MoS-HScTO is the lowest of all three as it is the minimum distance between the XCoM and BoS from HS to contralateral toe off (cTO). In addition, MoS-HScTO appears to occur shortly after HS, which explains why its value is comparable to MoS-HS.

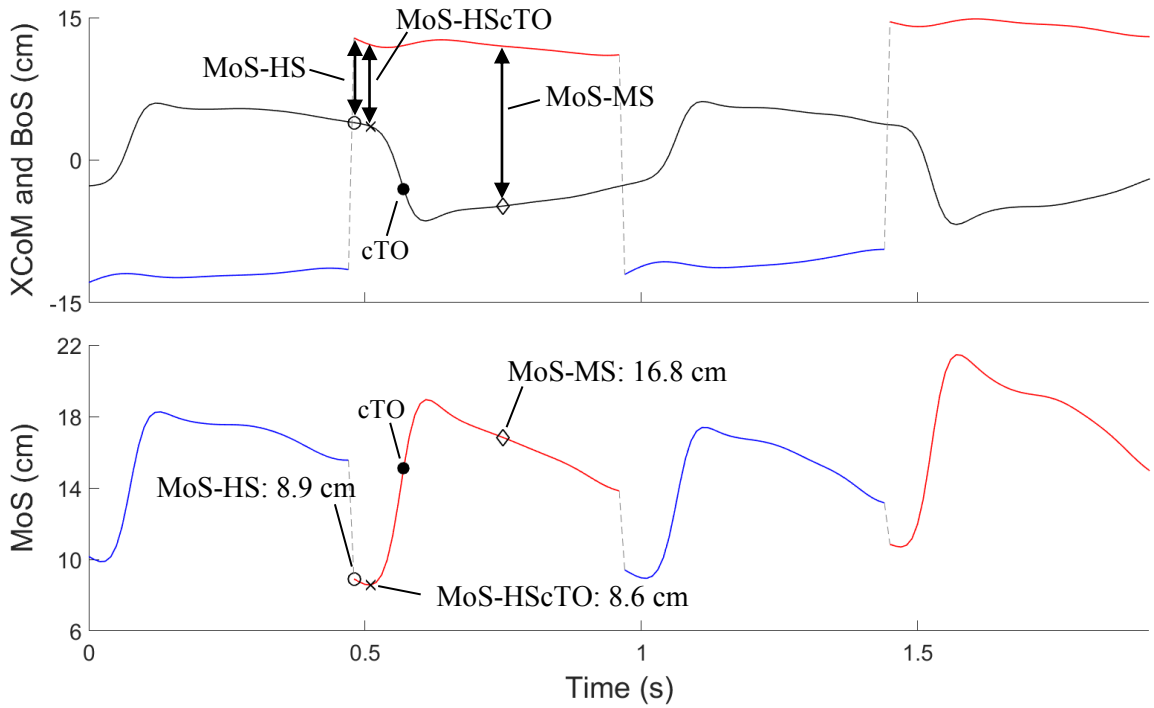

Figure 4.11: Temporal relationship between the locations of the extrapolated centre of mass (XCoM) and base of support (BoS), and the corresponding margin of stability (MoS) for two complete walking strides of a non-disabled participant in the mediolateral (ML) direction. Top: black curve is the XCoM, while the red and blue lines represent the limits of the BoS defined during the stance phase of the left and right feet, respectively. Bottom: MoS for left (red) and right (blue) body sides. Markers indicate the location of contralateral toe off (cTO) and indices of the gait cycle at which each MoS measure is taken for a single step. The MoS measures indicated are: heel strike (MoS-HS), mid-stance (MoS-MS), and the minimum between heel strike and cTO (MoS-HScTO). Values for MoS-HS, MoS-MS and MoS-HScTO are also provided for a single step.

Figure 4.12 provides a representative time series example of the relationship between the XCoM and BoS in the AP direction, along with the corresponding MoS for a non-disabled participant

during an unperturbed walking segment from the first level of the simulated rocky surface walking task. The time series include two complete walking strides (i.e., two steps per body side). Based on the plot of the XCoM and BoS, it can be seen that, in each step, the XCoM travels beyond the boundary of the BoS. This observation is confirmed by noting that the MoS repeatedly falls into the negative range shortly after MS. Contrary to what was observed in the ML direction, the trajectory of the MoS appears to be relatively consistent across successive steps. Representative values of the two MoS measures in the AP direction (MoS-HS and MoS-MS) for a single step indicate that results are relatively comparable between MoS-HS and MoS-MS, with MoS-MS being only slightly higher.

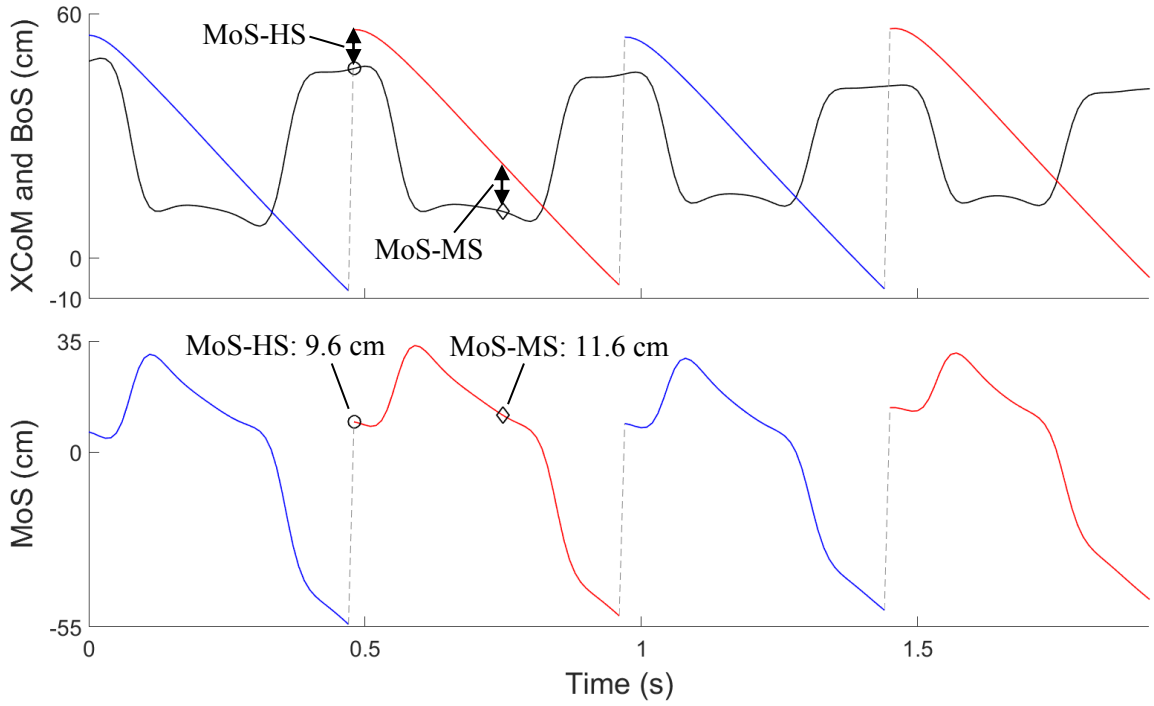

Figure 4.12: Temporal relationship between the locations of the extrapolated centre of mass (XCoM) and base of support (BoS), and the corresponding margin of stability (MoS) for two complete walking strides of a non-disabled participant in the anteroposterior (AP) direction. Top: black curve is the XCoM, while the red and blue lines represent the limits of the BoS defined during the stance phase of the left and right feet, respectively. Bottom: MoS for left (red) and right (blue) body sides. Markers indicate the location of contralateral toe off (cTO) and indices of the gait cycle at which each MoS measure is taken for a single step. The MoS measures indicated are: heel strike (MoS-HS) and mid-stance (MoS-MS). Values for MoS-HS and MoS-MS are also provided for a single step.

The Friedman test with factors task level and body side did not reveal any significant differences ($\alpha = 0.05$) between MoS values taken from level 1 and level 2 of the simulated rocky surface

walking task, for all MoS measures. Thus, for participants with insufficient data in level 1, values were drawn from level 2 to ensure a total of 15 steps (values) per body side. Additionally, the Friedman test identified significant differences between right and left steps for MoS-MS ($p = 0.002$) only. Since none of the other measures exhibited significant differences, all MoS measures were combined for the two body sides. Tables 4.4 and 4.5 present all MoS measures in the ML and AP directions. In line with the observations from Figure 4.11, the greatest MoS values occurred for MoS-MS, whereas MoS-HS and MoS-HScTO were comparable. In the AP direction, MoS-HS was much greater than MoS-MS, which differs from what is suggested by Figure 4.12.

In terms of the variability of the measures in the ML direction, the MoS-MS exhibited the lowest across-participant variability (given by standard deviation), in terms of both absolute and relative measurement (roughly 17% of the mean value). The MoS-HS and MoS-HScTO both had higher absolute measurements of across-participant variability, corresponding to approximately 30% of the mean value. Within-participant variability was generally in the 10 to 17% range for all cases. On average, relative across- and within-participant variability were greater for the MoS measures in the AP direction. For MoS-HS, across- and within- participant variability were 30% and 35% of the mean value, respectively, whereas for MoS-MS, both measurements of variability were approximately 40% of the mean value.

Table 4.4: Margin of stability measures at heel strike (MoS-HS), mid-stance (MoS-MS) and contralateral toe off (MoS-HScTO) in the mediolateral (ML) direction. Data are presented as group means and across-participant standard deviations (SD). Average within-participant variability (WPV) is also presented for each measure.

Measure	*Mean* ± *SD*	*WPV*
MoS-HS (cm)	13.2 ± 3.9	2.1
MoS-MS (cm)	18.3 ± 3.1	2.6
MoS-HScTO (cm)	12.8 ± 4.2	2.2

Table 4.5: Margin of stability measures at heel strike (MoS-HS) and mid-stance (MoS-MS) in the anteroposterior (AP) direction. Data are presented as group means and across-participant standard deviations (SD). Average within-participant variability (WPV) is also presented for each measure.

Measure	*Mean ± SD*	*WPV*
MoS-HS (cm)	17.6 ± 5.3	6.2
MoS-MS (cm)	7.5 ± 3.2	3.0

4.3.3 Between-Session Repeatability

Tables 4.6 and 4.7 present the between-session repeatability results for the MoS measures in the ML and AP directions, respectively. In the ML direction, all MoS measures presented good repeatability (ICC > 0.6), whereas in the AP direction, only the MoS-HS demonstrated good repeatability. The MoS-MS in the AP direction showed only fair repeatability (ICC > 0.4).

For all MoS measures in the ML direction, SEM values represented 10 to 20% of the average absolute value. In the AP direction, the SEM for MoS-HS was approximately 17% of the average absolute value, whereas for MoS-MS, the SEM was roughly 32% of the average absolute value.

In the ML direction, MDC values for MoS-HS and MoS-HScTO neared a mark of 50% of the average absolute value. For MoS-MS, the MDC value was 36%. In comparison, MDC values in the AP direction were 47% of the average absolute value for MoS-HS, and 88% of the average absolute value for MoS-MS.

Table 4.6: Repeatability results for the margin of stability measures at heel strike (MoS-HS), mid-stance (MoS-MS) and contralateral toe off (MoS-HScTO) in the mediolateral (ML) direction. Repeatability parameters include the intra-class correlation coefficient with corresponding 95% confidence intervals, standard error of measurement (SEM), and minimum detectable change (MDC). ICC values above 0.6 are presented in bold.

Measure	*ICC*	*SEM (cm)*	*MDC (cm)*
MoS-HS	**0.66 (0.26-0.87)**	2.3	6.3
MoS-MS	**0.63 (0.19-0.86)**	1.9	6.6
MoS-HScTO	**0.65 (0.25-0.86)**	2.5	6.8

Table 4.7: Repeatability results for the margin of stability measures at heel strike (MoS-HS) and mid-stance (MoS-MS) in the anteroposterior (AP) direction Repeatability parameters include the intra-class correlation coefficient with corresponding 95% confidence intervals, standard error of measurement (SEM) and minimum detectable change (MDC). ICC values above 0.6 are presented in bold.

Measure	*ICC*	*SEM (cm)*	*MDC (cm)*
MoS-HS	**0.67 (0.26-0.88)**	3.0	8.4
MoS-MS	0.44 (-0.09-0.77)	2.4	6.6

4.3.4 Comparison to Impaired Participants

Figure 4.13 provides a representative time series example of foot displacement for the participant with HA during an unperturbed walking segment from the first level of the simulated rocky surface walking task. Same as for the non-disabled individuals, the trajectory of either foot is provided by the position of the top, front marker on the outside of either foot (Figure 4.8, markers 8 and 12) for two complete walking strides (i.e., two steps per body side). By inspection of Figure 4.13, the participant appears to demonstrate a symmetric gait pattern as there do not seem to be any noticeable differences between body sides. Furthermore, neither of the feet demonstrate any major fluctuations in the ML direction. Example values of stride time, step time and step width are all larger than observed for non-disabled participants.

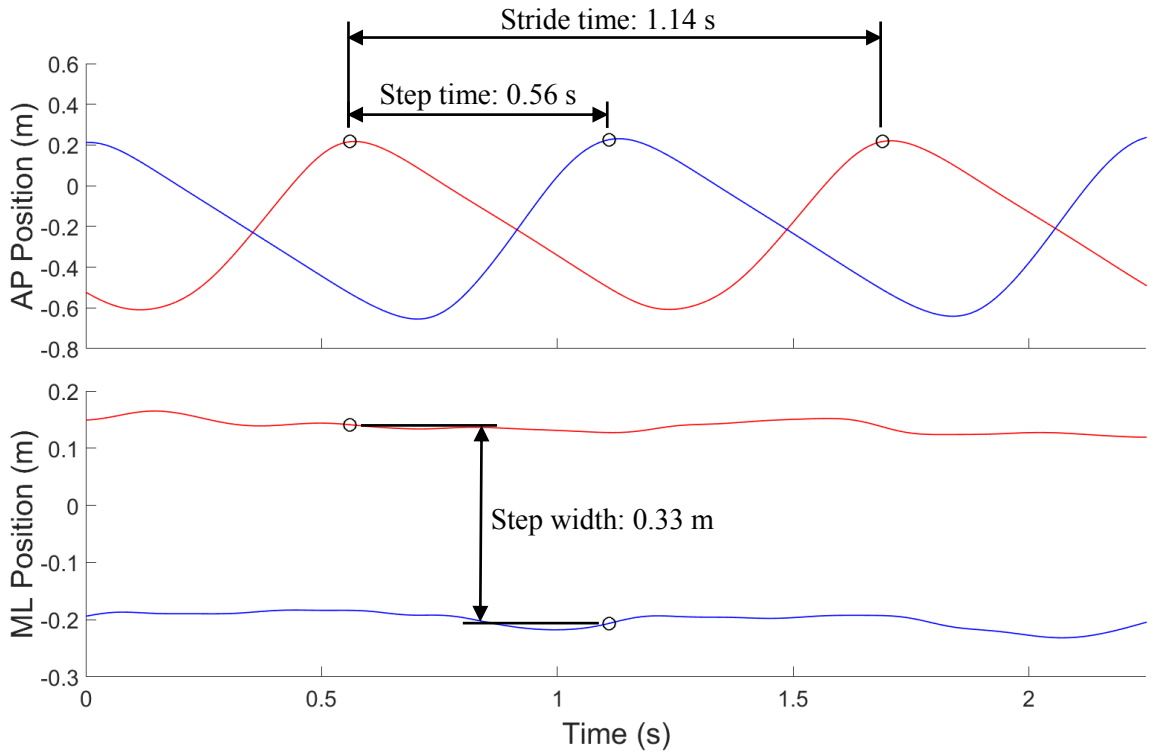

Figure 4.13: Displacement of the feet for two complete walking strides of the participant with hemophilic arthropathy in both the anteroposterior (AP) and mediolateral (ML) directions. Time series are obtained from an unperturbed walking segment within the first level of the simulated rocky surface walking task. Line color indicates body side: left (red) and blue (right). Circle markers indicate times of heel strike (HS). Values of stride time, step time and step width are shown, all beginning on left HS (right step).

Figure 4.14 provides a representative time series example of foot displacement for the participant with TTA during an unperturbed walking segment from the first level of the simulated rocky surface walking task. As before, the trajectory of either foot is provided by the position of the top, front marker on the outside of either foot (Figure 4.8, markers 8 and 12) for two complete walking strides (i.e., two steps per body side). Based on the AP position of the feet, the participant seems to demonstrate consistency across successive steps, thus, demonstrating a consistent and symmetric gait pattern. In the ML direction, there appear to be noticeable and repeated deviations in the foot location just prior to HS, for both body sides. Example values of stride and step time are both much larger than those of the non-disabled participants, while step width is slightly smaller.

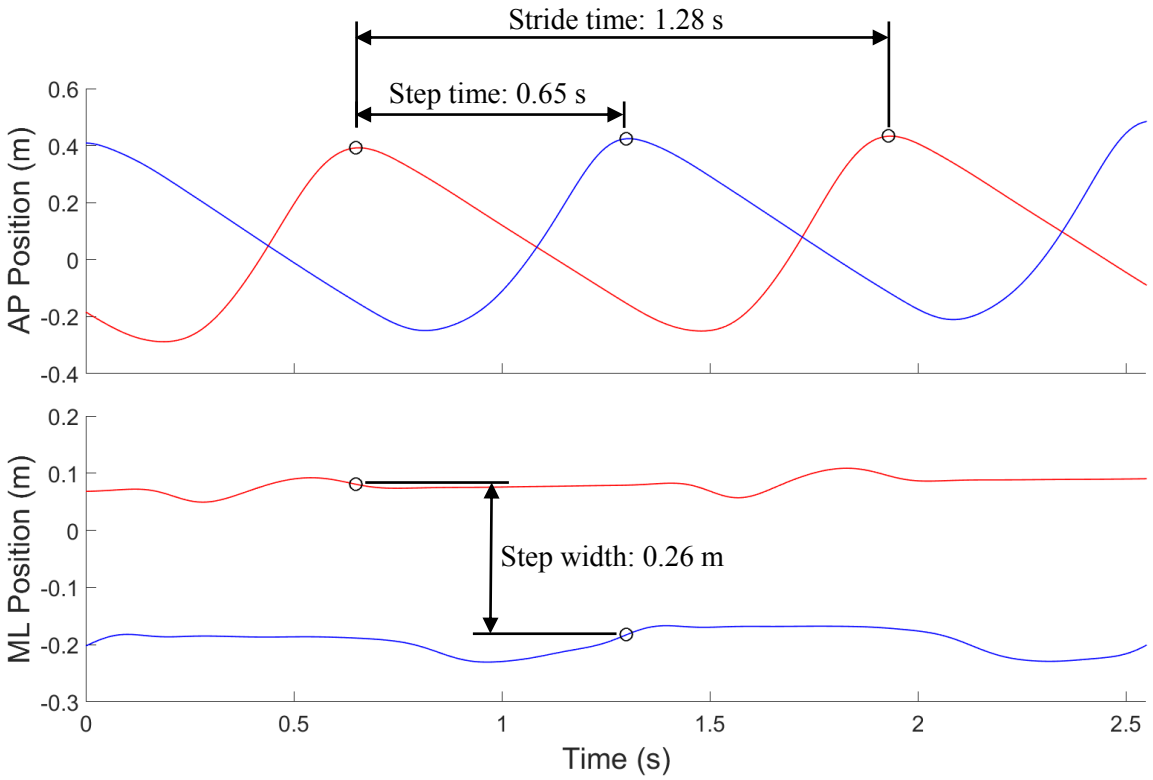

Figure 4.14: Displacement of the feet for two complete walking strides of the participant with transtibial amputation in both the anteroposterior (AP) and mediolateral (ML) directions. Time series are obtained from an unperturbed walking segment within the first level of the simulated rocky surface walking task. Line color indicates body side: left (red) and blue (right). Circle markers indicate times of heel strike (HS). Values of stride time, step time and step width are shown, all beginning on left HS (right step).

Figure 4.15 provides a representative time series example of foot displacement for the participant with mTBI during an unperturbed walking segment from the first level of the simulated rocky surface walking task. The trajectory of either foot is provided by the position of the top, front marker on the outside of either foot (Figure 4.8, markers 8 and 12) for two complete walking strides (i.e., two steps per body side). By observation of Figure 4.15, the participant does not appear to demonstrate any noticeable differences between body sides or in successive steps. This indicates a consistent and symmetric step-to-step gait pattern. In the ML direction, the participant appears to shift towards the right side near the end of the representative time series. Example values of stride and step time are both smaller than their non-disabled counterparts, while step width is larger than observed in the non-disabled sample.

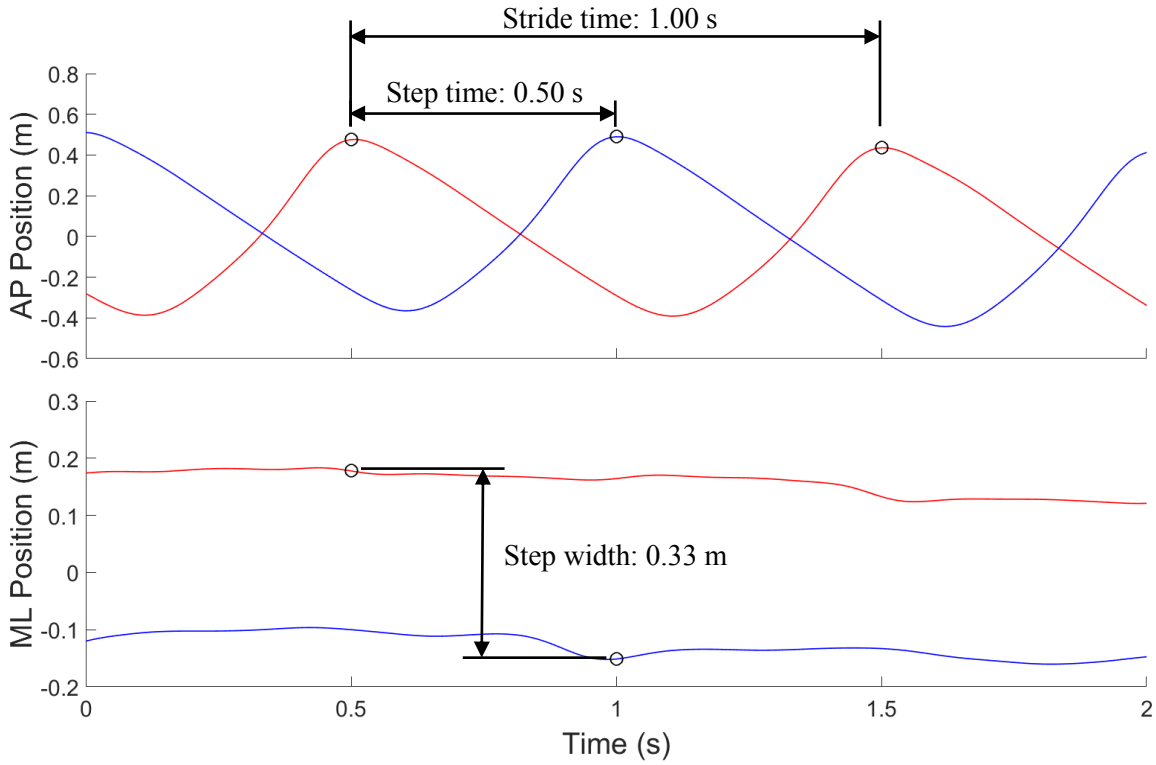

Figure 4.15: Displacement of the feet for two complete walking strides of the participant with mild traumatic brain injury in both the anteroposterior (AP) and mediolateral (ML) directions. Time series are obtained from an unperturbed walking segment within the first level of the simulated rocky surface walking task. Line color indicates body side: left (red) and blue (right). Circle markers indicate times of heel strike (HS). Values of stride time, step time and step width are shown, all beginning on left HS (right step).

Temporo-spatial parameters, including walking speed, stride length, stride time, step length, step time, step width, swing per stride, and stance per stride are provided in Table 4.8 for participants with: (1) HA, (2) TTA, and (3) mTBI. Obtained normative values are shown as well for comparison purposes. Note, again, that step width was calculated based on the lateral distance between the top, front markers on the rigid plates located on the outsides of the feet (Figure 4.8, markers 8 and 12), rather than markers located at the centre-line of either foot (e.g., heel markers). While the individual with HA walked at a comparable speed as the non-disabled participants, the stride length and time as well as the step lengths, times, and widths were larger on both body sides. By comparison of these parameters for body sides, the individual with HA walked with a symmetric gait pattern. Some slight asymmetries were revealed in looking at the separate phases of swing and stance as the individual appeared to spend more time in swing during a left step and more time in stance during a right step. The individual with TTA walked slower than the non-disabled participants, matched by a correspondingly lower stride length and higher stride time. Asymmetries between left and right body sides were revealed when scrutinizing the greater step

length and time on the right body side. Furthermore, the individual with TTA spent more time in right swing than left, and, thus, more time in left stance than right. Similar values for step width were found for both body sides. The individual with mTBI walked faster than the non-disabled participants, with a greater stride length and lower stride time. Per body side, greater step lengths were observed on the right, whereas step time and step width were similar for right and left.

Table 4.8: Temporo-spatial parameters of normal, level-surface walking on the CAREN for case study participants with: (1) hemophilic arthropathy (HA); (2) transtibial amputation (TTA); and (3) mild traumatic brain injury (mTBI). Data are presented as participant means and within-participant variability (WPV). Normative values (mean and across-participant variability) are shown for comparison purposes.

		HA	**TTA**	**mTBI**	**Norm**
Parameter		*Mean ± WPV*	*Mean ± WPV*	*Mean ± WPV*	*Mean ± SD*
Walking speed (m/s)		1.43 ± 0.05	0.99 ± 0.05	1.82 ± 0.12	1.43 ± 0.23
Stride length(m)		1.61 ± 0.07	1.26 ± 0.04	1.76 ± 0.06	1.48 ± 0.14
Stride time (s)		1.12 ± 0.01	1.28 ± 0.02	0.98 ± 0.03	1.05 ± 0.11
Step length (m)	Left	0.81 ± 0.03	0.61 ± 0.03	0.86 ± 0.04	0.74 ± 0.07
	Right	0.80 ± 0.04	0.66 ± 0.02	0.90 ± 0.03	
Step time (s)	Left	0.56 ± 0.01	0.63 ± 0.03	0.49 ± 0.02	0.52 ± 0.06
	Right	0.56 ± 0.01	0.65 ± 0.02	0.49 ± 0.02	
Step width (m)	Left	0.34 ± 0.02	0.31 ± 0.02	0.28 ± 0.03	0.29 ± 0.04
	Right	0.34 ± 0.02	0.31 ± 0.03	0.28 ± 0.04	
Swing per stride (%)	Left	38.77 ± 0.86	35.85 ± 1.09	39.81 ± 0.72	39.12 ± 1.29
	Right	36.36 ± 0.73	36.58 ± 1.67	39.57 ± 1.29	
Stance per stride (%)	Left	61.38 ± 1.03	64.36 ± 1.51	60.19 ± 0.72	60.90 ± 1.29
	Right	63.89 ± 0.62	63.58 ± 1.63	60.80 ± 1.35	

Figure 4.16 provides a representative time series example of the relationship between the XCoM and BoS in the ML direction, along with the corresponding MoS for the participant with HA during an unperturbed walking segment from the first level of the simulated rocky surface walking task. The figure shows that the participant's XCoM remained within the bounds of the BoS, which indicates a positive margin of stability throughout the entire interval. Based on the plot of the MoS, the overall trajectory seems relatively comparable between consecutive steps. Representative

values of MoS-HS, MoS-MS and MoS-HScTO indicate that all are larger than those observed in the non-disabled participants. However, similar to the non-disabled sample, MoS-MS is the largest, followed by MoS-HS and MoS-HScTO. In this case, MoS-HS and MoS-HScTO both occur at the same instant in time (i.e., HS) and, thus, have the same value.

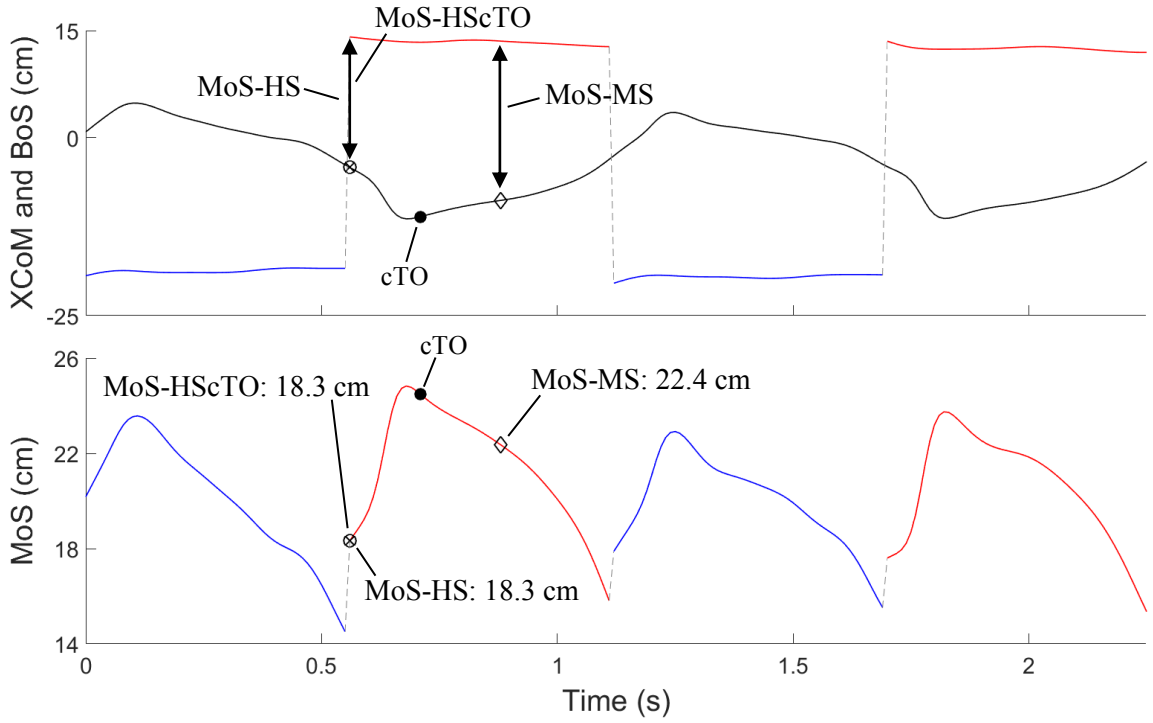

Figure 4.16: Temporal relationship between the locations of the extrapolated centre of mass (XCoM) and base of support (BoS), and the corresponding margin of stability (MoS) for two complete walking strides of the participant with hemophilic arthropathy in the mediolateral (ML) direction. Top: black curve is the XCoM, while the red and blue lines represent the limits of the BoS defined during the stance phase of the left and right feet, respectively. Bottom: MoS for left (red) and right (blue) body sides. Markers indicate the location of contralateral toe off (cTO) and indices of the gait cycle at which each MoS measure is taken for a single step. The MoS measures indicated are: heel strike (MoS-HS), mid-stance (MoS-MS), and the minimum between heel strike and cTO (MoS-HScTO). Values for MoS-HS, MoS-MS and MoS-HScTO are also provided for a single step.

Figure 4.17 provides a representative time series example of the relationship between the XCoM and BoS in the AP direction, along with the corresponding MoS for the participant with HA during an unperturbed walking segment from the first level of the simulated rocky surface walking task. The time series includes two complete walking strides (i.e., two steps per body side). As was observed in the representative time series from the non-disabled participant, the XCoM travels beyond the boundary of the BoS during each step, shortly after MS. The trajectory of the MoS

appears to be different across body sides, specifically from HS to the time the peak value is reached. The participant with HA looks to achieve a greater MoS-HS on the left body side rather than the right. Representative values indicate that MoS-HS is much larger, and MoS-MS is much smaller than for the non-disabled participants. Consistent with the findings from the non-disabled sample, MoS-HS is larger than MoS-MS.

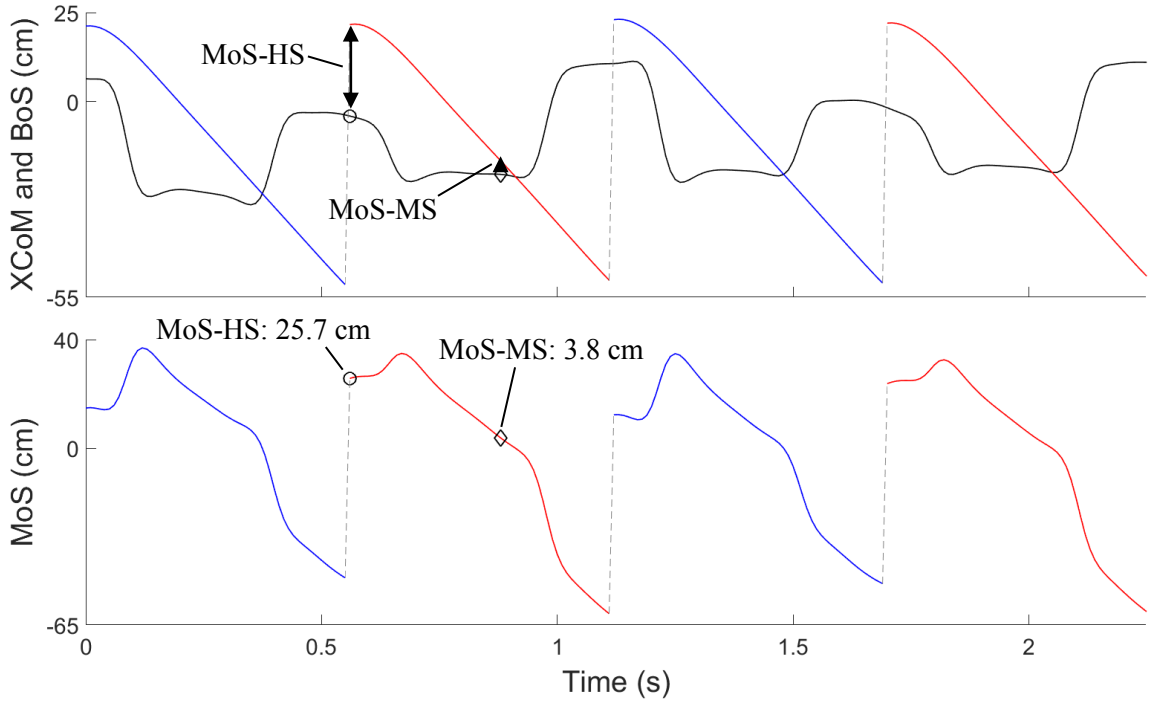

Figure 4.17: Temporal relationship between the locations of the extrapolated centre of mass (XCoM) and base of support (BoS), and the corresponding margin of stability (MoS) for two complete walking strides of the participant with hemophilic arthropathy in the anteroposterior (AP) direction. Top: black curve is the XCoM, while the red and blue lines represent the limits of the BoS defined during the stance phase of the left and right feet, respectively. Bottom: MoS for left (red) and right (blue) body sides. Markers indicate the location of contralateral toe off (cTO) and indices of the gait cycle at which each MoS measure is taken for a single step. The MoS measures indicated are: heel strike (MoS-HS) and mid-stance (MoS-MS). Values for MoS-HS and MoS-MS are also provided for a single step.

Figure 4.18 provides a representative time series example of the relationship between the XCoM and BoS in the ML direction, along with the corresponding MoS for the participant with TTA during an unperturbed walking segment from the first level of the simulated rocky surface walking task. Based on Figure 4.18, the participant's XCoM remained well within the limits of the BoS, which is confirmed by the positive values for the MoS. The MoS plot demonstrates clear differences between the MoS trajectory on each body side, as the MoS curve for the left body side

appears significantly more rounded than on the right. The representative values of MoS-HS and MoS-HScTO are both larger than those observed in the non-disabled sample, while MoS-MS is slightly smaller. However, as in the non-disabled sample, MoS-MS remains largest, followed by MoS-HS and MoS-HScTO. Similar to the participant with HA, the MoS-HS and MoS-HScTO both occur at the same instant in time (i.e., HS) and, thus, have the same value.

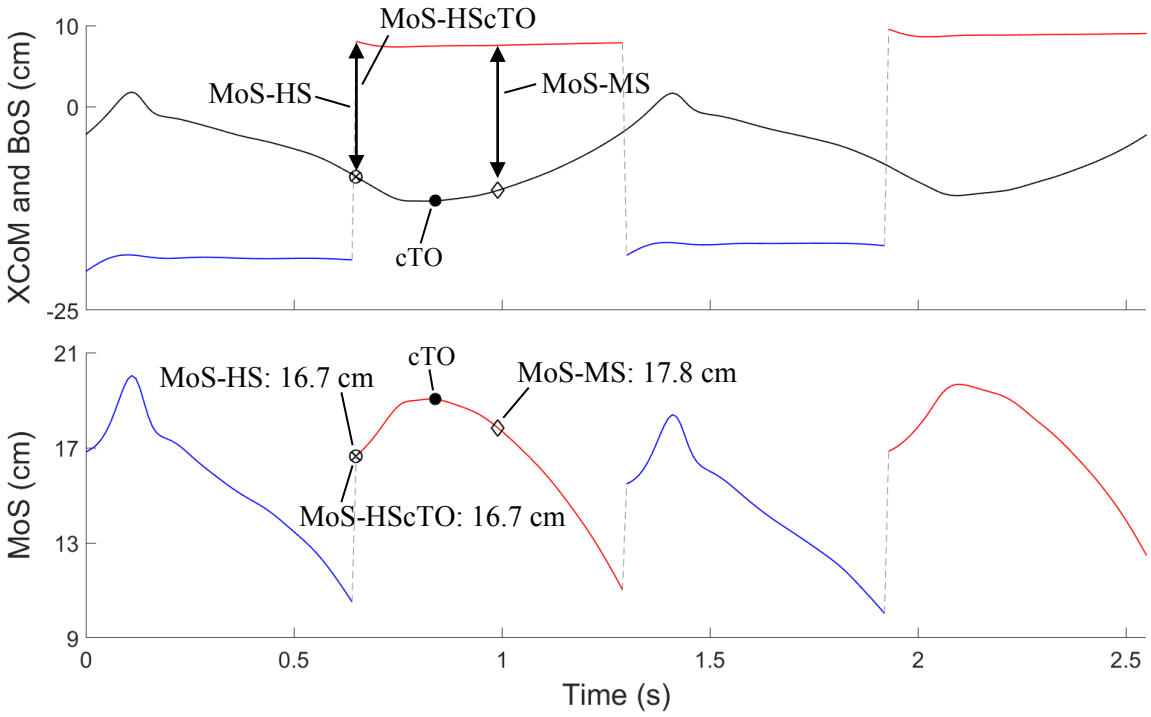

Figure 4.18: Temporal relationship between the locations of the extrapolated centre of mass (XCoM) and base of support (BoS), and the corresponding margin of stability (MoS) for two complete walking strides of the participant with transtibial amputation in the mediolateral (ML) direction. Top: black curve is the XCoM, while the red and blue lines represent the limits of the BoS defined during the stance phase of the left and right feet, respectively. Bottom: MoS for left (red) and right (blue) body sides. Markers indicate the location of contralateral toe off (cTO) and indices of the gait cycle at which each MoS measure is taken for a single step. The MoS measures indicated are: heel strike (MoS-HS), mid-stance (MoS-MS), and the minimum between heel strike and cTO (MoS-HScTO). Values for MoS-HS, MoS-MS and MoS-HScTO are also provided for a single step.

Figure 4.19 provides a representative time series example of the relationship between the XCoM and BoS in the AP direction, along with the corresponding MoS for the participant with TTA during an unperturbed walking segment from the first level of the simulated rocky surface walking task. The time series includes two complete walking strides (i.e., two steps per body side). As with the non-disabled participant and the participant with HA, the XCoM travels beyond the boundary

of the BoS shortly after MS in each step. Across body sides, the trajectory of the MoS appears comparable. Based on the representative values for a single step, MoS-HS nearly matches that of the non-disabled participants, while MoS-MS is larger. Similar to the non-disabled sample, MoS-HS is greater than MoS-MS in the AP direction.

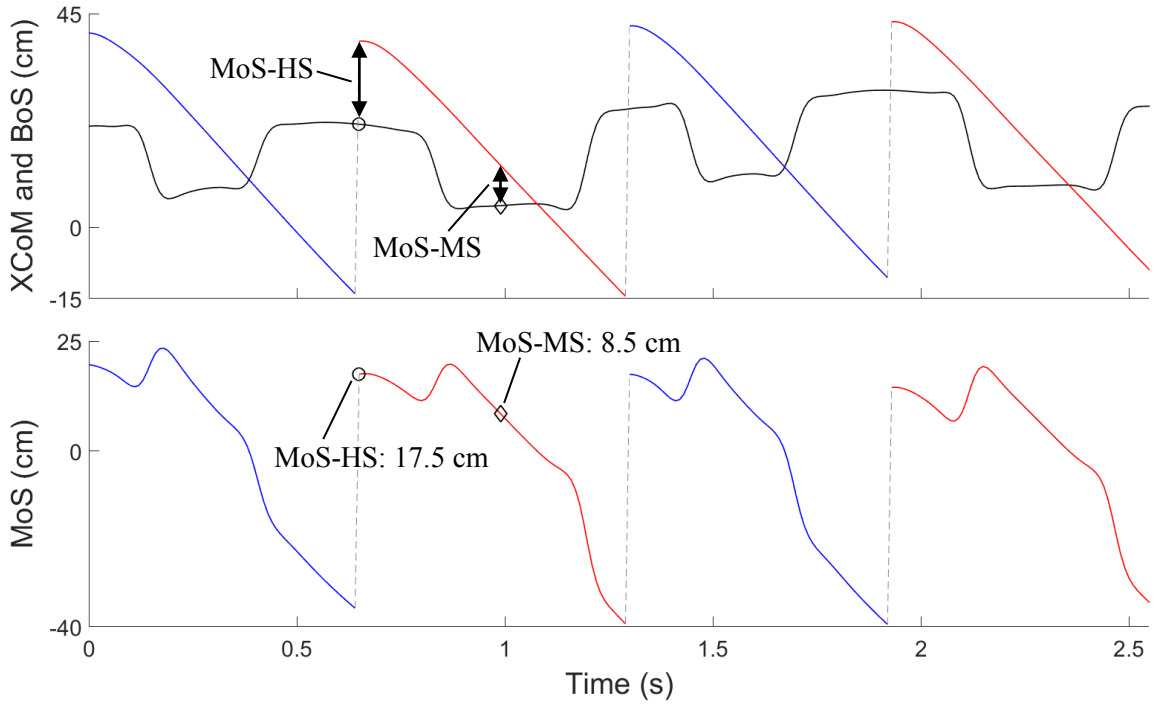

Figure 4.19: Temporal relationship between the locations of the extrapolated centre of mass (XCoM) and base of support (BoS), and the corresponding margin of stability (MoS) for two complete walking strides of the participant with transtibial amputation in the anteroposterior (AP) direction. Top: black curve is the XCoM, while the red and blue lines represent the limits of the BoS defined during the stance phase of the left and right feet, respectively. Bottom: MoS for left (red) and right (blue) body sides. Markers indicate the location of contralateral toe off (cTO) and indices of the gait cycle at which each MoS measure is taken for a single step. The MoS measures indicated are: heel strike (MoS-HS) and mid-stance (MoS-MS). Values for MoS-HS and MoS-MS are also provided for a single step.

Figure 4.20 provides a representative time series example of the relationship between the XCoM and BoS in the ML direction, along with the corresponding MoS for the participant with mTBI during an unperturbed walking segment from the first level of the simulated rocky surface walking task. Based on observations from Figure 4.20, the participant maintained their XCoM within the limits of the BoS, thereby preserving a positive MoS throughout both strides. In addition, it appears that the participant with mTBI walked with the XCoM shifted slightly towards the right side of the body. This observation is confirmed in seeing the larger overall trajectory of the MoS for the left

body side, with the participant maintaining a greater MoS during left stance. From the representative values, MoS-HS and MoS-HScTO are both smaller than those of the non-disabled sample, while MoS-MS is larger. As observed in the non-disabled sample, MoS-MS is largest, followed by MoS-HS and, last, MoS-HScTO. Again, it is not surprising that MoS-HScTO is smallest since it is identified as the minimum value between HS and cTO.

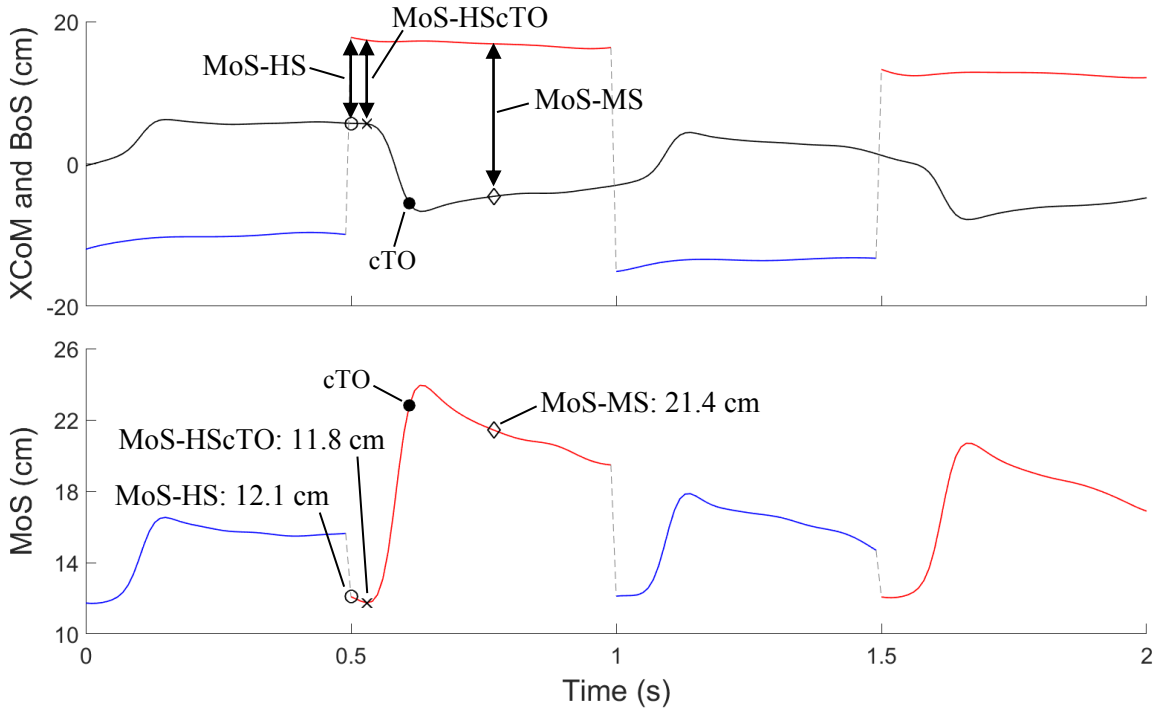

Figure 4.20: Temporal relationship between the locations of the extrapolated centre of mass (XCoM) and base of support (BoS), and the corresponding margin of stability (MoS) for two complete walking strides of the participant with mild traumatic brain injury in the mediolateral (ML) direction. Top: black curve is the XCoM, while the red and blue lines represent the limits of the BoS defined during the stance phase of the left and right feet, respectively. Bottom: MoS for left (red) and right (blue) body sides. Markers indicate the location of contralateral toe off (cTO) and indices of the gait cycle at which each MoS measure is taken for a single step. The MoS measures indicated are: heel strike (MoS-HS), mid-stance (MoS-MS), and the minimum between heel strike and cTO (MoS-HScTO). Values for MoS-HS, MoS-MS and MoS-HScTO are also provided for a single step.

Figure 4.21 provides a representative time series example of the relationship between the XCoM and BoS in the AP direction, along with the corresponding MoS for the participant with mTBI during an unperturbed walking segment from the first level of the simulated rocky surface walking task. The time series includes two complete walking strides (i.e., two steps per body side). As in all participants, the XCoM travels beyond the boundary of the BoS shortly after MS. Despite a

noticeable deviation in the third step where the XCoM nears the boundary of the BoS prior to mid-stance, the MoS trajectory appears similar between body sides. The representative value of MoS-MS is nearly twice that of the non-disabled sample, while the value of MoS-HS is smaller. Contrary to the non-disabled sample, MoS-MS is greater than MoS-HS for the participant with mTBI.

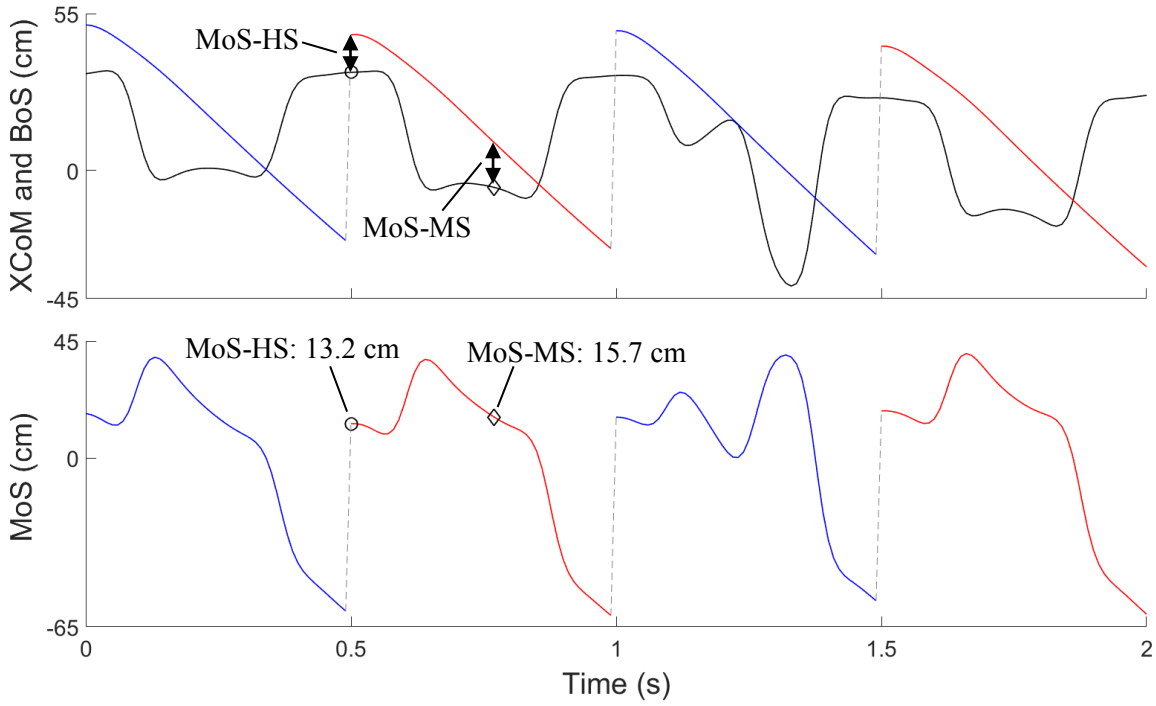

Figure 4.21: Temporal relationship between the locations of the extrapolated centre of mass (XCoM) and base of support (BoS), and the corresponding margin of stability (MoS) for two complete walking strides of the participant with mild traumatic brain injury in the anteroposterior (AP) direction. Top: black curve is the XCoM, while the red and blue lines represent the limits of the BoS defined during the stance phase of the left and right feet, respectively. Bottom: MoS for left (red) and right (blue) body sides. Markers indicate the location of contralateral toe off (cTO) and indices of the gait cycle at which each MoS measure is taken for a single step. The MoS measures indicated are: heel strike (MoS-HS) and mid-stance (MoS-MS). Values for MoS-HS and MoS-MS are also provided for a single step.

Presented in Tables 4.9 and 4.10 are mean MoS values in the ML and AP directions for all three case study participants: (1) HA, (2) TTA, and (3) mTBI. Mean values for non-disabled participants, along with standard deviations (across-participant variability) are also provided. In all but the individual with mTBI, MoS measures were generally larger for the case study participants, as compared to the non-disabled participants. Furthermore, for the ML direction, the largest values were attained for MoS-MS, followed by MoS-HS, and then MoS-HScTO. As for the AP direction, the largest values were observed for MoS-HS, as MoS-MS values were typically

much smaller. Both of the latter two observations are consistent with the findings from the non-disabled participants.

In the ML direction, the individual with HA demonstrated a greater MoS on the left body side, for all measures. Furthermore, higher variability was found for MoS measures on the right body side, in the ML direction. In the AP direction, the individual with HA exhibited an MoS-HS on the left body side that was nearly twice as large as on the right body side. As such, MoS-HS was larger on the left body side and smaller on the right body side in comparison to MoS-HS obtained from the non-disabled sample. A larger MoS-MS in the AP direction was observed on the right body side. Similar to the ML direction, greater variability occurred on the right body side.

The individual with TTA had greater mean MoS-HS and MoS-MS values on the left body side, in the ML direction. For both measures, greater variability was also observed on the left body side. The mean and within-participant variability of MoS-HScTO values was comparable between left and right body sides. In the AP direction, a larger MoS-HS was observed for the right body side, while a larger MoS-MS was seen on the left body side. The MoS-MS on the right body side was quite small and nearing instability (i.e., close to zero). Meanwhile, the MoS-HS on the left body side demonstrated a high variability (109% of mean value).

Finally, the individual with mTBI had a greater MoS on the left body side, for all measures in both the ML and AP directions. This is consistent with the visual observation made from Figure 4.20. In terms of variability, relatively high values (in comparison to the mean value) were observed in the AP direction, for MoS-HS and MoS-MS on both body sides.

Table 4.9: Margin of stability (MoS) measures in the mediolateral (ML) direction at heel strike (HS), mid-stance (MS), and the minimum between heel strike and contralateral toe off (HScTO) for case study participants with: (1) hemophilic arthropathy (HA); (2) transtibial amputation (TTA); and (3) mild traumatic brain injury (mTBI). Data are presented as group means and within-participant variability (WPV). Normative values (mean and across-participant variability) are shown for comparison purposes.

Measure		HA *Mean ± WPV*	TTA *Mean ± WPV*	mTBI *Mean ± WPV*	Norm *Mean ± SD*
MoS-HS (cm)	Left	19.4 ± 1.5	17.7 ± 3.0	11.4 ± 2.3	13.2 ± 3.9
	Right	18.8 ± 1.8	18.6 ± 1.9	10.1 ± 2.0	
MoS-MS (cm)	Left	22.8 ± 1.7	21.3 ± 2.6	19.0 ± 3.0	18.3 ± 3.1
	Right	19.6 ± 2.3	17.6 ± 1.8	16.8 ± 4.2	
MoS-HScTO (cm)	Left	19.4 ± 1.5	18.3 ± 1.8	11.6 ± 3.1	12.8 ± 4.2
	Right	18.1 ± 1.6	18.1 ± 1.6	10.0 ± 2.1	

Table 4.10: Margin of stability (MoS) measures in the anteroposterior (AP) direction at heel strike (HS), mid-stance (MS), and the minimum between heel strike and contralateral toe off (HScTO) for case study participants with: (1) hemophilic arthropathy (HA); (2) transtibial amputation (TTA); and (3) mild traumatic brain injury (mTBI). Data are presented as group means and within-participant variability (WPV). Normative values (mean and across-participant variability) are shown for comparison purposes.

Measure		HA *Mean ± WPV*	TTA *Mean ± WPV*	mTBI *Mean ± WPV*	Norm *Mean ± SD*
MoS-HS	Left	24.9 ± 2.7	12.9 ± 14.0	15.9 ± 7.1	17.6 ± 5.3
	Right	12.8 ± 4.6	19.8 ± 2.4	14.9 ± 4.9	
MoS-MS	Left	5.2 ± 1.7	11.0 ± 1.9	12.3 ± 5.2	7.5 ± 3.2
	Right	7.9 ± 3.8	1.4 ± 1.6	8.2 ± 6.6	

4.4 Discussion

The main objective of the present study was to evaluate the utility of the XCoM to quantify human gait stability in a clinical setting, using its corresponding dynamic MoS. By conducting experiments with human participants, it was found that: (1) the XCoM is a practically feasible measure to obtain, in terms of imposing minimal burden on the participant, a lack of extensive setup required, a reasonable duration of a trial, the versatility to be applied to multiple walking conditions, and a sound theoretical basis; (2) measurement of gait stability via the MoS is robust,

demonstrated by reasonable across- and within-participant variability; (3) the MoS was also a reliable measure of gait stability as it demonstrated good repeatability between sessions; and (4) the MoS has potential to be sensitive to detect impairments in gait through the deviation from normal gait values.

4.4.1 Practical Feasibility of Obtaining the XCoM and MoS

As discussed in Chapter 3, the expected burden on the patient and time constraints are two of the critical barriers to implementation of standardized outcome measures and functional assessment [194]–[196]. In the present study, we placed considerable attention to both obstacles in order to demonstrate the practical feasibility of obtaining the XCoM and MoS for use in a clinical setting. First, only 15 gait strides (i.e., 15 steps per body side) were used to compute the mean MoS values which, based on the average stride length of 1.48 m (Table 4.3), is less than 25 m of total walking distance. Granted, this does not include the time from gait initiation to the beginning of a steady-state gait pattern (i.e., comfortable pace); however, even taking this into account, the total walking distance is entirely reasonable. Furthermore, we extracted steps from multiple 10 m walking segments, which means that all 15 steps do not need to be from the same period of continuous walking. Therefore, if fatigue is of concern, it is possible to conduct multiple trials of shorter distances and allow the patient to rest in between. The relatively small number of steps also helps when considering time constraints as less walking means a shorter assessment time.

In assessing the time feasibility of an outcome measure, it is important to not only consider the overall trial time, but also the time necessary to prepare the patient and any data collection equipment. With respect to the XCoM, the greatest hindrance is regarding the CoM and v_{CoM} since the most commonly recommended method for estimating them, the kinematic method [83], [85], is relatively time-consuming. To overcome this issue, we employed an instrumented treadmill in combination with the ZPZP double-integration technique [88], [89], [182], which allowed the AP and ML components of CoM and v_{CoM} to be estimated via integration of the measured GRFs. As such, this eliminates the need for a full-body kinematic marker set. In the case where an instrumented treadmill is unavailable, the use of simplified marker sets should be explored. Havens et al. [248] suggest using either the lower extremity and trunk model, or the pelvis average model.

Although a total of 35 markers were attached to the participant's body during the protocol, only the 4-marker clusters on the back and feet were used in the analysis of the present study. By virtue of their rigid plate design, the time required to secure the marker clusters to the participant was minimal. Therefore, the use of these markers did not appreciably increase setup time or jeopardize the time feasibility of obtaining the XCoM and MoS.

4.4.2 Walking Performance by Temporo-Spatial Parameters

Overall, the temporo-spatial gait parameters obtained from non-disabled participants were comparable to similar gait studies conducted on the CAREN, such as that by Sinitski et al. [279]. Participants in the present study walked at a similar speed with slightly smaller stride and step lengths. The largest differences were observed in swing and stance time per stride (%) as Sinitski et al. [279] found lower swing time per stride and higher stance time per stride. However, the differences were less than 3% and most likely not of clinical significance. In comparison to normative values for overground walking [35], [51], the results of the present study indicate that participants walked at speeds between 'normal' and 'fast' for overground gait.

4.4.3 Gait Stability Based on the MoS

In comparing the three MoS measures for the normative sample in the ML direction, the MoS-MS was noticeably larger than both MoS-HS and MoS-HScTO. This is in contrast to the findings of Peebles et al. [97] who found lower values for MoS-MS compared to MoS-HS. Furthermore, the MoS-MS values of the present study were approximately 8 cm larger than those observed by Peebles et al. [97], while MoS-HS values were comparable. It is worth noting that participants in the comparative study walked overground, rather than on a treadmill. In addition, the position of the CoM was approximated as the geometric centre of a triangle formed by two anterior superior iliac spine markers and the midpoint between two posterior iliac spine markers.

It is also apparent that the MoS-HS and MoS-HScTO were comparable for the ML direction, based on their mean normative values and the instant at which they occur in the gait cycle. First, each lies well within the normative range (mean ± SD) of the other. Furthermore, the point at which MoS-HScTO occurs in a step is typically at HS or very shortly after (less than 0.05 s difference). Taking both details into consideration, it seems unnecessary to apply both measures when

estimating gait stability. Previous literature has cited HS to be the point at which stability is most compromised [30], [91], [280], leading to MoS-HS being the most commonly applied MoS measure [3], [19], [47], [97], [100], [266], [267]. Taking this into account, it appears sufficient to use only MoS-HS, rather than MoS-HScTO, moving forward; however, further work is necessary before altogether dismissing MoS-HScTO as a valid measure to quantify gait stability in the ML direction.

As is evident in the previous comparison to the work of Peebles et al. [97], a lack of consistency in the methods across previous studies [19], [47], [63], [70], [91], [92], [97], [98], [100], [202], [239], [266], [281]–[283] indicates that caution should be maintained when comparing to the present results. For instance, there is a high level of variation in the methods used to estimate the CoM, how the BoS is defined, and whether the MoS is quantified by the average over an entire step, or at a specific instant in each step. Differences in the prescribed walking conditions (e.g., overground, fixed treadmill speed) further complicate the comparisons.

As mentioned earlier, the normative MoS-HS estimate in the present study is comparable to that predicted by Peebles et al. [97], despite the differences in methods. As for other studies, both Hof et al. [47] and Curtze et al. [100] found very low mean MoS values for non-disabled participants. In both cases, the MoS estimates were only slightly above zero, indicating very low stability. Again, these differences may be a result of differences in methods as Hof et al. [47] low-pass filtered the CoP data to estimate CoM, used the CoP position to define the BoS, and found the minimum MoS value across an entire step, instead of directly at HS. Meanwhile, Curtze et al. [100] estimated the CoM using the kinematic method and calculated MoS-HS as the distance between the XCoM and the midline of the foot at HS during overground walking. McAndrew Young et al. [19] found higher values of MoS-HS, although still smaller than those of the present study. In this case, only the CoM estimation differed from the present study as the kinematic method was used in place of the double-integration technique.

In the AP direction, MoS-HS is much larger than MoS-MS. Given that MS is defined as the point at which the CoM passes over the stance foot in the AP direction, this observation is entirely reasonable. As the CoM travels over the foot, the two are aligned in the AP direction and, thus, the

separation distance approaches zero. As a result, MoS-MS is due only to the velocity component of the XCoM. Peebles et al. [97] also found larger values for MoS-HS than MoS-MS in non-disabled participants (AP direction), confirming our observation. However, similar to the ML direction, Peebles et al. [97] reported smaller MoS-MS and comparable MoS-HS values at preferred walking speeds, relative to the present study. At a similar walking speed (1.4 m/s) as the average for non-disabled participants in the present study (1.43 m/s), Süptitz et al. [98] found lower MoS-HS values for young adults. The normative MoS-HS values of the present study appear to match those achieved by participants walking at slower speeds (1.0-1.2 m/s). Süptitz et al. [98] calculated MoS-HS as the distance between the XCoM and a toe marker, which should effectively increase the MoS in comparison to the present study (toe marker versus marker at centre of the foot); however, participants also walked at a fixed speed. The other notable difference is that CoM was estimated using the kinematic method. Finally, McAndrew Young et al. [19] observed mean MoS-HS values for unperturbed gait that are roughly double those of the present study. While CoM estimation differed between studies, MoS-HS was measured from a toe marker at HS, rather than a marker closer to the centre of the foot. The latter distinction may explain some of the discrepancy, but certainly not all.

4.4.4 Variability and Robustness of the MoS

In evaluating the utility of a proposed outcome measure, it is important to consider the within-participant variability, as increased variability in motor performance is a key indicator of poor motor skill in some clinical populations [284]. In the context of gait, increased variability in temporo-spatial gait parameters is thought to be correlated with decreased stability and greater fall risk [8], [43], [119], [285]. Therefore, a proposed gait stability measure should demonstrate low within-participant variability in a normative sample so that accurate deductions can be made when comparing to the performance of impaired populations. For the current study, mean participant standard deviation as a measure of within-participant variability demonstrated reasonably low results for all MoS measures in the ML direction. Slightly larger within-participant variability was found for MoS-HScTO, in comparison to MoS-HS and MoS-MS. Given that the MoS-HS and MoS-MS were taken at a specific instant of the gait cycle, whereas the MoS-HScTO measure searched for the minimum MoS in the ML direction between HS and cTO, the corresponding increase in variability is entirely reasonable. In the AP direction, the MoS-HS and MoS-MS

demonstrated substantially higher within-participant variability values as they were more than twice as large as for their ML counterparts, relative to respective means. While this may question the utility of the AP measures, it is worth noting that the AP direction is the direction of travel, implying an inherent degree of variability of the measures. Adding to this, the use of the self-paced control of the treadmill may have induced greater stride-to-stride variability.

In order to be sensitive to differences, across-participant variability of a measure should, ideally, also remain low for a normative sample. However, too little variability among participants could be indicative of ceiling effects or restriction of range, both of which reveal poor measurement capabilities of the measure for the sample [286]. Keeping this in mind, estimates of across-participant variability, given by the standard deviation of the participants' means, are justifiable for all MoS measures in the ML direction, along with the MoS-HS in the AP direction. In the ML direction, the largest values in relation to the mean are again seen for MoS-HScTO, followed closely by MoS-HS. Meanwhile across-participant variability relative to the mean for MoS-MS is noticeably lower. The latter observation may be tied to the fact that MoS-MS is measured from the stance foot, whereas MoS-HScTO and MoS-HS are more closely tied to foot placement. At roughly 30% of their respective mean values, the across-participant variability for MoS-HScTO and MoS-HS in the ML direction, and MoS-HS in the AP direction are trending slightly higher. However, their utility cannot be ruled out without a comparison to measures obtained from known impairments.

As noted in the previous section, it is important to be careful when comparing the present results with other studies. However, it is still worthwhile discussing how the results relate. Contrary to Peebles et al. [97], greater across-participant variability relative to the mean was seen, in the ML direction, for MoS-MS than MoS-HS. Furthermore, across-participant variability relative to the mean was nearly identical for MoS-MS between studies, yet MoS-HS variability in the present study was nearly double that determined by Peebles et al. [97]. The results of Curtze et al. [100] revealed considerably high measurements of across-participant variability as values approached more than 100% of the mean value for MoS-HS. Again, with respect to MoS-HS, both Hof et al. [47] and McAndrew Young et al. [19] demonstrated reasonable across-participant variability relative to the mean; however, it was still slightly lower than in the present study. For MoS-

HScTO, Day et al. [202] demonstrated equal to slightly lower measurements of relative across-participant variability, whereas Rosenblatt et al. [91] reported higher results than the present study. While both of these studies used the kinematic method to estimate CoM position, each approximated the BoS differently. Day et al. [202] used the CoP position, and Rosenblatt et al. [91] used anthropometric measurements of the foot relative to body height to estimate the limits of the BoS.

In the AP direction, Peebles et al. [97] also observed greater across-participant variability relative to the mean for MoS-MS over MoS-HS. At the preferred walking speed, the variability estimates relative to their respective means were higher than those in the present study, for both MoS-MS and MoS-HS. In their study, MoS-MS demonstrated an across-participant variability greater than 100% of the mean value, making the relative value of 40% for our study seem somewhat reasonable. Concerning MoS-HS, McAndrew Young et al. showed relatively low across-participant variability as results represented less than 10% of their respective mean values. Given that Peebles et al. [97] approximated the CoM with a limited number of markers, while McAndrew Young et al. [19] used a full kinematic marker set, it is possible to speculate that this may provide reason for the difference in variability. However, the studies also differed with respect to the walking conditions studied: overground [97] versus treadmill [19].

4.4.5 Between-Session Repeatability of the MoS

To instill confidence in a measurement and, thus, ensure that it provides consistent results, a given outcome measure must demonstrate sufficient repeatability. Furthermore, in the clinical setting, patients are oftentimes evaluated on multiple occasions over a period of weeks or months to monitor changes in gait and evaluate the effectiveness of prescribed interventions. Adequate repeatability is a prerequisite for being able to detect change using a standard outcome measure. Thus, the between-session repeatability of all MoS measures was determined using an ICC(2,1) model [191]. Despite all MoS measures being calculated as the mean of 15 values (steps), an ICC(2,1) model was applied in place of ICC(2,*k*) as the value from one step does not constitute a single measurement of gait stability. Due to the natural stride-to-stride variability of gait, discrete measures, such as the MoS in this case, are computed as the mean across multiple strides (or steps)

[47], [93], [97], [100], [239], [257], [287], [288]. The mean value represents a single measure of gait stability, which was used in the assessment of repeatability for the present study.

The results of the repeatability study found that all MoS measures in the ML direction (MoS-HS, MoS-MS and MoS-HScTO) demonstrate good repeatability between sessions, whereas, in the AP direction, only the MoS-HS measure indicated good repeatability. Although this is believed to be the first study to investigate the between-session repeatability of the MoS, the ICC values are comparable to those of van Schooten et al. [272] who examined the between-session repeatability of local dynamic stability, another measure of gait stability presented in Chapter 2, for overground walking. Regardless, the indication of good repeatability, indicated by ICC values greater than 0.6, may not be sufficient for clinical application. According to the guidelines described by Kottner et al. [289], ICCs greater than 0.6 may be adequate for group-level comparisons in research, but when important clinical decisions are being made on behalf of an individual patient, ICC values of 0.9 may be necessary. Despite this, reasonable precision of these measures is indicated by the SEM values relative to their respective means. All MoS measures demonstrating good repeatability (MoS-HS, MoS-MS and MoS-HScTO in the ML direction, and MoS-HS in the AP direction) showed SEM values that were less than 20% of their respective mean values. Though the MDC values appear high relative to the mean MoS values from the normative sample, it remains possible that they still have the capacity to detect changes in gait stability. However, this observation can only be confirmed by monitoring change in individuals with a known gait impairment or balance deficit, or instances in which gait is known to be compromised (i.e., during perturbations).

Poor to fair agreement was observed for MoS-MS in the AP direction, which diminishes its suitability to be applied in future research and, certainly, in clinical settings. This is reinforced by taking a look at the poor level of precision demonstrated by the SEM in relation to the mean value. Furthermore, a high MDC value relative to the mean indicates a reduced capacity for MoS-MS to monitor change.

4.4.6 Ability to Detect Differences in Gait Stability

To evaluate the potential of the MoS to discriminate between normative participants and those with known impairments, pilot data from three case study participants were included. For this

purpose, measurements from the case study participants were compared to the estimated ranges of the mean normative values (mean ± 2SD). In doing so for the present study, all MoS measures in both the ML and AP directions remained within their respective normative range for all three case study participants. Thus, none of the MoS measures were able to detect differences in gait stability for the selected case study participants. Though this has the potential to call into question the capacity of the MoS to detect differences in gait stability for individuals with known impairments, further work is needed before dismissing the MoS as an appropriate tool for clinical gait stability assessment. It is important to note that the case study participants present a limited sample of pilot data, and it is entirely possible that their stability during gait is not representative of a larger sample. Despite all three case study participants having a diagnosed impairment, the extent to which those impairments affected their balance was unknown. It is believed, however, that all three participants were on the higher end of balance ability as all walked without walking aids at community-level ambulation (i.e., over various terrains). In the future, clinical balance assessments (e.g., Berg Balance Scale) should be included in the protocol to assist in characterizing impaired participants. Furthermore, these balance scores may be used to correlate known balance deficits to differences observed in the MoS measures.

By comparison of the within-participant variability between the normative sample and the case studies, only the individual with mTBI demonstrated higher variability throughout all measures. Interestingly, the individual with TTA demonstrated notably more variability for MoS-HS and MoS-MS in the ML direction, and MoS-HS in the AP direction, on the left side, which is the prosthetic side. Both of these observations suggest that within-participant variability of the MoS may be indicative of a difference in stability.

Despite the apparent lack of sensitivity of the MoS measures to detect differences in gait stability for the three case study participants, they do demonstrate capacity to identify asymmetries between right and left body sides. Most notable is the MoS-HS in the AP direction for the participant with HA as the value on the left body side was nearly twice as large as the one on the right. What is particularly interesting about this asymmetry is that it is only observed for MoS-HS since the temporo-spatial parameters are nearly identical across body sides. Based on the lower MoS-HS value on the right body side, it might be inferred that the participant with HA is less stable at right

HS than left HS. Given that the participant with HA is more restricted on the right body side, in terms of range of motion at the knee, this inference is plausible. However, it is difficult to confirm the validity of this observation only, without knowledge of the actual balance scores from clinical balance assessments. With respect to the participant with TTA, MoS-HS in the AP direction again provides indication of an asymmetry between body sides as the value on the left body side was roughly two-thirds of the value on the right. With the left body side being the prosthetic side, it makes sense that stability is more heavily compromised on the left side (at left HS) than on the right. This is in alignment with previous work comparing MoS values for prosthetic and non-prosthetic sides for individuals with lower-limb amputation [100], [239], [283]. While making this observation, it is worth noting that MoS-HS in the AP direction on the left body side for the participant with TTA is met with considerably high variability (109% of the mean value) in comparison to the right body side (12% of the mean value), which likely provides stronger insight into the asymmetry and compromised stability at left HS.

Although the case study participants provided only a limited sample of pilot data, their inclusion does highlight the feasibility of the overall assessment: participants with three different types of impairment were tested, all of which could perform the necessary protocol. Moving forward, the practical feasibility of the assessment should be investigated in a larger sample of participants with a wider range of functional balance impairments. Furthermore, to characterize balance impairments, future work should include balance scores based on clinical balance assessments such as the Berg Balance Scale. This would strongly assist in shedding more light on the sensitivity of MoS measures to detect differences in gait stability. Alternatively, a repeated measures investigation could be conducted in a non-disabled sample with and without an implemented intervention, such as bracing the lower-limb to restrict movement of the joints and impair balance. The body side asymmetries demonstrated by the MoS measures in the case study participants present another intriguing possibility: could a body side ratio of MoS values be used as a measure of balance asymmetry and compromised gait stability? Again, this should be evaluated in future investigations.

4.5 Conclusions

The overarching goal of this study was to evaluate the utility of the XCoM concept to quantify human gait stability (via the MoS) in a clinical setting, based on experiments conducted in human participants. As such, careful attention was given to choose data collection and analysis techniques that would overcome common barriers to clinical implementation and support its feasibility in that respect. The protocol was designed to minimize the burden on the patient, as well as the time required for setup and overall trial length. All three MoS measures in the ML direction (MoS-HS, MoS-MS and MoS-HscTO), as well as MoS-HS in the AP direction, demonstrated reasonable within- and across-participant variability, along with good repeatability between sessions. Although the repeatability results are not large enough to support clinical implementation, they are sufficient for continued use of the MoS in research. With respect to the case study comparisons, none of the MoS measures demonstrated the sensitivity necessary to detect differences in gait stability from the normative sample. However, in the AP direction, MoS-HS did indicate a potential capacity to highlight asymmetries between right and left body sides. In addition, for the ML direction, differences between MoS-HS and MoS-HScTO of the normative sample were minimal; thus, it is likely sufficient to apply only one measure moving forward. The literature would suggest this to be MoS-HS since it is more commonly used and presents the simpler option, along with lower variability. However, before altogether dismissing MoS-HScTO, further investigation is warranted to determine if the overlap between MoS-HS and MoS-HScTO is consistent across multiple populations and gait conditions. Additional work is necessary to achieve the repeatability necessary for clinical purposes and investigate the ability of the MoS measures to detect differences in gait stability a larger sample of impaired participants.

5 Conclusion

For many individuals with balance impairments, falls are a common occurrence and can result in serious injury which, in turn, also places an unsustainable burden on the healthcare system. Several targeted interventions (e.g., gait training, assistive devices) exist to mediate the risk of falls and subsequent injury; however, it is imperative that we accurately identify individuals at risk of falling and optimize interventions to suit their needs. Furthermore, a means to evaluate the effectiveness of a prescribed intervention over successive follow-up assessments is required. Unfortunately, there is yet to be a universally accepted measure to quantify dynamic gait stability and diagnose fall risk during gait (Chapter 1).

The first objective of this thesis was to conduct a literature review to identify the characteristics of proposed gait stability measures, define a set of clinical feasibility criteria, and select those measures that best adhere to the criteria for clinical implementation. In total, nine proposed gait stability measures were reviewed (Chapter 2). Of these, only the extrapolated centre of mass (XCoM), stabilizing and destabilizing forces, and gait sensitivity norm (GSN) demonstrated the required characteristics; i.e., imposing little burden on the patient; requiring minimal time to obtain the measure; being versatile in terms of applying it to multiple walking conditions; and ensuring the measure's sound theoretical link to gait mechanics (Chapter 3).

The second objective of this thesis was to evaluate the utility of one of those three identified measures – the XCoM – to quantify human stability in a clinical setting, via the margin of stability (MoS), by conducting experiments involving human participants (Chapter 4). The practical feasibility of obtaining the XCoM and MoS was demonstrated by employing data collection methods and analysis techniques that minimized the setup and overall trial time. Furthermore, the burden on the patient was lessened by collecting data across multiple intervals of shorter walking distances. The robustness of the MoS measures in the ML and AP directions was shown by assessing both the across- and within-participant variability in a sample of non-disabled participants. In addition, a between-session reliability study exhibited good results, which are sufficient for continued scientific work, but not direct clinical implementation. Finally, the capacity of all measures to detect differences in gait stability were assessed in case studies

involving three participants with known impairments: (1) hemophilia arthropathy, (2) unilateral transtibial amputation, and (3) mild traumatic brain injury. Overall, the MoS-HS provided the best combination of robustness and repeatability. Furthermore, MoS-HS was able to highlight body side differences in the AP direction. Though further work is certainly warranted, it is recommended to focus attention on using MoS-HS to quantify gait stability for both directions in future work.

5.1 Future Directions

To be considered for clinical implementation, the XCoM and MoS require further investigation. First and foremost, a protocol adequate to achieve reliability sufficient for clinical use (ICC > 0.9) is necessary. One suggestion might be to assess the change in ICCs for MoS values computed from a greater number of steps. The ability to obtain reliable estimates at an individual, patient-specific level over successive sessions is vital to the clinical validation of the XCoM and MoS.

Further investigation is also warranted, in impaired populations, when assessing the sensitivity of the MoS to detect differences in gait stability. This is a critical step towards identifying individuals with reduced gait stability and diagnosing the risk of falling. The MoS also needs to have adequate sensitivity to detect changes in gait stability as a result of prescribed interventions, and to grade the effect that those have on balance during walking. Thus, additional studies aimed at assessing stability before and after an intervention, or through the course of an intervention (e.g., gait training), should be conducted.

Finally, a standardized means of determining the MoS, in terms of how the value over a step is quantified and how the BoS is defined, is absolutely necessary. As it stands now, it is incredibly difficult to make comparisons across studies due to a lack of consistency in the methods used. Developing a standard definition for the above quantities, similar to those of the temporo-spatial parameters, will be critical for collecting standardized normative reference values against which to make comparisons.

References

[1] M. D. Chang, E. Sejdić, V. Wright, and T. Chau, "Measures of dynamic stability: Detecting differences between walking overground and on a compliant surface," *Hum. Mov. Sci.*, vol. 29, no. 6, pp. 977–986, 2010.

[2] F. Reynard, P. Vuadens, O. Deriaz, and P. Terrier, "Could local dynamic stability serve as an early predictor of falls in patients with moderate neurological gait disorders? A reliability and comparison study in healthy individuals and in patients with paresis of the lower extremities," *PLoS One*, vol. 9, no. 6, 2014.

[3] V. Lugade, V. Lin, and L. S. Chou, "Center of mass and base of support interaction during gait," *Gait Posture*, vol. 33, no. 3, pp. 406–411, 2011.

[4] S. M. O'Connor and A. D. Kuo, "Direction-Dependent Control of Balance During Walking and Standing," *J. Neurophysiol.*, vol. 102, pp. 1411–1419, 2009.

[5] K. Terry, E. H. Sinitski, J. B. Dingwell, and J. M. Wilken, "Amplitude effects of medio-lateral mechanical and visual perturbations on gait," *J. Biomech.*, vol. 45, no. 11, pp. 1979–1986, 2012.

[6] M. Millard, D. Wight, J. McPhee, E. Kubica, and D. Wang, "Human foot placement and balance in the sagittal plane.," *J. Biomech. Eng.*, vol. 131, no. December 2009, p. 121001, 2009.

[7] J. B. Dingwell and H. G. Kang, "Differences Between Local and Orbital Dynamic Stability During Human Walking," *J. Biomech. Eng.*, vol. 129, no. 4, p. 586, 2006.

[8] J. M. Hausdorff, D. A. Rios, and H. K. Edelberg, "Gait variability and fall risk in community-living older adults: A 1-year prospective study," *Arch. Phys. Med. Rehabil.*, vol. 82, no. 8, pp. 1050–1056, 2001.

[9] V. Scott, L. Wagar, and S. Elliott, "Falls & Related Injuries among Older Canadians: Fall-related Hospitalizations & Prevention Initiatives," *Div. Aging Seniors, Public Heal. Agency Canada*, pp. 1–43, 2011.

[10] A. Stinchcombe, N. Kuran, and S. Powell, *Seniors' falls in Canada: Second report: Key highlights*, vol. 34, no. 2–3. 2014.

[11] W. P. Berg, H. M. Alessio, E. M. Mills, and C. Tong, "Circumstances and consequences of falls in independent community-dwelling older adults," *Age Ageing*, vol. 26, no. 4, pp. 261–

268, 1997.

[12] J. R. Center, “Mortality after all major types of osteoporotic fracture in men and women: an observational study.,” *Lancet*, vol. 153, pp. 878–882, 1999.

[13] J. Howcroft, J. Kofman, and E. D. Lemaire, “Review of fall risk assessment in geriatric populations using inertial sensors,” *J. Neuroeng. Rehabil.*, vol. 10, no. 1, p. 91, 2013.

[14] C. Tiseo and W. T. Ang, “The Balance: An energy management task,” *Proc. IEEE RAS EMBS Int. Conf. Biomed. Robot. Biomechatronics*, vol. 2016–July, pp. 723–728, 2016.

[15] S. M. Bruijn, O. G. Meijer, P. J. Beek, and J. H. van Dieën, “Assessing the stability of human locomotion: a review of current measures.,” *J. R. Soc. Interface*, vol. 10, no. 83, p. 20120999, 2013.

[16] S. N. Robinovitch, F. Feldman, Y. Yang, R. Schonnop, P. M. Leung, T. Sarraf, J. Sims-Gould, and M. Loughin, “Video capture of the circumstances of falls in elderly people residing in long-term care: An observational study,” *Lancet*, vol. 381, no. 9860, pp. 47–54, 2013.

[17] F. Yang and Y. C. Pai, “Can stability really predict an impending slip-related fall among older adults?,” *J. Biomech.*, vol. 47, no. 16, pp. 3876–3881, 2014.

[18] J. B. Dingwell, J. P. Cusumano, D. Sternad, and P. R. Cavanagh, “Slower speeds in patients with diabetic neuropathy,” *J. Biomech.*, vol. 33, pp. 1269–1277, 2000.

[19] P. M. McAndrew Young, J. M. Wilken, and J. B. Dingwell, “Dynamic margins of stability during human walking in destabilizing environments,” *J. Biomech.*, vol. 45, no. 6, pp. 1053–1059, 2012.

[20] H. Leipholz, *Stability theory: An Introduction to the Stability of Dynamic Systems and Rigid Bodies*. 1970.

[21] N. Peter Reeves, K. S. Narendra, and J. Cholewicki, “Spine stability: The six blind men and the elephant,” *Clin. Biomech.*, vol. 22, no. 3, pp. 266–274, 2007.

[22] E. H. Sinitksi, K. Terry, J. M. Wilken, and J. B. Dingwell, “Effects of perturbation magnitude on dynamic stability when walking in destabilizing environments,” *J. Biomech.*, vol. 45, no. 12, pp. 2084–2091, 2012.

[23] A. Bruton, J. H. Conway, and S. T. Holgate, “Reliability: What is it, and how is it measured?,” *Physiotherapy*, vol. 86, no. 2, pp. 94–99, 2000.

[24] R. Bellman, *Stability Theory of Differential Equations*. New York: McGraw-Hill, 1953.

[25] N. P. Reeves and J. Cholewicki, “Modeling the human lumbar spine for assessing spinal loads, stability, and risk of injury.,” *Crit. Rev. Biomed. Eng.*, vol. 31, no. 1–2, pp. 73–139, 2003.

[26] F. Riva, M. C. Bisi, and R. Stagni, “Orbital stability analysis in biomechanics: A systematic review of a nonlinear technique to detect instability of motor tasks,” *Gait Posture*, vol. 37, no. 1, pp. 1–11, 2013.

[27] S. M. Bruijn, “Is stability an unstable concept ? Quantifying dynamic stability of human locomotion,” no. October, p. 102, 2010.

[28] P. M. McAndrew, J. M. Wilken, and J. B. Dingwell, “Dynamic stability of human walking in visually and mechanically destabilizing environments,” *J. Biomech.*, vol. 44, no. 4, pp. 644–649, 2010.

[29] Y. Hurmuzlu, C. Basdogan, Y. Hurmuzlue, and C. Basdogan, “On the measurement of dynamic stability of human locomotion,” *J. Biomech. Eng.*, vol. 116, no. February 1994, pp. 30–36, 1994.

[30] A. L. Hof, “The ‘extrapolated center of mass’ concept suggests a simple control of balance in walking,” *Hum. Mov. Sci.*, vol. 27, no. 1, pp. 112–125, 2008.

[31] C. Duclos, P. Desjardins, S. Nadeau, A. Delisle, D. Gravel, B. Brouwer, and H. Corriveau, “Destabilizing and stabilizing forces to assess equilibrium during everyday activities - Supporting Info B,” p. 3.

[32] S. M. Bruijn, M. Wisse, E. Draaijers, J. H. van Dieën, O. G. Meijer, and P. J. Beek, “The gait sensitivity norm in human walking,” *Dyn. Walk. 2008*, p. 9023121, 2008.

[33] S. Damouras, M. D. Chang, E. Sejdić, and T. Chau, “An empirical examination of detrended fluctuation analysis for gait data,” *Heal. Environ. Res. Des. J.*, vol. 4, no. 1, pp. 11–33, 2009.

[34] D. Hamacher, N. B. Singh, J. H. Van Dieën, M. O. Heller, and W. R. Taylor, “Kinematic measures for assessing gait stability in elderly individuals: a systematic review.,” *J. R. Soc. Interface*, vol. 8, no. 65, pp. 1682–98, 2011.

[35] T. Oberg, A. Karsznia, and K. Oberg, “Basic gait parameters: reference data for normal subjects, 10-79 years of age.,” *J. Rehabil. Res. Dev.*, vol. 30, no. 2, pp. 210–23, 1993.

[36] J. H. Hollman, E. M. McDade, and R. C. Petersen, “Normative Spatiotemporal Gait Parameters in Older Adults,” vol. 86, no. 12, pp. 3279–3288, 2011.

[37] A. Wolf, J. B. Swift, H. L. Swinney, and J. A. Vastano, "Determining Lyapunov exponents from a time series," *Phys. D Nonlinear Phenom.*, vol. 16, no. 3, pp. 285–317, 1985.

[38] M. T. Rosenstein, J. J. Collins, and C. J. De Luca, "A practical method for calculating largest Lyapunov exponents from small data sets," *Phys. D*, vol. 65, pp. 117–134, 1993.

[39] A. L. Hof, M. G. J. Gazendam, and W. E. Sinke, "The condition for dynamic stability," *J. Biomech.*, vol. 38, no. 1, pp. 1–8, 2005.

[40] C. Duclos, P. Desjardins, S. Nadeau, A. Delisle, D. Gravel, B. Brouwer, and H. Corriveau, "Destabilizing and stabilizing forces to assess equilibrium during everyday activities," *J. Biomech.*, vol. 42, no. 3, pp. 379–382, 2009.

[41] D. G. E. Hobbelen and M. Wisse, "A disturbance rejection measure for limit cycle walkers: The gait sensitivity norm," *IEEE Trans. Robot.*, vol. 23, no. 6, pp. 1213–1224, 2007.

[42] L. D. Aarts, S. M. Bruijn, J. C. van den Noort, L. H. Sloot, and J. Harlaar, "The Gait Sensitivity Norm as a measure of human gait stability," *Pap. Present. Motek User Gr. Meet. World Congr. ISGPR*, vol. 2014, no. September, 2014.

[43] T. M. Owings and M. D. Grabiner, "Measuring step kinematic variability on an instrumented treadmill: How many steps are enough?," *J. Biomech.*, vol. 36, no. 8, pp. 1215–1218, 2003.

[44] J. M. Hausdorff, C. K. Peng, Z. Ladin, J. Y. Wei, and a L. Goldberger, "Is walking a random walk? Evidence for long-range correlations in stride interval of human gait.," *J. Appl. Physiol.*, vol. 78, no. 1, pp. 349–358, 1995.

[45] D. L. Wight, E. G. Kubica, and D. W. L. Wang, "Introduction of the Foot Placement Estimator: A Dynamic Measure of Balance for Bipedal Robotics," *J. Comput. Nonlinear Dyn.*, vol. 3, no. 1, p. 011009, 2008.

[46] M. Millard, J. McPhee, and E. Kubica, "Foot Placement and Balance in 3D," *J. Comput. Nonlinear Dyn.*, vol. 7, no. 2, p. 021015, 2012.

[47] A. L. Hof, R. M. van Bockel, T. Schoppen, and K. Postema, "Control of lateral balance in walking. Experimental findings in normal subjects and above-knee amputees," *Gait Posture*, vol. 25, no. 2, pp. 250–258, 2007.

[48] L. Hak, H. Houdijk, P. J. Beek, and J. H. Van Dieë, "Steps to take to enhance gait stability: The effect of stride frequency, stride length, and walking speed on local dynamic stability and margins of stability," *PLoS One*, vol. 8, no. 12, 2013.

[49] S. A. England and K. P. Granata, “The influence of gait speed on local dynamic stability of walking,” *Gait Posture*, vol. 25, no. 2, pp. 172–178, 2007.

[50] J. B. Dingwell, J. P. Cusumano, P. R. Cavanagh, and D. Sternad, “Local Dynamic Stability Versus Kinematic Variability of Continuous Overground and Treadmill Walking,” *J. Biomech. Eng.*, vol. 123, no. 1, p. 27, 2001.

[51] B. Auvinet, G. Berrut, C. Touzard, L. Moutel, N. Collet, D. Chaleil, and E. Barrey, “Reference data for normal subjects obtained with an accelerometric device,” *Gait Posture*, vol. 16, no. 2, pp. 124–134, 2002.

[52] J. C. Menant, J. R. Steele, H. B. Menz, B. J. Munro, and S. R. Lord, “Effects of walking surfaces and footwear on temporo-spatial gait parameters in young and older people,” *Gait Posture*, vol. 29, no. 3, pp. 392–397, 2009.

[53] D. H. Gates, J. M. Wilken, S. J. Scott, E. H. Sinitski, and J. B. Dingwell, “Kinematic strategies for walking across a destabilizing rock surface,” *Gait Posture*, vol. 35, no. 1, pp. 36–42, 2012.

[54] M. Punt, S. M. Bruijn, H. Wittink, I. G. van de Port, G. Wubbels, and J. H. van Dieën, “Virtual obstacle crossing: Reliability and differences in stroke survivors who prospectively experienced falls or no falls,” *Gait Posture*, vol. 58, no. March, pp. 533–538, 2017.

[55] J. W. Chow, S. a Yablon, T. S. Horn, and D. S. Stokic, “Temporospatial characteristics of gait in patients with lower limb muscle hypertonia after traumatic brain injury.,” *Brain Inj.*, vol. 24, no. 13–14, pp. 1575–84, 2010.

[56] L. Hak, J. H. Van Dieën, P. Van Der Wurff, M. R. Prins, A. Mert, P. J. Beek, and H. Houdijk, “Walking in an unstable environment: Strategies used by transtibial amputees to prevent falling during gait,” *Arch. Phys. Med. Rehabil.*, vol. 94, no. 11, pp. 2186–2193, 2013.

[57] A. L. Hof, S. M. Vermerris, and W. A. Gjaltema, “Balance responses to lateral perturbations in human treadmill walking,” *J. Exp. Biol.*, vol. 213, no. Pt 15, pp. 2655–64, 2010.

[58] A. Forner Cordero, H. F. J. M. Koopman, and F. C. T. Van der Helm, “Multiple-step strategies to recover from stumbling perturbations,” *Gait Posture*, vol. 18, no. 1, pp. 47–59, 2003.

[59] A. M. Schillings, B. M. H. Van Wezel, and J. Duysens, “Mechanically induced stumbling during human treadmill walking,” *J. Neurosci. Methods*, vol. 67, no. 1, pp. 11–17, 1996.

[60] a M. Schillings, B. M. van Wezel, T. Mulder, and J. Duysens, “Muscular responses and

movement strategies during stumbling over obstacles.," *J. Neurophysiol.*, vol. 83, no. 4, pp. 2093–2102, 2000.

[61] C. Shirota, A. M. Simon, E. J. Rouse, and T. A. Kuiken, "The effect of perturbation onset timing and length on tripping recovery strategies," *Proc. Annu. Int. Conf. IEEE Eng. Med. Biol. Soc. EMBS*, pp. 7833–7836, 2011.

[62] C. Shirota, A. M. Simon, and T. A. Kuiken, "Trip recovery strategies following perturbations of variable duration," *J. Biomech.*, vol. 47, no. 11, pp. 2679–2684, 2014.

[63] H. Reimann, T. D. Fettrow, E. D. Thompson, P. Agada, B. J. McFadyen, and J. J. Jeka, "Complementary mechanisms for upright balance during walking," *PLoS One*, vol. 12, no. 2, pp. 1–16, 2017.

[64] F. B. Horak and L. M. Nashner, "Central programming of postural movements: adaptation to altered support-surface configurations.," *J. Neurophysiol.*, vol. 55, no. 6, pp. 1369–1381, 1986.

[65] V. A. Stanhope, B. A. Knarr, D. S. Reisman, and J. S. Higginson, "Frontal plane compensatory strategies associated with self-selected walking speed in individuals post-stroke," *Clin. Biomech.*, vol. 29, no. 5, pp. 518–522, 2014.

[66] M. J. Major, R. L. Stine, and S. A. Gard, "The effects of walking speed and prosthetic ankle adapters on upper extremity dynamics and stability-related parameters in bilateral transtibial amputee gait," *Gait Posture*, vol. 38, no. 4, pp. 858–863, 2013.

[67] S. Kimel-Naor, A. Gottlieb, and M. Plotnik, "The effect of uphill and downhill walking on gait parameters: A self-paced treadmill study," *J. Biomech.*, vol. 60, pp. 142–149, 2017.

[68] B. L. Rankin, S. K. Buffo, and J. C. Dean, "A neuromechanical strategy for mediolateral foot placement in walking humans.," *J. Neurophysiol.*, vol. 112, no. 2, pp. 374–83, 2014.

[69] L. I. E. Oddsson, C. Wall, M. D. McPartland, D. E. Krebs, and C. A. Tucker, "Recovery from perturbations during paced walking," *Gait Posture*, vol. 19, no. 1, pp. 24–34, 2004.

[70] L. Hak, H. Houdijk, P. Van Der Wurff, M. R. Prins, A. Mert, P. J. Beek, and J. H. Van Dieën, "Stepping strategies used by post-stroke individuals to maintain margins of stability during walking," *Clin. Biomech.*, vol. 28, no. 9–10, pp. 1041–1048, 2013.

[71] R. A. Brady, B. T. Peters, and J. J. Bloomberg, "Strategies of healthy adults walking on a laterally oscillating treadmill," *Gait Posture*, vol. 29, no. 4, pp. 645–649, 2009.

[72] R. Senden, H. H. C. M. Savelberg, J. Adam, B. Grimm, I. C. Heyligers, and K. Meijer, "The

influence of age, muscle strength and speed of information processing on recovery responses to external perturbations in gait," *Gait Posture*, vol. 39, no. 1, pp. 513–517, 2014.

[73] S. M. Bruijn, J. H. van Dieën, O. G. Meijer, and P. J. Beek, "Statistical precision and sensitivity of measures of dynamic gait stability," *J. Neurosci. Methods*, vol. 178, no. 2, pp. 327–333, 2009.

[74] A. M. Fraser and H. L. Swinney, "Independent coordinates for strange attractors from mutual information," *Physical Review A*, vol. 33, no. 2. pp. 1134–1140, 1986.

[75] C. A. Rabago, J. B. Dingwell, and J. M. Wilken, "Reliability and minimum detectable change of temporal-spatial, kinematic, and dynamic stability measures during perturbed gait," *PLoS One*, vol. 10, no. 11, pp. 1–22, 2015.

[76] M. Kennel, R. Brown, and H. Abarbanel, "Determining the embedding dimension for phase-space reconstruction using a geometrical construction," vol. 24, no. 1, pp. 5–6, 1991.

[77] L. H. Sloot, K. S. Van Schooten, S. M. Bruijn, H. Kingma, M. Pijnappels, and J. H. Van Dieën, "Sensitivity of local dynamic stability of over-ground walking to balance impairment due to galvanic vestibular stimulation," *Ann. Biomed. Eng.*, vol. 39, no. 5, pp. 1563–1569, 2011.

[78] J. L. Chen and D. Y. Gu, "Local dynamic stability of lower extremity joints in lower limb amputees during slope walking," *Proc. Annu. Int. Conf. IEEE Eng. Med. Biol. Soc. EMBS*, pp. 7241–7244, 2013.

[79] J. Stenum, S. M. Bruijn, and B. R. Jensen, "The effect of walking speed on local dynamic stability is sensitive to calculation methods," *J. Biomech.*, vol. 47, no. 15, pp. 3776–3779, 2014.

[80] D. H. Gates and J. B. Dingwell, "Comparison of different state space definitions for local dynamic stability analyses," *J. Biomech.*, vol. 42, no. 9, pp. 1345–1349, 2009.

[81] R. Beurskens, J. M. Wilken, and J. B. Dingwell, "Dynamic stability of superior vs. inferior body segments in individuals with transtibial amputation walking in destabilizing environments," *J. Biomech.*, vol. 47, no. 12, pp. 3072–3079, 2014.

[82] Y. C. Pai and J. Patton, "Center of mass velocity-position predictions for balance control," *J. Biomech.*, vol. 30, no. 4, pp. 347–354, 1997.

[83] D. Lafond, M. Duarte, and F. Prince, "Comparison of three methods to estimate the center of mass during balance assessment," *J. Biomech.*, vol. 37, no. 9, pp. 1421–1426, 2004.

[84] F. Yang and Y. C. Pai, “Can sacral marker approximate center of mass during gait and slip-fall recovery among community-dwelling older adults?,” *J. Biomech.*, vol. 47, no. 16, pp. 3807–3812, 2014.

[85] R. Tisserand, T. Robert, R. Dumas, and L. Chèze, “A simplified marker set to define the center of mass for stability analysis in dynamic situations,” *Gait Posture*, vol. 48, pp. 64–67, 2016.

[86] D. Lenzi, A. Cappello, and L. Chiari, “Influence of body segment parameters and modeling assumptions on the estimate of center of mass trajectory,” *J. Biomech.*, vol. 36, no. 9, pp. 1335–1341, 2003.

[87] D. L. King and V. M. Zatsiorsky, “Extracting gravity line displacement from stabilographic recordings,” *Gait Posture*, vol. 6, no. 1, pp. 27–38, 1997.

[88] V. M. Zatsiorsky and M. Duarte, “Instant Equilibrium Point and Its Migration in Standing Tasks: Rambling and Trembling Components of the Stabilogram,” *Motor Control*, vol. 3, no. 1, pp. 28–38, 1999.

[89] V. M. Zatsiorsky and D. L. King, “An algorithm for determining gravity line location from posturographic recordings,” *J. Biomech.*, vol. 31, no. 2, pp. 161–164, 1997.

[90] O. Caron, B. Faure, and Y. Brenière, “Estimating the centre of gravity of the body on the basis of the centre of pressure in standing posture,” *J. Biomech.*, vol. 30, no. 11–12, pp. 1169–1171, 1997.

[91] N. J. Rosenblatt and M. D. Grabiner, “Measures of frontal plane stability during treadmill and overground walking,” *Gait Posture*, vol. 31, no. 3, pp. 380–384, 2010.

[92] N. J. Rosenblatt, C. P. Hurt, and M. D. Grabiner, “Sensitivity of dynamic stability to changes in step width during treadmill walking by young adults,” *J. Appl. Biomech.*, vol. 28, no. 5, pp. 616–621, 2012.

[93] T. Caderby, E. Yiou, N. Peyrot, M. Begon, and G. Dalleau, “Influence of gait speed on the control of mediolateral dynamic stability during gait initiation,” *J. Biomech.*, vol. 47, no. 2, pp. 417–423, 2014.

[94] W. Nakano, T. Fukaya, Y. Kanai, K. Akizuki, and Y. Ohashi, “Effects of temporal constraints on medio-lateral stability when negotiating obstacles,” *Gait Posture*, vol. 42, no. 2, pp. 158–164, 2015.

[95] F. Aprigliano, D. Martelli, P. Tropea, S. Micera, and V. Monaco, “Effects of slipping-like

perturbation intensity on the dynamical stability," *Proc. Annu. Int. Conf. IEEE Eng. Med. Biol. Soc. EMBS*, vol. 2015–Novem, no. Figure 1, pp. 5295–5298, 2015.

[96] M. Vlutters, E. H. F. Van Asseldonk, and H. Van der Kooij, "Center of mass velocity based predictions in balance recovery following pelvis perturbations during human walking," *J. Exp. Biol.*, pp. 1514–1523, 2016.

[97] A. T. Peebles, A. Reinholdt, A. P. Bruetsch, S. G. Lynch, and J. M. Huisinga, "Dynamic margin of stability during gait is altered in persons with multiple sclerosis," *J. Biomech.*, vol. 49, no. 16, pp. 3949–3955, 2016.

[98] F. Süptitz, K. Karamanidis, M. M. Catalá, and G. P. Brüggemann, "Symmetry and reproducibility of the components of dynamic stability in young adults at different walking velocities on the treadmill," *J. Electromyogr. Kinesiol.*, vol. 22, no. 2, pp. 301–307, 2012.

[99] L. Hak, H. Houdijk, F. Steenbrink, A. Mert, P. Van der Wurff, P. J. Beek, and J. H. Van Dieën, "Speeding up or slowing down?: Gait adaptations to preserve gait stability in response to balance perturbations," *Gait Posture*, vol. 36, no. 2, pp. 260–264, 2012.

[100] C. Curtze, A. L. Hof, K. Postema, and B. Otten, "Over rough and smooth: Amputee gait on an irregular surface," *Gait Posture*, vol. 33, no. 2, pp. 292–296, 2011.

[101] Y. Koyama, H. Tateuchi, R. Nishimura, X. Ji, H. Umegaki, M. Kobayashi, and N. Ichihashi, "Relationships between performance and kinematic/kinetic variables of stair descent in patients with medial knee osteoarthritis: An evaluation of dynamic stability using an extrapolated center of mass," *Clin. Biomech.*, vol. 30, no. 10, pp. 1066–1070, 2015.

[102] F. Yang, T. Bhatt, and Y.-C. Pai, "Role of stability and limb support in recovery against a fall following a novel slip induced in different daily activities," *Phys. Ther.*, vol. 42, no. 12, pp. 1903–1908, 2010.

[103] A. Delisle, M. Gagnon, and P. Desjardins, "Knee flexion and base of support in asymmetrical handling: Effects on the worker's dynamic stability and the moments of the L5/S1 and knee joints," *Clin. Biomech.*, vol. 13, no. 7, pp. 506–514, 1998.

[104] É. Desrosiers, S. Nadeau, and C. Duclos, "Balance during walking on an inclined instrumented pathway following incomplete spinal cord injury," *Spinal Cord*, vol. 53, no. 5, pp. 387–394, 2015.

[105] J.-F. Lemay, C. Duclos, S. Nadeau, and D. H. Gagnon, "Postural control during gait initiation and termination of adults with incomplete spinal cord injury," *Hum. Mov. Sci.*,

vol. 41, pp. 20–31, 2015.

[106] J. F. Lemay, C. Duclos, S. Nadeau, D. Gagnon, and É. Desrosiers, “Postural and dynamic balance while walking in adults with incomplete spinal cord injury,” *J. Electromyogr. Kinesiol.*, vol. 24, no. 5, pp. 739–746, 2014.

[107] Y. Mullie and C. Duclos, “Role of proprioceptive information to control balance during gait in healthy and hemiparetic individuals,” *Gait Posture*, vol. 40, no. 4, pp. 610–615, 2014.

[108] C. Duclos, C. Miéville, D. Gagnon, and C. Leclerc, “Dynamic stability requirements during gait and standing exergames on the wii fit® system in the elderly.,” *J. Neuroeng. Rehabil.*, vol. 9, p. 28, 2012.

[109] N. Ilmane, S. Croteau, and C. Duclos, “Quantifying dynamic and postural balance difficulty during gait perturbations using stabilizing/destabilizing forces,” *J. Biomech.*, vol. 48, no. 3, pp. 441–448, 2015.

[110] S. N. M. Thangal, M. Talaty, and S. Balasubramanian, “Assessment of gait sensitivity norm as a predictor of risk of falling during walking in a neuromusculoskeletal model,” *Med. Eng. Phys.*, vol. 35, no. 10, pp. 1483–1489, 2013.

[111] D. G. E. Hobbelen and M. Wisse, “Swing-leg retraction for limit cycle walkers improves disturbance rejection,” *IEEE Trans. Robot.*, vol. 24, no. 2, pp. 377–389, 2008.

[112] D. G. E. Hobbelen and M. Wisse, “Controlling the Walking Speed in Limit Cycle Walking,” *Int. J. Rob. Res.*, vol. 27, no. 9, pp. 989–1005, 2008.

[113] T. Hayashi, M. Yamakita, Y. Hanazawa, and F. Asano, “Robust walking of biped robot on uneven terrain using effect of wobbling mass,” *2014 IEEE Int. Conf. Robot. Biomimetics, IEEE ROBIO 2014*, pp. 2080–2085, 2014.

[114] T. Hayashi and M. Yamakita, “Robust analysis of biped walking on uneven terrain using output zeroing controls,” *2015 IEEE Int. Conf. Robot. Biomimetics, IEEE-ROBIO 2015*, pp. 505–510, 2016.

[115] X. Zang, X. Liu, Y. Zhu, and J. Zhao, “Study of human walking patterns based on the parameter optimization of a passive dynamic walking robot,” *Technol. Heal. Care*, vol. 24, pp. S849–S858, 2016.

[116] N. Stergiou and L. M. Decker, “Human Movement Variability, Nonlinear Dynamics, and Pathology: Is There A Connection?,” *Hum. Mov. Sci.*, vol. 30, no. 5, pp. 869–888, 2011.

[117] L. M. Decker, C. Moraiti, N. Stergiou, and A. D. Georgoulis, “New insights into anterior

cruciate ligament deficiency and reconstruction through the assessment of knee kinematic variability in terms of nonlinear dynamics," *Knee Surgery, Sport. Traumatol. Arthrosc.*, vol. 19, no. 10, pp. 1620–1633, 2011.

[118] C. Moraiti, N. Stergiou, S. Ristanis, and A. D. Georgoulis, "ACL deficiency affects stride-to-stride variability as measured using nonlinear methodology," *Knee Surgery, Sport. Traumatol. Arthrosc.*, vol. 15, no. 12, pp. 1406–1413, 2007.

[119] B. E. Maki, "Gait changes in older adults: predictors of falls or indicators of fear.," *J. Am. Geriatr. Soc.*, vol. 45, no. 3, pp. 313–320, 1997.

[120] P. C. Grabiner, S. T. Biswas, and M. D. Grabiner, "Age-related changes in spatial and temporal gait variables," *Arch. Phys. Med. Rehabil.*, vol. 82, no. 1, pp. 31–35, 2001.

[121] C. K. Peng, S. Havlin, H. E. Stanley, and A. L. Goldberger, "Long-range anti-correlations and non- Gaussian Behavior of the heartbeat," *Phys. Rev. Lett.*, vol. 70, no. 9, pp. 1343–1346, 1995.

[122] K. Jordan, J. H. Challis, and K. M. Newell, "Speed influences on the scaling behavior of gait cycle fluctuations during treadmill running," *Hum. Mov. Sci.*, vol. 26, no. 1, pp. 87–102, 2007.

[123] A. D. Kuo, J. M. Donelan, and A. Ruina, "Energetic consequences of walking like an inverted pendulum: step-to-step transitions.," *Exerc. Sport Sci. Rev.*, vol. 33, no. 2, pp. 88–97, 2005.

[124] S. M. Bruijn, M. Millard, L. van Gestel, P. Meyns, I. Jonkers, and K. Desloovere, "Gait stability in children with Cerebral Palsy," *Res. Dev. Disabil.*, vol. 34, no. 5, pp. 1689–1699, 2013.

[125] S. R. Geiringer, "The biomechanics of running," *J. Back Musculoskelet. Rehabil.*, vol. 5, no. 4, pp. 273–279, 1995.

[126] H. Haruna, S. Sugihara, K. Kon, T. Miyasaka, Y. Hayakawa, T. Nosaka, and K. Kimura, "Change in the Mechanical Energy of the Body Center of Mass in Hemiplegic Gait after Continuous Use of a Plantar Flexion Resistive Ankle-foot Orthosis," *J. Phys. Ther. Sci.*, vol. 25, no. 11, pp. 1437–1443, 2013.

[127] P. Meyns, J. Duysens, and K. Desloovere, "The arm posture in children with unilateral Cerebral Palsy is mainly related to antero-posterior gait instability," *Gait Posture*, vol. 49, pp. 132–135, 2016.

[128] D. A. Winter, *Biomechanics and motor control of human movement*. 2009.

[129] H. M. Herr and M. Popovic, "Angular momentum in human walking.," *J. Exp. Biol.*, vol. 211, no. Pt 4, pp. 467–81, 2008.

[130] M. J. Pearcy and R. J. Hindle, "New method for the non-invasive three-dimensional measurement of human back movement," *Clin. Biomech.*, vol. 4, no. 2, pp. 73–79, 1989.

[131] A. M. J. Bull, F. H. Berkshire, and A. A. Amis, "Accuracy of an electromagnetic measurement device and application to the measurement and description of knee joint motion," *Proc. Inst. Mech. Eng. Part H J. Eng. Med.*, vol. 212, no. 5, pp. 347–355, 1998.

[132] K. N. An, M. C. Jacobsen, L. J. Berglund, and E. Y. S. Chao, "Application of a magnetic tracking device to kinesiolgic studies.," *J. Biomech.*, vol. 21, no. 7, pp. 613–620, 1988.

[133] P. M. Mills, S. Morrison, D. G. Lloyd, and R. S. Barrett, "Repeatability of 3D gait kinematics obtained from an electromagnetic tracking system during treadmill locomotion," *J. Biomech.*, vol. 40, no. 7, pp. 1504–1511, 2007.

[134] E. A. Hassan, T. R. Jenkyn, and C. E. Dunning, "Direct comparison of kinematic data collected using an electromagnetic tracking system versus a digital optical system," *J. Biomech.*, vol. 40, no. 4, pp. 930–935, 2007.

[135] C. Wong, Z. Q. Zhang, B. Lo, and G. Z. Yang, "Wearable Sensing for Solid Biomechanics: A Review," *IEEE Sens. J.*, vol. 15, no. 5, pp. 2747–2760, 2015.

[136] P. B. Shull, W. Jirattigalachote, M. A. Hunt, M. R. Cutkosky, and S. L. Delp, "Quantified self and human movement: A review on the clinical impact of wearable sensing and feedback for gait analysis and intervention," *Gait Posture*, vol. 40, no. 1, pp. 11–19, 2014.

[137] A. Salarian, H. Russmann, F. J. G. Vingerhoets, C. Dehollain, Y. Blanc, P. R. Burkhard, and K. Aminian, "Gait assessment in Parkinson's disease: Toward an ambulatory system for long-term monitoring," *IEEE Trans. Biomed. Eng.*, vol. 51, no. 8, pp. 1434–1443, 2004.

[138] A. M. Sabatini, "Integration Method for Applications of Inertial Sensing To Gait Analysis," *Med. Biol. Eng.*, vol. 43, no. 2002, 2005.

[139] J. R. Rebula, L. V. Ojeda, P. G. Adamczyk, and A. D. Kuo, "Measurement of foot placement and its variability with inertial sensors," *Gait Posture*, vol. 38, no. 4, pp. 974–980, 2013.

[140] T. Liu, Y. Inoue, and K. Shibata, "Development of a wearable sensor system for quantitative gait analysis," *Meas. J. Int. Meas. Confed.*, vol. 42, no. 7, pp. 978–988, 2009.

[141] H. Dejnabadi, B. M. Jolles, E. Casanova, P. Fua, and K. Aminian, "Estimation and

visualization of sagittal kinematics of lower limbs orientation using body-fixed sensors," *IEEE Trans. Biomed. Eng.*, vol. 53, no. 7, pp. 1385–1393, 2006.

[142] F. B. van Meulen, D. Weenk, J. H. Buurke, B.-J. F. van Beijnum, and P. H. Veltink, "Ambulatory assessment of walking balance after stroke using instrumented shoes," *J. Neuroeng. Rehabil.*, vol. 13, no. 1, p. 48, 2016.

[143] C. Paiman, D. Lemus, D. Short, and H. Vallery, "Observing the State of Balance with a Single Upper-Body Sensor," *Front. Robot. AI*, vol. 3, no. April, pp. 1–17, 2016.

[144] X. Xu, R. W. McGorry, L. S. Chou, J. hua Lin, and C. chi Chang, "Accuracy of the Microsoft Kinect™ for measuring gait parameters during treadmill walking," *Gait Posture*, vol. 42, no. 2, pp. 145–151, 2015.

[145] A. Schmitz, M. Ye, R. Shapiro, R. Yang, and B. Noehren, "Accuracy and repeatability of joint angles measured using a single camera markerless motion capture system," *J. Biomech.*, vol. 47, no. 2, pp. 587–591, 2014.

[146] M. Sandau, H. Koblauch, T. B. Moeslund, H. Aanæs, T. Alkjær, and E. B. Simonsen, "Markerless motion capture can provide reliable 3D gait kinematics in the sagittal and frontal plane," *Med. Eng. Phys.*, vol. 36, no. 9, pp. 1168–1175, 2014.

[147] S. Corazza, L. Mündermann, A. M. Chaudhari, T. Demattio, C. Cobelli, and T. P. Andriacchi, "A markerless motion capture system to study musculoskeletal biomechanics: Visual hull and simulated annealing approach," *Ann. Biomed. Eng.*, vol. 34, no. 6, pp. 1019–1029, 2006.

[148] E. Ceseracciu, Z. Sawacha, and C. Cobelli, "Comparison of markerless and marker-based motion capture technologies through simultaneous data collection during gait: Proof of concept," *PLoS One*, vol. 9, no. 3, pp. 1–7, 2014.

[149] B. Bonnechère, B. Jansen, P. Salvia, H. Bouzahouene, L. Omelina, F. Moiseev, V. Sholukha, J. Cornelis, M. Rooze, and S. Van Sint Jan, "Validity and reliability of the Kinect within functional assessment activities: Comparison with standard stereophotogrammetry," *Gait Posture*, vol. 39, no. 1, pp. 593–598, 2014.

[150] M. Sandau, "Applications of markerless motion capture in gait recognition," *Dan. Med. J.*, vol. 63, no. 3, pp. 1–18, 2016.

[151] A. Cappozzo, U. Della Croce, A. Leardini, and L. Chiari, "Human movement analysis using stereophotogrammetry. Part 1: Theoretical background," *Gait Posture*, vol. 21, no. 2, pp.

186–196, 2005.

[152] M. P. Kadaba, H. K. Ramakrishnan, and M. E. Wootten, “Measurement of lower extremity kinematics during level walking,” *Class. Pap. Orthop.*, pp. 397–398, 1990.

[153] L. D. Duffell, N. Hope, and A. H. McGregor, “Comparison of kinematic and kinetic parameters calculated using a clusterbased model and Vicon’s plug-in gait,” *Proc. Inst. Mech. Eng. Part H J. Eng. Med.*, vol. 228, no. 2, pp. 206–210, 2014.

[154] A. Leardini, F. Biagi, C. Belvedere, and M. G. Benedetti, “Quantitative comparison of current models for trunk motion in human movement analysis,” *Clin. Biomech.*, vol. 24, no. 7, pp. 542–550, 2009.

[155] G. Mantovani and M. Lamontagne, “How Different Marker Sets Affect Joint Angles in Inverse Kinematics Framework,” *J. Biomech. Eng.*, vol. 139, no. 4, p. 044503, 2017.

[156] K. D. Taylor, F. M. Mottier, D. W. Simmons, W. Cohen, R. J. Pavlak, D. P. Cornell, and G. B. Hankins, “An automated motion measurement system for clinical gait analysis,” *J. Biomech.*, vol. 15, no. 7, pp. 505–516, 1982.

[157] L. Zheng, R. Carey, E. Thorhauer, S. Tashman, C. Harner, and X. Zhang, “In vivo tibiofemoral skeletal kinematics and cartilage contact arthrokinematics during decline walking after isolated meniscectomy,” *Med. Eng. Phys.*, vol. 51, pp. 41–48, 2018.

[158] R. H. Brown, A. H. Burstein, C. L. Nash, and C. C. Schock, “Spinal analysis using a three-dimensional radiographic technique,” *J. Biomech.*, vol. 9, no. 6, 1976.

[159] W. P. Stevens, “Reconstruction of three-dimensional anatomical landmark coordinates using video-based stereophotogrammetry,” *J. Anat.*, vol. 191, no. 2, pp. 277–284, 1997.

[160] D. . Sutherland, “The evolution of clinical gait analysis: Part II Kinematics,” *Gait Posture*, vol. 16, no. 2, pp. 159–179, 2002.

[161] A. Cappozzo, F. Catani, U. Della Croce, and A. Leardini, “Position and orientation in space of bones during movement: anatomical frame definition and determination,” *Clinincal Biomech.*, vol. 10, no. 4, pp. 171–178, 1995.

[162] L. Chiari, U. Della Croce, A. Leardini, and A. Cappozzo, “Human movement analysis using stereophotogrammetry. Part 2: Instrumental errors,” *Gait Posture*, vol. 21, no. 2, pp. 197–211, 2005.

[163] A. Muro-de-la-Herran, B. García-Zapirain, and A. Méndez-Zorrilla, “Gait analysis methods: An overview of wearable and non-wearable systems, highlighting clinical

applications," *Sensors (Switzerland)*, vol. 14, no. 2, pp. 3362–3394, 2014.

[164] A. Leardini, A. Chiari, U. Della Croce, and A. Cappozzo, "Human movement analysis using stereophotogrammetry Part 3. Soft tissue artifact assessment and compensation," *Gait Posture*, vol. 21, no. 2, pp. 212–225, 2005.

[165] U. Della Croce, A. Leardini, L. Chiari, and A. Cappozzo, "Human movement analysis using stereophotogrammetry Part 4: Assessment of anatomical landmark misplacement and its effects on joint kinematics," *Gait Posture*, vol. 21, no. 2, pp. 226–237, 2005.

[166] M. Rabuffetti, G. Baroni, M. Ferrarin, G. Ferrigno, and A. Pedotti, "Self-marking of anatomical landmarks for on-orbit experimental motion analysis compared to expert direct-marking," *Hum. Mov. Sci.*, vol. 21, no. 4, pp. 439–455, 2002.

[167] D. H. Sutherland, "The evolution of clinical gait analysis part III - Kinetics and energy assessment," *Gait Posture*, vol. 21, no. 4, pp. 447–461, 2005.

[168] D. A. Winter, "The biomechanics and motor control of human gait." pp. 1–27, 1987.

[169] T. Shimba, "An estimation of center of gravity from force platform data," *J. Biomech.*, vol. 17, no. 1, 1984.

[170] E. K. Antonsson and R. W. Mann, "The frequency content of gait," *EmbaseHereditas*, vol. I, 1989.

[171] A. Crowe, P. Schiereck, R. W. Deboer, and W. Keessen, "Characterization of Human Gait by Means of Body Center-of-Mass Oscillations Derived from Ground Reaction Forces," *Ieee Trans. Biomed. Eng.*, vol. 42, no. 3, pp. 293–303, 1995.

[172] K. Monaghan, E. Delahunt, and B. Caulfield, "Increasing the number of gait trial recordings maximises intra-rater reliability of the CODA motion analysis system," *Gait Posture*, vol. 25, no. 2, pp. 303–315, 2007.

[173] D. Stephensen, W. I. Drechsler, and O. M. Scott, "Influence of ankle plantar flexor muscle architecture and strength on gait in boys with haemophilia in comparison to typically developing children," *Haemophilia*, vol. 20, no. 3, pp. 413–420, 2014.

[174] J. M. Donelan, R. Kram, and A. D. Kuo, "Simultaneous positive and negative external mechanical work in human walking," *J. Biomech.*, vol. 35, no. 1, pp. 117–124, 2002.

[175] S. A. Gard, S. C. Miff, and A. D. Kuo, "Comparison of kinematic and kinetic methods for computing the vertical motion of the body center of mass during walking," *Hum. Mov. Sci.*, vol. 22, no. 6, pp. 597–610, 2004.

[176] G. M. Blenkinsop, M. T. G. Pain, and M. J. Hiley, “Evaluating feedback time delay during perturbed and unperturbed balance in handstand,” *Hum. Mov. Sci.*, vol. 48, pp. 112–120, 2016.

[177] G. M. Blenkinsop, M. T. G. Pain, and M. J. Hiley, “Balance control strategies during perturbed and unperturbed balance in standing and handstand,” *R. Soc. Open Sci.*, vol. 4, no. 7, p. 161018, 2017.

[178] E. H. Sinitski, E. D. Lemaire, N. Baddour, M. Besemann, N. L. Dudek, and J. S. Hebert, “Fixed and self-paced treadmill walking for able-bodied and transtibial amputees in a multi-terrain virtual environment,” *Gait Posture*, vol. 41, no. 2, pp. 568–573, 2015.

[179] R. K. Begg, R. Wytch, and R. E. Major, “Instrumentation used in clinical gait studies: a review,” *J. Med. Eng. Technol.*, vol. 13, no. 6, pp. 290–295, 1989.

[180] G. Beckham, T. Suchomel, and S. Mizuguchi, “Force Plate Use in Performance Monitoring and Sport Science Testing,” *New Stud. Athl.*, vol. 29, no. 3, pp. 25–37, 2014.

[181] T. E. Prieto, J. B. Myklebust, R. G. Hoffmann, E. G. Lovett, and B. M. Myklebust, “Measures of postural steadiness: Differences between healthy young and elderly adults,” *IEEE Trans. Biomed. Eng.*, vol. 43, no. 9, pp. 956–966, 1996.

[182] V. M. Zatsiorsky and M. Duarte, “Rambling and Trembling in Quiet Standing,” *Language, Speech, and Hearing Services in Schools*, vol. 26, no. 1. pp. 185–200, 2000.

[183] R. Bartlett, *Introduction to Sports Biomechanics*. 1997.

[184] S. G. Psycharakis and S. Miller, “Estimation of Errors in Force Platform Data,” *Res. Q. Exerc. Sport*, vol. 77, no. 4, pp. 514–518, 2015.

[185] T. Kleckers, “Force sensors for strain gauge and piezoelectric crystal-based mechatronic systems- A comparison,” *2012 IEEE I2MTC - Int. Instrum. Meas. Technol. Conf. Proc.*, pp. 2306–2308, 2012.

[186] M. F. Bobbert and H. C. Schamhardt, “Accuracy of determining the point of force application with piezoelectric force plates,” *J. Biomech.*, vol. 23, no. 7, pp. 705–710, 1990.

[187] H. B. Schmiedmayer and J. Kastner, “Enhancements in the accuracy of the center of pressure (COP) determined with piezoelectric force plates are dependent on the load distribution.,” *J. Biomech. Eng.*, vol. 122, no. 5, pp. 523–527, 2000.

[188] H. B. Schmiedmayer and J. Kastner, “Parameters influencing the accuracy of the point of force application determined with piezoelectric force plates,” *J. Biomech.*, vol. 32, no. 11,

pp. 1237–1242, 1999.

[189] T. K. Koo and M. Y. Li, "A Guideline of Selecting and Reporting Intraclass Correlation Coefficients for Reliability Research," *J. Chiropr. Med.*, vol. 15, no. 2, pp. 155–163, 2016.

[190] R. Trevethan, "Intraclass correlation coefficients: clearing the air, extending some cautions, and making some requests," *Heal. Serv. Outcomes Res. Methodol.*, vol. 17, no. 2, pp. 127–143, 2017.

[191] J. P. Weir, "Quantifying test-retest reliability using the intraclass correlation coefficient and the SEM," *J. Strength Cond. Res.*, vol. 19, no. 1, pp. 231–240, 2005.

[192] P. E. Shrout and J. L. Fleiss, "Intraclass correlations: Uses in assessing rater reliability," *Psychol. Bull.*, vol. 86, no. 2, pp. 420–428, 1979.

[193] K. O. Mcgraw and S. P. Wong, "Forming Inferences About Some Intraclass Correlation Coefficients," *Psychol. Methods*, vol. 1, no. 1, pp. 30–46, 1996.

[194] L. J. Cochrane, C. A. Olson, S. Murray, M. Dupuis, T. Tooman, and S. Hayes, "Gaps between knowing and doing: Understanding and assessing the barriers to optimal health care," *J. Contin. Educ. Health Prof.*, vol. 27, no. 2, 2007.

[195] K. Wales, L. Clemson, N. Lannin, and I. Cameron, "Functional assessments used by occupational therapists with older adults at risk of activity and participation limitations: A systematic review," *PLoS One*, vol. 11, no. 2, pp. 2–7, 2016.

[196] R. A. H. M. Swinkels, R. P. S. Van Peppen, H. Wittink, J. W. H. Custers, and A. J. H. M. Beurskens, "Current use and barriers and facilitators for implementation of standardised measures in physical therapy in the Netherlands," *BMC Musculoskelet. Disord.*, vol. 12, no. 1, p. 106, 2011.

[197] B. F. Chorpita, E. L. Daleiden, and J. R. Weisz, "Modularity in the design and application of therapeutic interventions," *Appl. Prev. Psychol.*, vol. 11, no. 3, pp. 141–156, 2005.

[198] S. M. Bruijn, D. J. J. Bregman, O. G. Meijer, P. J. Beek, and J. H. van Dieën, "The validity of stability measures: A modelling approach," *J. Biomech.*, vol. 44, no. 13, pp. 2401–2408, 2011.

[199] E. C. Wonsetler and M. G. Bowden, "A systematic review of mechanisms of gait speed change post- stroke. Part 2: Exercise capacity, muscle activation, kinetics, and kinematics Elizabeth David S.," *Anal Chem.*, vol. 25, no. 4, pp. 368–379, 2015.

[200] J. B. Dingwell and J. P. Cusumano, "Re-interpreting detrended fluctuation analyses of

stride-to-stride variability in human walking," *Gait Posture*, vol. 32, no. 3, pp. 348–353, 2010.

[201] D. Engelhart, T. A. Boonstra, R. G. K. M. Aarts, A. C. Schouten, and H. van der Kooij, "Comparison of closed-loop system identification techniques to quantify multi-joint human balance control," *Annu. Rev. Control*, vol. 41, pp. 58–70, 2015.

[202] K. V. Day, S. A. Kautz, S. S. Wu, S. P. Suter, and A. L. Behrman, "Foot placement variability as a walking balance mechanism post-spinal cord injury," *Clin. Biomech.*, vol. 27, no. 2, pp. 145–150, 2012.

[203] S. M. Bruijn, W. R. T. Ten Kate, G. S. Faber, O. G. Meijer, P. J. Beek, and J. H. Van Dieën, "Estimating dynamic gait stability using data from non-aligned inertial sensors," *Ann. Biomed. Eng.*, vol. 38, no. 8, pp. 2588–2593, 2010.

[204] K. S. van Schooten, L. H. Sloot, S. M. Bruijn, H. Kingma, O. G. Meijer, M. Pijnappels, and J. H. Van Dieën, "Sensitivity of trunk variability and stability measures to balance impairments induced by galvanic vestibular stimulation during gait," *Gait Posture*, vol. 33, no. 4, pp. 656–660, 2011.

[205] M. J. P. Toebes, M. J. M. Hoozemans, R. Furrer, J. Dekker, and J. H. Van Dieën, "Local dynamic stability and variability of gait are associated with fall history in elderly subjects," *Gait Posture*, vol. 36, no. 3, pp. 527–531, 2012.

[206] G. Pavei, E. Seminati, D. Cazzola, and A. E. Minetti, "On the estimation accuracy of the 3D body center of mass trajectory during human locomotion: Inverse vs. forward dynamics," *Front. Physiol.*, vol. 8, no. MAR, pp. 1–13, 2017.

[207] J. Pijlman, A. L. Hof, and E. Otten, "Balanced walking. The inverted pendulum model as tool for computing centre-of-mass position from centre-of-pressure data." pp. 871–875, 2001.

[208] T. Geijtenbeek and F. Steenbrink, "D-Flow : Immersive Virtual Reality and Real-Time Feedback for Rehabilitation," *10th Int. Conf. Virtual Real. Contin. Its Appl. Ind.*, vol. 1, no. 212, pp. 201–208, 2011.

[209] E. Ageberg, D. Roberts, E. Holmström, and T. Fridén, "Balance in single-limb stance in healthy subjects - Reliability of testing procedure and the effect of short-duration sub-maximal cycling," *BMC Musculoskelet. Disord.*, vol. 4, pp. 1–16, 2003.

[210] F. Horak, D. Wrisley, and J. Frank, "The Balance Evaluation Systems Test (BESTest) to

Differentiate Balance Deficit," vol. 3, no. 800, pp. 7–8, 2009.

[211] M. A. Hunt, F. J. Mcmanus, R. S. Hinman, and K. L. Bennell, "Predictors of single-leg standing balance in individuals with medial knee osteoarthritis," *Arthritis Care Res.*, vol. 62, no. 4, pp. 496–500, 2010.

[212] A. Huurnink, D. P. Fransz, I. Kingma, and J. H. van Dieën, "Comparison of a laboratory grade force platform with a Nintendo Wii Balance Board on measurement of postural control in single-leg stance balance tasks," *J. Biomech.*, vol. 46, no. 7, pp. 1392–1395, 2013.

[213] B. L. Riemann and R. Schmitz, "The relationship between various modes of single leg postural control assessment.," *Int. J. Sports Phys. Ther.*, vol. 7, no. 3, pp. 257–66, 2012.

[214] A. Schneiders, K. Gregory, S. Karas, and A. Mündermann, "Effect of foot position on balance ability in single-leg stance with and without visual feedback," *J. Biomech.*, vol. 49, no. 9, pp. 1969–1972, 2016.

[215] T. C. Sell, N. C. Clark, D. Wood, J. P. Abt, M. Lovalekar, and S. M. Lephart, "Single-leg balance impairments persist in fully operational military special forces operators with a previous history of low back pain," *Orthop. J. Sport. Med.*, vol. 2, no. 5, pp. 1–6, 2014.

[216] B. A. Springer, R. Marin, T. Cyhan, H. Roberts, and N. W. Gill, "Normative values for the unipedal stance test with eyes open and closed," *J. Geriatr. Phys. Ther.*, vol. 30, no. 1, pp. 8–15, 2007.

[217] T. H. Trojian, "Single leg balance test to identify risk of ankle sprains * Commentary 1 * Commentary 2," *Br. J. Sports Med.*, vol. 40, no. 7, pp. 610–613, 2006.

[218] B. J. Vellas, S. J. Wayne, L. Romero, R. N. Baumgartner, L. Z. Rubernstein, and P. J. Garry, "One-leg balance is an important predictor of injuious falls in older persons," *J. Am Geriatr Soc*, vol. 45, pp. 735–738, 1997.

[219] T. R. Fujisawa H., "A new clinical test of dynamic standing balance in the frontal plane: the side-step test," *Clin. Rehabil.*, vol. 20, pp. 340–346, 2006.

[220] M. Kobayashi, K. Takahashi, M. Sato, and S. Usuda, "The characteristics of multi-directional step distance and the association between stepping laterality and walking ability of patients with stroke," *J. Phys. Ther. Sci.*, vol. 27, no. 3, pp. 905–909, 2015.

[221] J. C. Singer, S. D. Prentice, and W. E. McIlroy, "Dynamic stability control during volitional stepping: A focus on the restabilisation phase at movement termination," *Gait Posture*, vol. 35, no. 1, pp. 106–110, 2012.

[222] F. Ishii, N. Matsukawa, M. Horiba, T. Yamanaka, M. Hattori, I. Wada, and K. Ojika, "Impaired ability to shift weight onto the non-paretic leg in right-cortical brain-damaged patients," *Clin. Neurol. Neurosurg.*, vol. 112, no. 5, pp. 406–412, 2010.

[223] S. Kasahara and H. Saito, "Effect of loading parameters on motor performance during a dynamic weight-shift task," *Gait Posture*, vol. 41, no. 1, pp. 100–105, 2015.

[224] M. W. Kennedy, T. Bretl, and J. P. Schmiedeler, "Interpreting lateral dynamic weight shifts using a simple inverted pendulum model," *Gait Posture*, vol. 40, no. 1, pp. 134–139, 2014.

[225] P. V. Tsaklis, W. J. A. Grooten, and E. Franzén, "Effects of Weight-Shift Training on Balance Control and Weight Distribution in Chronic Stroke: A Pilot Study," *Top. Stroke Rehabil.*, vol. 19, no. 1, pp. 23–31, 2012.

[226] E. M. J. Bekkers, S. Van Rossom, E. Heremans, K. Dockx, S. Devan, S. M. P. Verschueren, and A. Nieuwboer, "Adaptations to postural perturbations in patients with freezing of gait," *Front. Neurol.*, vol. 9, no. JUL, pp. 1–9, 2018.

[227] F. B. Horak, S. M. Henry, and a Shumway-Cook, "Postural perturbations: new insights for treatment of balance disorders.," *Phys. Ther.*, vol. 77, no. 5, pp. 517–533, 1997.

[228] B. E. Maki, W. E. McIlroy, and S. D. Perry, "Influence of lateral destabilization on compensatory stepping responses," *J. Biomech.*, vol. 29, no. 3, pp. 343–353, 1996.

[229] C.-L. Chen, S.-Z. Lou, H.-W. Wu, S.-K. Wu, K.-T. Yeung, and F.-C. Su, "Effects of the type and direction of support surface perturbation on postural responses," *J. Neuroeng. Rehabil.*, vol. 11, no. 1, p. 50, 2014.

[230] S. A. Chvatal and L. H. Ting, "Common muscle synergies for balance and walking," *Front. Comput. Neurosci.*, vol. 7, no. May, pp. 1–14, 2013.

[231] T. D. J. Welch and L. H. Ting, "Mechanisms of motor adaptation in reactive balance control," *PLoS One*, vol. 9, no. 5, 2014.

[232] B. D. Hendershot, C. E. Mahon, and A. L. Pruziner, "A comparison of kinematic-based gait event detection methods in a self-paced treadmill application," *J. Biomech.*, vol. 49, no. 16, pp. 4146–4149, 2016.

[233] J. Sturdy, D. H. Gates, B. J. Darter, and J. M. Wilken, "Assessing preparative gait adaptations in persons with transtibial amputation in response to repeated medial-lateral perturbations," *Gait Posture*, vol. 39, no. 3, pp. 995–998, 2014.

[234] S. Kruger, "A virtual reality approach to gait training in service members with lower

extremity amputations," *Int. J. Disabil. Hum. Dev.*, vol. 10, no. 4, pp. 313–316, 2011.

[235] S. L. Carey, K. B. Reed, and A. Martori, "Wearable Robotics: Challenges and Trends," vol. 16, pp. 219–224, 2017.

[236] B. M. Isaacson, T. M. Swanson, and P. F. Pasquina, "The use of a computer-assisted rehabilitation environment (CAREN) for enhancing wounded warrior rehabilitation regimens.," *J. Spinal Cord Med.*, vol. 36, no. 4, pp. 296–9, 2013.

[237] J. Fung, C. L. Richards, F. Malouin, B. J. McFadyen, and A. Lamontagne, "A Treadmill and Motion Coupled Virtual Reality System for Gait Training Post-Stroke," *CyberPsychology Behav.*, vol. 9, no. 2, pp. 157–162, 2006.

[238] A. Leroux, J. Fung, and H. Barbeau, "Postural adaptation to walking on inclined surfaces: II. Strategies following spinal cord injury," *Clin. Neurophysiol.*, vol. 117, no. 6, pp. 1273–1282, 2006.

[239] D. H. Gates, S. J. Scott, J. M. Wilken, and J. B. Dingwell, "Frontal Plane Dynamic Margins of Stability in Individuals With and Without Transtibial Amputation Walking on a Loose Rock Surface," vol. 6, no. 8, pp. 570–575, 2013.

[240] F. Madehkhaksar, J. Klenk, K. Sczuka, K. Gordt, I. Melzer, and M. Schwenk, "The effects of unexpected mechanical perturbations during treadmill walking on spatiotemporal gait parameters, and the dynamic stability measures by which to quantify postural response," *PLoS One*, vol. 13, no. 4, pp. 1–15, 2018.

[241] S. Roeles, P. J. Rowe, S. M. Bruijn, C. R. Childs, G. D. Tarfali, F. Steenbrink, and M. Pijnappels, "Gait stability in response to platform, belt, and sensory perturbations in young and older adults," *Med. Biol. Eng. Comput.*, no. Ml, pp. 1–11, 2018.

[242] S. Chvatal and L. Ting, "Voluntary and reactive recruitment of locomotor muscle synergies during perturbed walking," *Computer (Long. Beach. Calif).*, vol. 144, no. 5, pp. 724–732, 2012.

[243] a. S. C. Oliveira, L. Gizzi, U. G. Kersting, and D. Farina, "Modular organization of balance control following perturbations during walking," *J. Neurophysiol.*, vol. 108, no. July, pp. 1895–1906, 2012.

[244] D. H. Gates, B. J. Darter, J. B. Dingwell, and J. M. Wilken, "Comparison of walking overground and in a Computer Assisted Rehabilitation Environment (CAREN) in individuals with and without transtibial amputation.," *J. Neuroeng. Rehabil.*, vol. 9, no. 1,

p. 81, 2012.

[245] J. Forero, R. Rubuliak, A. H. Vette, and J. S. Hebert, “Development of a Simplified Motion Capture Cluster Marker set to Enhance Rehabilitation in the CAREN System,” *Poster Present. 6th Annu. Can. Inst. Mil. Veteran Heal. Res. Forum*, 2016.

[246] B. Malfait, F. Staes, A. De Vries, A. Smeets, M. Hawken, M. A. Robinson, J. Vanrenterghem, and S. Verschueren, “Dynamic neuromuscular control of the lower limbs in response to unexpected single-planar versus multi-planar support perturbations in young, active adults,” *PLoS One*, vol. 10, no. 7, pp. 1–17, 2015.

[247] A. H. Vrieling, H. G. van Keeken, T. Schoppen, E. Otten, A. L. Hof, J. P. K. Halbertsma, and K. Postema, “Balance control on a moving platform in unilateral lower limb amputees,” *Gait Posture*, vol. 28, no. 2, pp. 222–228, 2008.

[248] K. L. Havens, T. Mukherjee, and J. M. Finley, “Analysis of biases in dynamic margins of stability introduced by the use of simplified center of mass estimates during walking and turning,” *Gait Posture*, vol. 59, no. October 2017, pp. 162–167, 2018.

[249] M. Wuehr, R. Schniepp, C. Pradhan, J. Ilmberger, M. Strupp, T. Brandt, and K. Jahn, “Differential effects of absent visual feedback control on gait variability during different locomotion speeds,” *Exp. Brain Res.*, vol. 224, no. 2, pp. 287–294, 2013.

[250] J. C. van den Noort, L. H. Sloot, S. M. Bruijn, and J. Harlaar, “How to measure responses of the knee to lateral perturbations during gait? A proof-of-principle for quantification of knee instability,” *J. Biomech.*, vol. 61, pp. 111–122, 2017.

[251] P. Moin, *Fundamentals of Engineering Numerical Analysis*. Cambridge University Press, 2010.

[252] J. Nilsson, M. Panizza, and M. Hallett, “Principles of digital sampling of a physiologic signal,” *Electroencephalogr. Clin. Neurophysiol. Evoked Potentials*, vol. 89, no. 5, pp. 349–358, 1993.

[253] E. H. Sinitski, E. D. Lemaire, and N. Baddour, “Characteristics of a dual force plate system embedded in a six degree of freedom motion platform,” *MeMeA 2013 - IEEE Int. Symp. Med. Meas. Appl. Proc.*, no. Ml, pp. 241–245, 2013.

[254] G. Paolini, U. Della Croce, P. O. Riley, F. K. Newton, and D. Casey Kerrigan, “Testing of a tri-instrumented-treadmill unit for kinetic analysis of locomotion tasks in static and dynamic loading conditions,” *Med. Eng. Phys.*, vol. 29, no. 3, pp. 404–411, 2007.

[255] J. A. Zeni, J. G. Richards, and J. S. Higginson, “Two simple methods for determining gait events during treadmill and overground walking using kinematic data,” *Gait Posture*, vol. 27, no. 4, pp. 710–714, 2008.

[256] R. Moraes, F. Allard, and A. E. Patla, “Validating Determinants for an Alternate Foot Placement Selection Algorithm During Human Locomotion in Cluttered Terrain,” *J Neurophysiol*, vol. 98, pp. 1928–1940, 2007.

[257] S. Bohm, F. Mersmann, S. Bierbaum, R. Dietrich, and A. Arampatzis, “Cognitive demand and predictive adaptational responses in dynamic stability control,” *J. Biomech.*, vol. 45, no. 14, pp. 2330–2336, 2012.

[258] J. Song, S. Sigward, B. Fisher, and G. J. Salem, “Altered dynamic postural control during step turning in persons with early-stage Parkinson’s disease,” *Parkinsons. Dis.*, vol. 2012, 2012.

[259] D. A. Winter, A. E. Patla, J. S. Frank, and S. E. Walt, “Biomechanical Walking Pattern Changes in the Fit and Healthy Elderly,” no. 6, pp. 340–347, 1990.

[260] T. E. Te Lockhart and J. Liu, “Differentiating fall-prone and healthy adults using local dynamic stability,” *Ergonomics*, vol. 51, no. 12, pp. 1860–1872, 2008.

[261] L. Bassi Luciani, V. Genovese, V. Monaco, L. Odetti, E. Cattin, and S. Micera, “Design and Evaluation of a new mechatronic platform for assessment and prevention of fall risks,” *J. Neuroeng. Rehabil.*, vol. 9, p. 51, 2012.

[262] J. H. Chien, D. J. A. Eikema, M. Mukherjee, and N. Stergiou, “Locomotor Sensory Organization Test: A Novel Paradigm for the Assessment of Sensory Contributions in Gait,” *Ann. Biomed. Eng.*, vol. 42, no. 12, pp. 2512–2523, 2014.

[263] E. H. Sinitski, E. D. Lemaire, and N. Baddour, “Evaluation of motion platform embedded with force plate-instrumented treadmill,” *J. Rehabil. Res. Dev.*, vol. 52, no. 2, pp. 221–233, 2015.

[264] R. Senden, B. Grimm, I. C. Heyligers, H. H. C. M. Savelberg, and K. Meijer, “Acceleration-based gait test for healthy subjects: Reliability and reference data,” *Gait Posture*, vol. 30, no. 2, pp. 192–196, 2009.

[265] D. Martelli, V. Vashista, S. Micera, and S. K. Agrawal, “Direction-dependent adaptation of dynamic gait stability following waist-pull perturbations,” *IEEE Trans. Neural Syst. Rehabil. Eng.*, vol. PP, no. 99, pp. 1304–1313, 2015.

[266] X. Lin, O. G. Meijer, J. Lin, W. Wu, X. Lin, B. Liang, J. H. Van Dieën, and S. M. Bruijn, "Frontal plane kinematics in walking with moderate hip osteoarthritis: Stability and fall risk," *Clin. Biomech.*, vol. 30, no. 8, pp. 874–880, 2015.

[267] A.-L. Simon, V. Lugade, K. Bernhardt, A. N. Larson, and K. Kaufman, "Assessment of stability during gait in patients with spinal deformity—A preliminary analysis using the dynamic stability margin," *Gait Posture*, vol. 55, no. June 2016, pp. 37–42, 2017.

[268] C. R. Lee and C. T. Farley, "Determinants of the center of mass trajectory in human walking and running.," *J. Exp. Biol.*, vol. 201, no. Pt 21, pp. 2935–2944, 1998.

[269] J. M. Wilken, K. M. Rodriguez, M. Brawner, and B. J. Darter, "Reliability and minimal detectible change values for gait kinematics and kinetics in healthy adults," *Gait Posture*, vol. 35, no. 2, pp. 301–307, 2012.

[270] M. Henriksen, H. Lund, R. Moe-Nilssen, H. Bliddal, and B. Danneskiod-Samsøe, "Test-retest reliability of trunk accelerometric gait analysis," *Gait Posture*, vol. 19, no. 3, pp. 288–297, 2004.

[271] L. Allet, S. Armand, R. A. de Bie, A. Golay, D. Monnin, K. Aminian, and E. D. de Bruin, "Reliability of diabetic patients' gait parameters in a challenging environment," *Gait Posture*, vol. 28, no. 4, pp. 680–686, 2008.

[272] K. S. van Schooten, S. M. Rispens, M. Pijnappels, A. Daffertshofer, and J. H. van Dieen, "Assessing gait stability: The influence of state space reconstruction on inter- and intra-day reliability of local dynamic stability during over-ground walking," *J. Biomech.*, vol. 46, no. 1, pp. 137–141, 2013.

[273] P. E. Shrout, "Measurement reliability and reliability in psychiatry," *Stat. Methods Med. Res.*, vol. 7, no. 98, pp. 301–317, 1998.

[274] J. L. Fleiss, "The measurement of interrater agreement," *Stat. Methods Rates Proportions*, vol. 52, no. 2, pp. 695–702, 1981.

[275] J. L. Fleiss, "The design and analysis of clinical experiments," *Stat. Med.*, vol. 7, no. 3, p. 454, 1986.

[276] S. Chinn, "Repeatability and method comparison.," *Thorax*, vol. 46, no. 6, pp. 454–456, 1991.

[277] M. Al-Amri, H. Al Balushi, and A. Mashabi, "Intra-rater repeatability of gait parameters in healthy adults during self-paced treadmill-based virtual reality walking," *Comput. Methods*

Biomech. Biomed. Engin., vol. 20, no. 16, pp. 1669–1677, 2017.

[278] S. Taş, S. Güneri, B. Kaymak, and Z. Erden, "A comparison of results of 3-dimensional gait analysis and observational gait analysis in patients with knee osteoarthritis," *Acta Orthop. Traumatol. Turc.*, vol. 49, no. 2, pp. 151–159, 2015.

[279] E. H. Sinitski, E. D. Lemaire, N. Baddour, M. Besemann, N. L. Dudek, and J. S. Hebert, "Supplemental material to: Fixed and self-paced treadmill walking for able-bodied and transtibial amputees in a multi-terrain virtual environment," *Gait Posture*, vol. 41, no. 2, pp. 568–573, 2015.

[280] A. L. Hof, "Comments about the article titled: Comparison of three methods to estimate the center of mass during balance assessment," *J. Biomech.*, vol. 38, no. 10, pp. 2134–2135, 2005.

[281] M. Moreno Catalá, D. Woitalla, and A. Arampatzis, "Reactive but not predictive locomotor adaptability is impaired in young Parkinson's disease patients," *Gait Posture*, vol. 48, pp. 177–182, 2016.

[282] W. Nakano, T. Fukaya, S. Kobayashi, and Y. Ohashi, "Age effects on the control of dynamic balance during step adjustments under temporal constraints," *Hum. Mov. Sci.*, vol. 47, pp. 29–37, 2016.

[283] L. Hak and J. H. Van Diee, "Limb Loss Might Be Functional in Terms of Gait Stability," vol. 94, no. 10, 2014.

[284] A. M. Valevicius, Q. A. Boser, E. B. Lavoie, C. S. Chapman, P. M. Pilarski, A. H. Vette, and J. S. Hebert, "Characterization of normative hand movements during two functional upper limb tasks," *PLoS ONE, Revis. requested*, pp. 1–22, 2017.

[285] M. J. P. Toebes, M. J. M. Hoozemans, S. E. Mathiassen, J. Dekker, and J. H. van Dieën, "Measurement strategy and statistical power in studies assessing gait stability and variability in older adults," *Aging Clin. Exp. Res.*, vol. 28, no. 2, pp. 257–265, 2016.

[286] W. J. Coster, "Making the best match: selecting outcome measures for clinical trials and outcome studies.," *Am. J. Occup. Ther.*, vol. 67, no. 2, pp. 162–70, 2013.

[287] S. Bierbaum, A. Peper, K. Karamanidis, and A. Arampatzis, "Adaptive feedback potential in dynamic stability during disturbed walking in the elderly," *J. Biomech.*, vol. 44, no. 10, pp. 1921–1926, 2011.

[288] S. Bierbaum, A. Peper, K. Karamanidis, and A. Arampatzis, "Adaptational responses in

dynamic stability during disturbed walking in the elderly," *J. Biomech.*, vol. 44, no. 10, pp. 1921–1926, 2010.

[289] J. Kottner, L. Audige, S. Brorson, A. Donner, B. J. Gajewski, A. Hroóbjartsson, C. Roberts, M. Shoukri, and D. L. Streiner, "Guidelines for Reporting Reliability and Agreement Studies (GRRAS) were proposed," *Int. J. Nurs. Stud.*, vol. 48, no. 6, pp. 661–671, 2011.

[290] G. M. Blenkinsop, M. T. G. Pain, and M. J. Hiley, "Balance control strategies during perturbed and unperturbed balance in standing and handstand Subject Category : Subject Areas :," *R. Soc. Open Sci.*, vol. 4, pp. 1–12, 2017.

Appendices

Appendix A: Consent Forms

A.1 Non-Disabled Participants

Information Sheet and Consent Form: Healthy Adult

Study Title: "Development of a Performance Assessment Tool for the CAREN"

Research Investigators: Dr. Jacqueline Hebert 780.735.8218
Dr. Albert Vette 780.492.1534
Juan Forero, PhD 780.735.7972

Funding source: CIMVHR/Surgeon General Health Research Program

Introduction

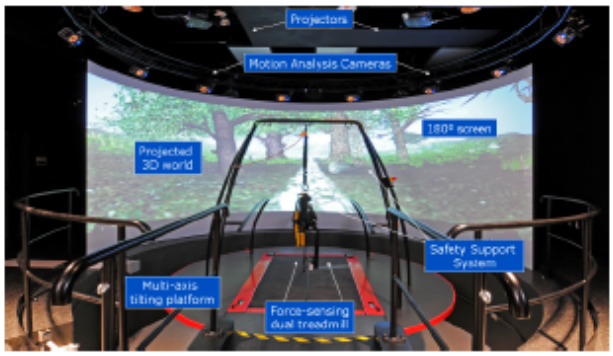

You are being asked to participate in this research project to measure how people perform while sitting, standing and walking on a treadmill in a virtual reality (VR) system. The Computer-Assisted Rehabilitation Environment (CAREN) simulates different environments that include slopes (uphill/downhill) as well as perturbations to give the feeling of real-life scenarios during sitting, standing and walking. We are developing an assessment tool for the CAREN to better identify balance and mobility impairments due to lower limb amputation and traumatic brain injury. The outcomes of this project will provide information that healthcare professionals can use to better understand balance and performance, and thereby improve rehabilitation decision-making.

Please read this Information Sheet and Consent Form carefully and ask as many questions as you like before deciding whether to participate in this research study. You can discuss this study with your family, friends and your health-care team.

Background and Purpose of the Study

The accurate assessment of balance, gait and mobility is an important aspect of clinical practice for clinicians working on the rehabilitation of balance and mobility. Such assessment is usually performed through the use of different measures aimed at characterizing different characteristics of balance and mobility. Although those measures are reliable in assessing individuals with different impairments, they are still limited to the specific population they have been designed for. The CAREN represents an ideal environment for assessing balance and mobility in a wide range of individuals, including not only injured individuals (e.g., lower limb amputation, traumatic brain injury, stroke), but also high performance populations (e.g., military personnel).

Study Procedures

We are looking for healthy adult individuals between the ages of 18 and 60 years of age that have no pain or medical problems affecting their walking ability.

The study will require you to attend the Glenrose Rehabilitation Hospital (GRH) for three sessions on different days. The first and second sessions will take place within the Courage In Motion (C I M) Centre and the third session will take place at the gymnasium. You will be asked to wear athletic shorts or pants, and comfortable shoes on both sessions.

First and second sessions:

Upon arriving at the C I M Centre, a project assistant will review the protocol, answer any questions you might have, and ask you to sign the attached consent form if you wish to participate. The project assistant will record your age, weight, and gender, as well as contact information such as address, telephone number or email address. No other information about you will be recorded.

The project assistant will fit you with a safety harness and attach small plastic plates with reflective markers to your back, thighs, shanks and feet so that we can track how you move. The marker plates will be attached with Velcro® straps. You will be led onto the CAREN platform where the safety harness will be attached to the CAREN safety portal. Note that this setup will ensure that you do not fall to the ground during a stumble. The CAREN system operator will explain all safety procedures at the beginning of the session.

You will be asked to follow the instructions that will be displayed on the screen of the CAREN system while the infra-red cameras record the movement of the reflective markers. Your image (actual face or body) is not recorded with the infra-red cameras, just the reflection of the markers. Although these cameras will not record your image, we may ask you to allow us to record an additional conventional video of the experiments. This video will be used when analyzing the experimental data and will be disposed of after the analysis has been completed. This kind of video will **only be recorded if you give us consent to do so**.

Third session:

Upon arriving to the gymnasium, a project assistant will review the protocol, answer any questions you might have, and ask you to confirm on the consent you signed before on the first session if you wish to participate.

You will be asked to follow the instructions for each of the following balance and agility tests. You will be directed by a research assistant to complete the tasks. Those tests are the Activities-specific Balance Confidence Scale (ABC) questionnaire, the Berg Balance Scale (BBS), the Dynamic Gait Index (DGI), the Amputee Mobility Predictor (AMP) and the Comprehensive High-level Activity Mobility Predictor (CHAMP).

Study Duration

The entire test sessions on the CAREN (sessions 1 and 2) are expected to last less than 2.5 hours in total. The marker placements will take about 10 minutes. The trials on the CAREN will take about 5 minutes each. Between trials, you can take a break if necessary. After the test session, you will

be invited to come back for a second session on a different day to complete the test again, and possibly for a third session to complete standard balance and agility tests in the gymnasium of the GRH. The entire test session at the gymnasium (session 3) is expected to last less than 1.5 hour in total. Each of the 5 tests will take about 15 minutes to complete.

Possible Side Effects and/or Risks

The risks in the study are minimal and may include chaffing from the harness on the CAREN system. Some people experience dizziness when completing tasks on the CAREN system. If this occurs, more time can be spent on getting used to the system. You can also choose to withdraw from the study at any time. If you feel uncomfortable during any part of the study, the study can be stopped at your request.

Benefits of the Study

You may not receive any direct benefit from participating in this study. Your participation in this research may allow the researchers to discover better ways to assess balance and performance, leading to better decisions for therapy to help people walk and perform functional tasks again after injury or illness.

Withdrawal from the Study

You have the right to withdraw from the study at any time without any impact on your current and future care. If you decide to withdraw, you can discuss this with any member of the research team.

Compensation

In the event of a research-related injury or illness, you will be provided with appropriate medical treatment/care. You are not waiving your legal rights by agreeing to participate in this study. Note that you will be paid $20 on each visit for participating in this study (compensation of your time).

Confidentiality

All information will be kept confidential. You will not be identifiable in any publications or presentations resulting from this study. The only information kept after you complete the study is your age, gender, and weight. That information will be coded with an independent study number, with no identifying information linked to you. These data will be stored in an encrypted electronic file which is password protected on an encrypted and secured hard drive. Only the research team at the Glenrose Rehabilitation Hospital will be able to access these data.

Voluntary Participation

Your participation in this study is voluntary. If you choose not to participate, your decision will not affect the potential care you receive at the GRH, at this time or in the future.

Further Information

If you have any questions regarding this study, please do not hesitate to contact the investigator: Dr. Jacqueline Hebert, Glenrose Rehabilitation Hospital, 10230-111 Avenue, Edmonton AB T5G0B7; email: jacqueline.hebert@ahs.ca, phone 780-725-8218.

The plan for this study has been reviewed for its adherence to ethical guidelines by a Research Ethics Board at the University of Alberta. For questions regarding participant rights and ethical conduct of research, contact the Research Ethics Office at (780) 492-2615. This office has no direct involvement with this project.

INFORMED CONSENT FORM

Study Title: "Development of a Performance Assessment Tool for the CAREN"

Research Investigators: Dr. Jacqueline Hebert 780.735.8218
Dr. Albert Vette 780.492.1534
Juan Forero, PhD 780.735.7972

	Yes
Do you understand that you have been asked to be in a research study?	☐
Have you read and received a copy of the attached Information Sheet?	☐
Do you understand the benefits and risks involved in taking part in this research study?	☐
Have you had an opportunity to ask questions and discuss this study?	☐
Do you understand that you are free to leave the study at any time, without having to give a reason and without affecting your future medical care?	☐
Has the issue of confidentiality been explained to you?	☐
Do you understand who will have access to your records?	☐
Do you agree to be video recorded during the study? Your image (mainly your body) will be digitally captured on video and the file be destroyed after the data has been analyzed).	☐

Who explained this study to you? _____

I agree to take part in this study:

Signature of Research Participant _____

Printed Name: _____ Date: _____

I believe that the person signing this form understands what is involved in the study and voluntarily agrees to participate.

Signature of Investigator or Designee_____ Date _____

THE INFORMATION SHEET MUST BE ATTACHED TO THIS CONSENT FORM AND A COPY GIVEN TO THE RESEARCH PARTICIPANT

A.2 Impaired Participants

Information Sheet and Consent Form

Study Title: "Development of a Performance Assessment Tool for the CAREN"

Research Investigators: Dr. Jacqueline Hebert 780.735.8218
Dr. Albert Vette 780.492.1534
Juan Forero, PhD 780.735.7972

Funding source: CIMVHR/Surgeon General Health Research Program

Introduction

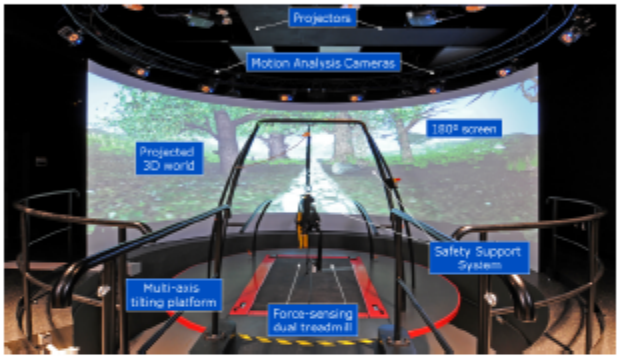

You are being asked to participate in this research project to measure how people perform while sitting, standing and walking on a treadmill in a virtual reality (VR) system. The Computer-Assisted Rehabilitation Environment (CAREN) simulates different environments that include slopes (uphill/downhill) as well as perturbations to give the feeling of real-life scenarios during sitting, standing and walking. We are developing an assessment tool for the CAREN to better identify balance and mobility impairments due to lower limb amputation and traumatic brain injury. The outcomes of this project will provide information that healthcare professionals can use to better understand balance and performance, and thereby improve rehabilitation decision-making.

Please read this Information Sheet and Consent Form carefully and ask as many questions as you like before deciding whether to participate in this research study. You can discuss this study with your family, friends and your health-care team.

Background and Purpose of the Study

The accurate assessment of balance, gait and mobility is an important aspect of clinical practice for clinicians working on the rehabilitation of balance and mobility. Such assessment is usually performed through the use of different measures aimed at characterizing different characteristics of balance and mobility. Although those measures are reliable in assessing individuals with different impairments, they are still limited to the specific population they have been designed for. The CAREN represents an ideal environment for assessing balance and mobility in a wide range of individuals, including not only injured individuals (e.g., lower limb amputation, traumatic brain injury, stroke), but also high performance populations (e.g., military personnel).

Study Procedures

We are looking for individuals with traumatic brain injury or lower limb amputation between the ages of 18 and 60 years of age that have no pain or medical problems affecting their walking ability.

The study will require you to attend the Glenrose Rehabilitation Hospital (GRH) for two sessions on different days. The first session will take place within the Courage In Motion (C I M) Centre and the second session will take place at the gymnasium. You will be asked to wear athletic shorts or pants, and comfortable shoes on both sessions.

First session:

Upon arriving at the C I M Centre, a project assistant will review the protocol, answer any questions you might have, and ask you to sign the attached consent form if you wish to participate. The project assistant will record your age, weight, and gender, as well as contact information such as address, telephone number or email address. No other information about you will be recorded.

The project assistant will fit you with a safety harness and attach small plastic plates with reflective markers to your back, thighs, shanks and feet so that we can track how you move. The marker plates will be attached with Velcro® straps. You will be led onto the CAREN platform where the safety harness will be attached to the CAREN safety portal. Note that this setup will ensure that you do not fall to the ground during a stumble. The CAREN system operator will explain all safety procedures at the beginning of the session.

You will be asked to follow the instructions that will be displayed on the screen of the CAREN system while the infra-red cameras record the movement of the reflective markers. Your image (actual face or body) is not recorded with the infra-red cameras, just the reflection of the markers. Although these cameras will not record your image, we may ask you to allow us to record an additional conventional video of the experiments. This video will be used when analyzing the experimental data and will be disposed of after the analysis has been completed. This kind of video will **only be recorded if you give us consent to do so**.

Second session:

Upon arriving to the gymnasium, a project assistant will review the protocol, answer any questions you might have, and ask you to confirm on the consent you signed before on the first session if you wish to participate.

You will be asked to follow the instructions for each of the following balance and agility tests. You will be directed by a research assistant to complete the tasks. Those tests are the Activities-specific Balance Confidence Scale (ABC) questionnaire, the Berg Balance Scale (BBS), the Dynamic Gait Index (DGI), the Amputee Mobility Predictor (AMP) and the Comprehensive High-level Activity Mobility Predictor (CHAMP).

Study Duration

The entire test session on the CAREN (session 1) is expected to last less than 2.5 hours in total. The marker placements will take about 10 minutes. The trials on the CAREN will take about 5 minutes each. Between trials, you can take a break if necessary. After the test session, you will be

invited to come back for a second session on a different day to complete standard balance and agility tests in the gymnasium of the GRH. The entire test session at the gymnasium (session 2) is expected to last less than 1.5 hours in total. Each of the 5 tests will take about 15 minutes to complete.

Possible Side Effects and/or Risks

The risks in the study are minimal and may include chaffing from the harness on the CAREN system. Some people experience dizziness when completing tasks on the CAREN system. If this occurs, more time can be spent on getting used to the system. You can also choose to withdraw from the study at any time. If you feel uncomfortable during any part of the study, the study can be stopped at your request.

Benefits of the Study

You may not receive any direct benefit from participating in this study. Your participation in this research may allow the researchers to discover better ways to assess balance and performance, leading to better decisions for therapy to help people walk and perform functional tasks again after injury or illness.

Withdrawal from the Study

You have the right to withdraw from the study at any time without any impact on your current and future care. If you decide to withdraw, you can discuss this with any member of the research team.

Compensation

In the event of a research-related injury or illness, you will be provided with appropriate medical treatment/care. You are not waiving your legal rights by agreeing to participate in this study. Note that you will be paid $20 on each visit for participating in this study (compensation of your time).

Confidentiality

All information will be kept confidential. You will not be identifiable in any publications or presentations resulting from this study. The only information kept after you complete the study is your age, gender, and weight. That information will be coded with an independent study number, with no identifying information linked to you. These data will be stored in an encrypted electronic file which is password protected on an encrypted and secured hard drive. Only the research team at the Glenrose Rehabilitation Hospital will be able to access these data.

Voluntary Participation

Your participation in this study is voluntary. If you choose not to participate, your decision will not affect the potential care you receive at the GRH, at this time or in the future.

Further Information

If you have any questions regarding this study, please do not hesitate to contact the investigator: Dr. Jacqueline Hebert, Glenrose Rehabilitation Hospital, 10230-111 Avenue, Edmonton AB T5G0B7; email: jacqueline.hebert@ahs.ca, phone 780-725-8218.

The plan for this study has been reviewed for its adherence to ethical guidelines by a Research Ethics Board at the University of Alberta. For questions regarding participant rights and ethical conduct of research, contact the Research Ethics Office at (780) 492-2615. This office has no direct involvement with this project.

INFORMED CONSENT FORM

Study Title: "Development of a Performance Assessment Tool for the CAREN"

Research Investigators: Dr. Jacqueline Hebert 780.735.8218
Dr. Albert Vette 780.492.1534
Juan Forero, PhD 780.735.7972

	Yes
Do you understand that you have been asked to be in a research study?	☐
Have you read and received a copy of the attached Information Sheet?	☐
Do you understand the benefits and risks involved in taking part in this research study?	☐
Have you had an opportunity to ask questions and discuss this study?	☐
Do you understand that you are free to leave the study at any time, without having to give a reason and without affecting your future medical care?	☐
Has the issue of confidentiality been explained to you?	☐
Do you understand who will have access to your records?	☐
Do you agree to be video recorded during the study? Your image (mainly your body) will be digitally captured on video).	☐

Who explained this study to you? _____

I agree to take part in this study:

Signature of Research Participant _____

Printed Name: _____ Date: _____

I believe that the person signing this form understands what is involved in the study and voluntarily agrees to participate.

Signature of Investigator or Designee_____ Date _____

THE INFORMATION SHEET MUST BE ATTACHED TO THIS CONSENT FORM AND A COPY GIVEN TO THE RESEARCH PARTICIPANT

A.3 Photograph and Video Consent

Consent to the Use of a Recording Device or Camera for Photographs, Video or Sound Recordings

Principal Investigator: Dr. Jacqueline Hebert, Division of Physical Medicine and Rehabilitation
Email: jhebert@ualberta.ca
Phone: (780) 248-5767

Name of Individual being photographed or recorded			
Address			
City/Town	**Province**	**Postal Code**	**Phone Number**
Name of Individual giving consent			
Type of recording *Digital Photographs and/or Video Recordings (with or without sound).*			
Specific Purpose *Subjective evaluation of body movement, education, presentation to the academic population or the general public, and publication in the public domain including both paper and electronic formats.*			
I understand that I have been made aware of the reasons that photographs and/or video recordings are needed. I consent to the use of my image and likeness in the form of still pictures and/or video for the communication of this research to the academic community or the general public. I understand that I have the right to refuse to grant this consent and that I can withdraw consent at any time by contacting the investigator listed above; notwithstanding any dissemination or use that may have occurred prior to the date of withdrawal of consent.			
Signature of Individual giving consent		**Date** *(yyyy-Mon-dd)*	
Person obtaining consent:			
Name	**Signature**	**Date (yyyy-Mon-dd)**	

Appendix B: Standing-Based Tasks

The single-leg balance task (Figure B.1a) included a virtual scene in which blocks of variable length (1, 5, 15 or 30 m) and height (2, 5, 10, 20 cm) would travel towards the participant in the direction of either the left or right leg. To avoid the blocks, participants had to raise the foot above the block and hold until it passed. Blocks traveled at 1 m/s, and the time between them was randomized between 5 to 8 s. During the step-to-target task (Figure B.1b), virtual targets (foot prints) would appear on-screen at angles of 0, ±45, and ±90 from the anterior direction, and on one of five different arcs. A scaling factor *S* was defined as:

$$S = 100/\,\text{leg length}, \tag{1}$$

where leg length is the length of the participant's leg in cm. The radii of the five arcs were then specified to be 30%, 50%, 70%, 90%, and 110% of the value of *S*. Depending on the target presented, the participant had to step with either one or both feet. This was specified by the number of foot prints on the current target. For the weight-shift task (Figure B.1c), the participant stood, virtually, at the centre of an eight-lined star. Essentially, each of the lines of the star acted as a track on which coins were displayed. Participants were required to collect as many coins as possible by keeping both feet on the platform (i.e., no stepping) and shifting their weight (i.e., centre of pressure) in the direction of the required track. Scaling factors $S1$ and $S2$ were defined as:

$$S1 = 100/\,\text{foot distance} \tag{2}$$

$$S2 = 100/\,\text{foot length}, \tag{3}$$

where foot distance and foot length were defined based on the foot separation distance and length, respectively, before starting each trial. The coins were then located at the following distances away from the centre: 35%, 55%, 75%, 95%, and 115% scaled to $S1$ in the mediolateral (ML) direction and $S2$ in the anteroposterior (AP) direction. The centre of pressure (CoP) displacement was visualized by a red ball, which provided real-time feedback to the participant. The final standing-based task involved a virtual simulation of the participant standing while riding on a bus travelling on a three-lane road through a metropolitan area (Figure B.1d). Horizontal platform translations (i.e., right, left, forward, backward, and diagonally) were introduced to simulate the bus speeding up or slowing down (forward and backward, respectively), switching lanes (right and left), and a combination of both (diagonally). Four different perturbation levels were used, defined by the time

for the platform to reach maximum displacement (25 cm for all levels). The magnitudes and their corresponding times to reach maximum displacement were: low (2.4 s), medium (1.6 s), high (0.8 s), and extreme (0.4 s). The platform moved back to its original position at the same speed 5 s after reaching maximum displacement. Participants were instructed to maintain balance however possible, including taking a step. As part of each of the standing-based tasks, including the calibration routine, an avatar (blue character in Figure B.1) demonstrated the task to be performed.

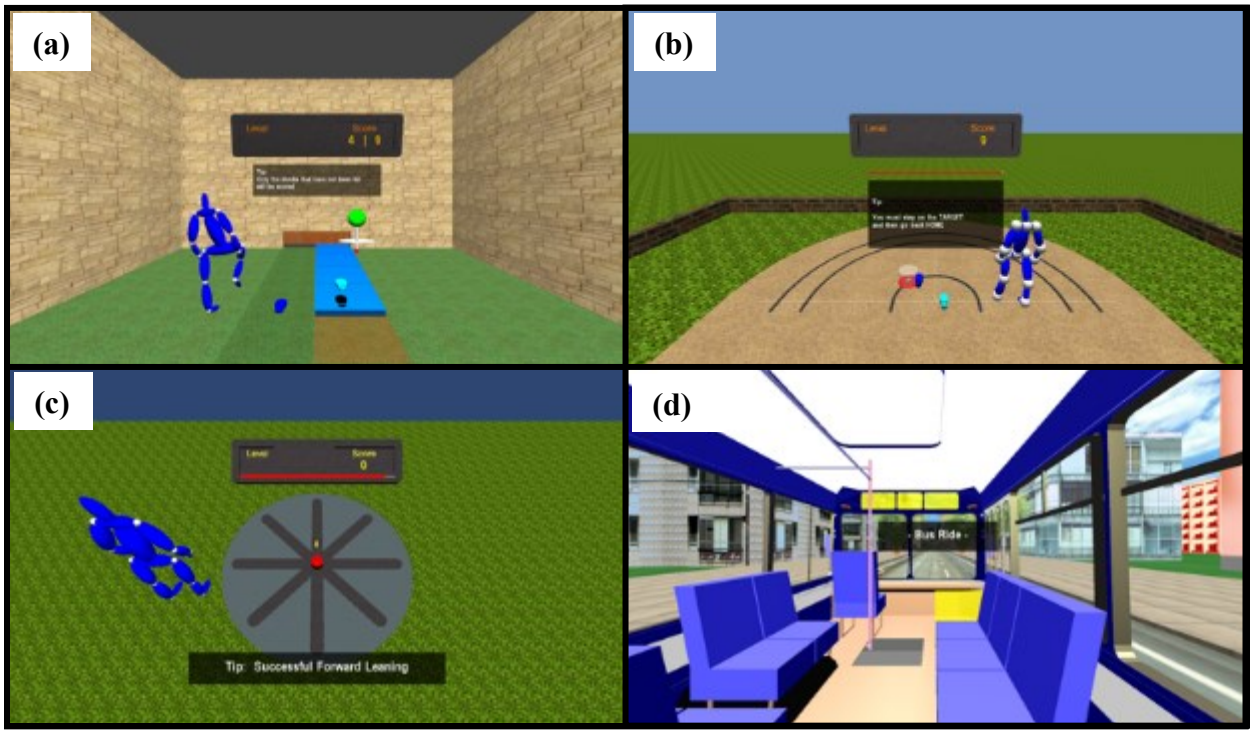

Figure B.1: Standing-based tasks as part of the experimental protocol. (a) single-leg balance task; (b) step-to-target task; (c) weight-shift task; and (d) balance in response to lateral perturbations task.

Appendix C: Marker Sorting and Identification Algorithm

This following custom Matlab code was designed to sort through all 39 markers used during the experimental protocol, and identify those belonging to both feet and the back. First, the algorithm used the built-in *cluster* function to group the markers into one of two groups based on whether or not they belonged to a 4-marker cluster. Next, from the group of 4-marker clusters, each cluster was identified by the mean position of its respective markers relative to the others. Finally, individual markers on each plate were identified by the relative distances between them, as they remained fixed.

```
function data_rev = IDmarkers_v03(data_all)
% Sorts the markers frame by frame. First, markers are
% grouped by their cluster plates. Next, specific
% markers from each cluster are identified
% based on the euclidean distance between them.
% DATA_ALL - struct containing data from a single walking
% segment

num_totalmarkers = 39;
num_totalclusters = 14;

num_usedmarkers = 12;
num_usedclusters = 3;

fields = fieldnames(data_all);

data_marker = [];
for i = 1:num_totalmarkers
    data_marker = [data_marker data_all.(fields{i})];
end

data_marksort = [];
for i = 1:length(data_marker(:,1))
    markers =
reshape(data_marker(i,1:num_totalmarkers*3),[3,num_totalmarkers])';

    Z = linkage(markers,'weighted','euclidean');
    clusters = cluster(Z,'maxclust',num_totalclusters);

    % Determine number of clusters
    clustercenters = zeros(num_totalclusters,3);
    clustercounts = zeros(num_totalclusters,1);
    for j = 1:num_totalclusters
        clustercenters(j,:) = mean(markers(clusters==j,:),1);
        clustercounts(j) = sum(clusters==j);
    end
```

```
    try
        % Group clusters by number of markers contained
        idx_noplates = find(clustercounts < 3);     % count = 1 or 2
        idx_plates = find(clustercounts >= 3);      % count = 4 (3 or
5 with error)

        % Ensure plate cluster count is 8
        while length(idx_plates) < 8
            [~,idx] = sort(clustercenters(idx_noplates,2),'ascend');
            idx_plates = [idx_plates; idx_noplates(idx(1))];
            idx_noplates(idx(1)) = [];
        end

        % Sort plate clusters from high to low
        [~,idx] = sort(clustercenters(idx_plates,2),'descend');
        idx_platesA = idx_plates(idx);

        % Back cluster (highest cluster)
        idx_back = idx_platesA(1);

        % Remove back cluster
        idx_platesB = idx_platesA(2:end);

        % Sort plate clusters from right to left
        [~,idx] = sort(clustercenters(idx_platesB,1),'descend');
        idx_platesC_L = idx_platesB(idx(4:6));
        idx_platesC_R = idx_platesB(idx(1:3));

        % Sort plate clusters from lowest to highest
        [~,idx] = sort(clustercenters(idx_platesC_L,2),'ascend');
        idx_footL = idx_platesC_L(idx(1));
        [~,idx] = sort(clustercenters(idx_platesC_R,2),'ascend');
        idx_footR = idx_platesC_R(idx(1));

        idx_sorted = [idx_footL idx_footR idx_back];

        idx_unusedclusters = setxor(idx_sorted,1:14);

        for j = 1:length(idx_unusedclusters)
            clusters(clusters == idx_unusedclusters(j)) = 0;
        end

        clusters_used = find(clusters);

        clusters_used = [clusters_used clusters(clusters_used)];

        temp_clusters_used = zeros(num_usedmarkers,1);
        for j = 1:num_usedmarkers
            temp_clusters_used(j) =
find(clusters_used(j,2)==idx_sorted);
        end

        temp_clusters_used = [clusters_used(:,1) temp_clusters_used];
```

```
        markers_sorted = [];
        clusters_sorted = [];
        for j = 1:num_usedclusters
            idx = find(temp_clusters_used(:,2)==j);
            for k = 1:length(idx)
            markers_sorted = [markers_sorted;
markers(clusters_used(idx(k)),:)];
            clusters_sorted = [clusters_sorted; j];
            end
        end

    catch
        idx_sorted = [];
        clusters_sorted = [];
        markers_sorted = [];
    end

    if length(unique(clusters_sorted)) == num_usedclusters
        D = cell(num_usedclusters,1);
        markers_ID = [];
        for j = 1:num_usedclusters
            idx_m = [];
            idx = find(clusters_sorted == j);
            if length(idx) == 4
                D{j} = squareform(pdist(markers_sorted(idx,:)));
                [P,~] = find(D{j} == max(max(D{j})));
                Q = setxor(1:length(idx),P);
                [~,tmp] = max(D{j}(P,Q(1)));
                idx_m(1) = idx(P(tmp));
                idx_m(2) = idx(P(not(tmp-1)+1));
                if j == 1 || j == 2
                    if markers_sorted(idx(Q(1)),3) >
markers_sorted(idx(Q(2)),3)
                        idx_m(3) = idx(Q(1));
                        idx_m(4) = idx(Q(2));
                    else
                        idx_m(3) = idx(Q(2));
                        idx_m(4) = idx(Q(1));
                    end
                end
                if j == 3
                    [~,tmp] = sort(markers_sorted(idx,2),'ascend');
                    if markers_sorted(idx(tmp(1)),1) <
markers_sorted(idx(tmp(2)),1)
                        idx_m(1) = idx(tmp(1));
                        idx_m(4) = idx(tmp(2));
                    else
                        idx_m(1) = idx(tmp(2));
                        idx_m(4) = idx(tmp(1));
                    end
```

```
                    if markers_sorted(idx(tmp(3)),1) <
markers_sorted(idx(tmp(4)),1)
                        idx_m(2) = idx(tmp(3));
                        idx_m(3) = idx(tmp(4));
                    else
                        idx_m(2) = idx(tmp(4));
                        idx_m(3) = idx(tmp(3));
                    end
                end
            else
                idx_m = idx;
                markers_sorted(idx,:) = nan;
            end
            markers_ID = [markers_ID; markers_sorted(idx_m,:)];
        end
    else
        markers_ID = nan(num_usedmarkers,3);
    end
    data_marksort = [data_marksort;
reshape(markers_ID',1,num_usedmarkers*3)];
end

for i = 1:num_usedmarkers
    data_rev.(fields{i}) = data_marksort(:,1:3);
    data_marksort(:,1:3) = [];
end
for i = num_usedmarkers+1:length(fields)
    data_rev.(fields{i}) = data_all.(fields{i});
end
```

Appendix D: Experimental Signal Processing

D.1 Frequency Spectrum Analysis of Kinematic Data

When reconstructing gaps in kinematic marker data through cubic spline interpolation [251], it is imperative that a true representation of the signal be maintained. Based on Nyquist's sampling theorem, a signal must be sampled at a frequency that is at least twice as high as the maximum meaningful frequency component within that signal [128], [251], which, thus, defines a limit for the maximum number of consecutively missing frames that can be reconstructed without loss of accuracy in the information [252]. To determine the largest meaningful frequency component, a frequency spectrum analysis must be conducted on the signal of interest. In the present study, markers fixed to rigid plates on the back and feet were used in the analysis, therefore, an examination of the frequency spectrums for both must be completed.

D.1.1 Back

A frequency domain plot, from 0 to the 50 Hz (Nyquist frequency), of the raw signals of a marker fixed to the back plate is shown in Figure B1. An initial observation of this plot indicates that most of the signal occurs at low frequencies, typically below 5 Hz. This is reinforced by the inset plot in Figure B1 which shows a zoomed in view of the plot from 0 to 10 Hz. Based on this observation, the largest meaningful frequency contained within the kinetic signal of the back is 5 Hz.

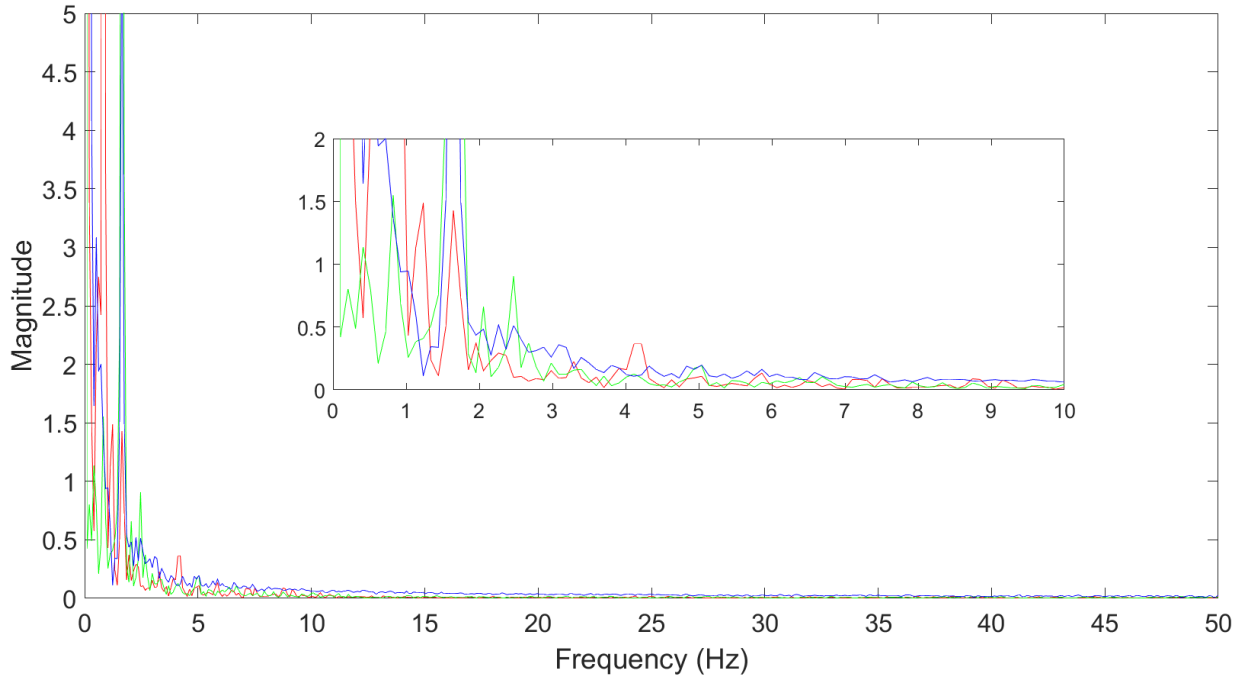

Figure D.1: Frequency domain plot of the raw signal from a marker fixed to the rigid plate on the left foot. Line color indicates dimension of interest: x-direction (red), y-direction (green), z-direction (blue).

D.1.2 Feet

A frequency domain plot, from 0 to the 50 Hz (Nyquist frequency), of the raw signals of a marker fixed to the foot plate is shown in Figure B2. An initial observation of this plot indicates that most of the signal occurs at low frequencies, typically below 5 Hz. This is reinforced by the inset plot in Figure B2 which shows a zoomed in view of the plot from 0 to 10 Hz. Based on this observation, the largest meaningful frequency contained within the kinematic signal of the foot is 5 Hz.

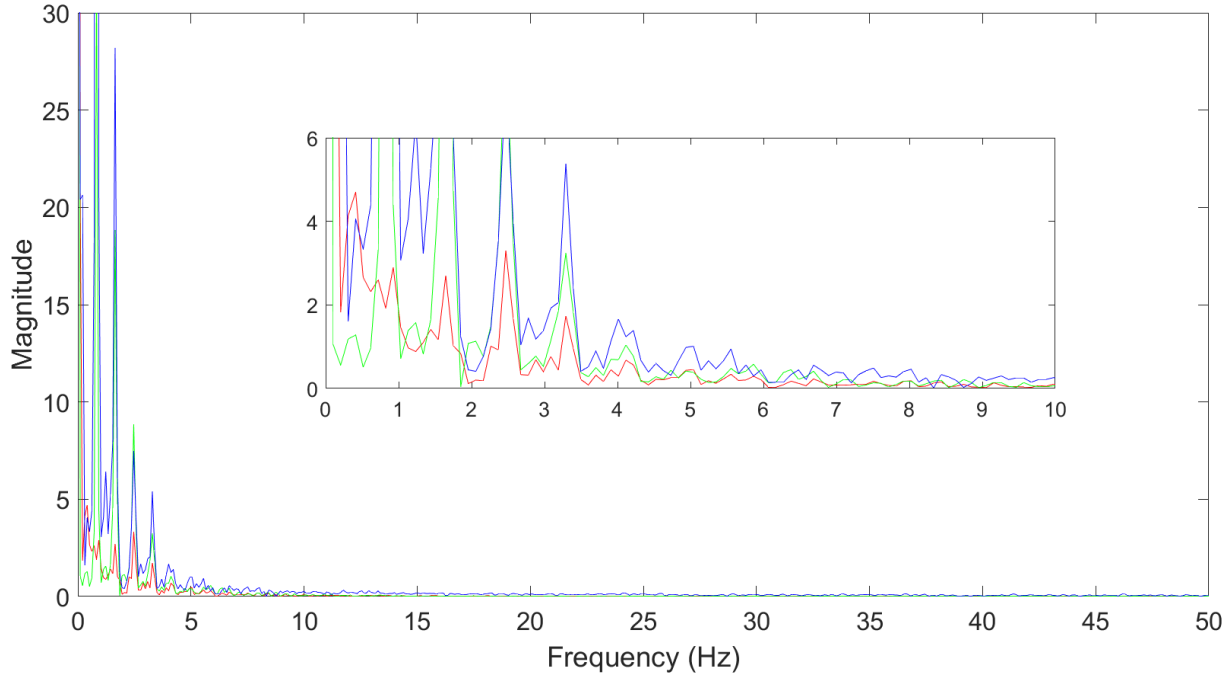

Figure D.2: Frequency domain plot of the raw signal from a marker fixed to the rigid plate on the left foot. Line color indicates dimension of interest: x-direction (red), y-direction (green), z-direction (blue).

D.2 Kinematic and Kinetic Signal Filter Design

High frequency components included in the kinematic and kinetic signals measured by the motion capture and force plate systems, respectively, may be artifacts of noise in each of the measurement systems. As noted by Antonsson and Mann [170], the dominant frequencies during human gait are typically less than 10 Hz. Therefore, experimentally recorded kinematic and kinetic gait signals are often filtered using low-pass digital Butterworth filters with cut-off frequencies between 6-10 Hz and 10-20 Hz, respectively. Butterworth filters have a nearly monotonic frequency response in the passband, so low-frequency components of the signal are and reverse directions, which eliminates any phase distortion.

D.2.1 Kinematic Data

The built-in Matlab function *butter* was used to design a fourth order, low-pass Butterworth filter with a cut-off frequency of 6 Hz for kinematic data, as used in [46], [53], [55], [94], [101], [256]–[260]. The amplitude and phase response of this filter are shown in Figure B3 and Figure B4,

respectively. The pole-zero plot is shown in Figure B5. Since all poles are within the unit circle, the filter is stable for any stable input.

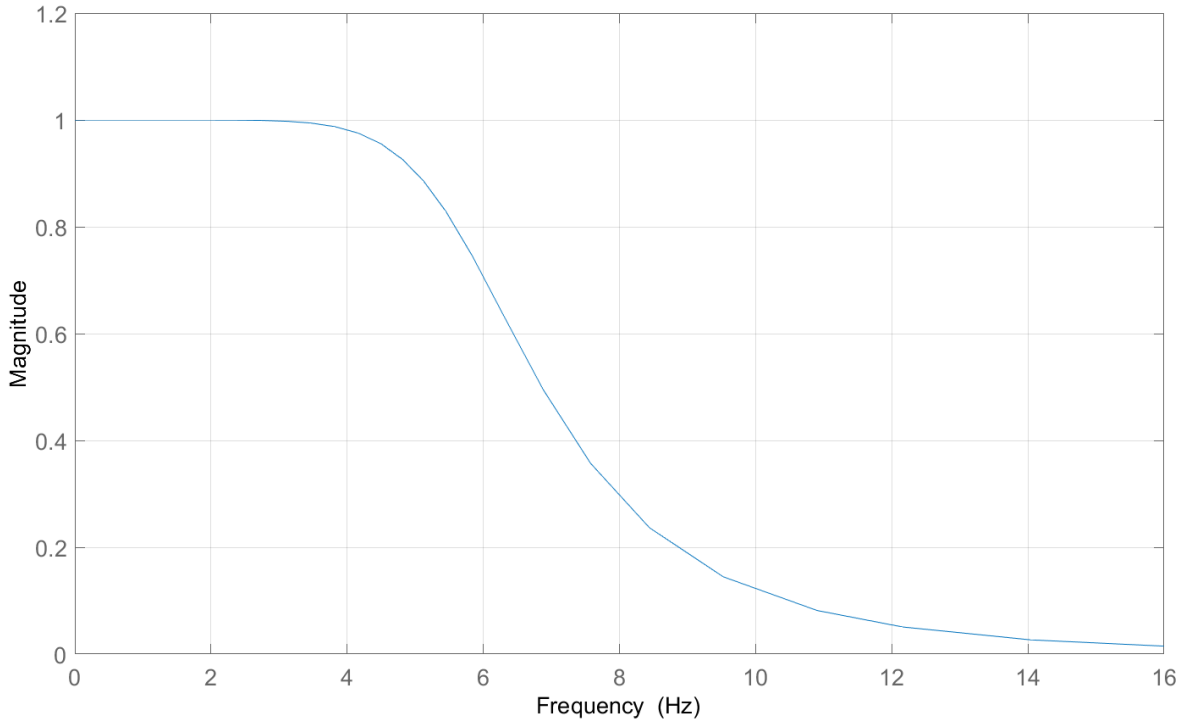

Figure D.3: Magnitude response of a fourth-order, low-pass Butterworth filter with cut-off frequency of 6 Hz.

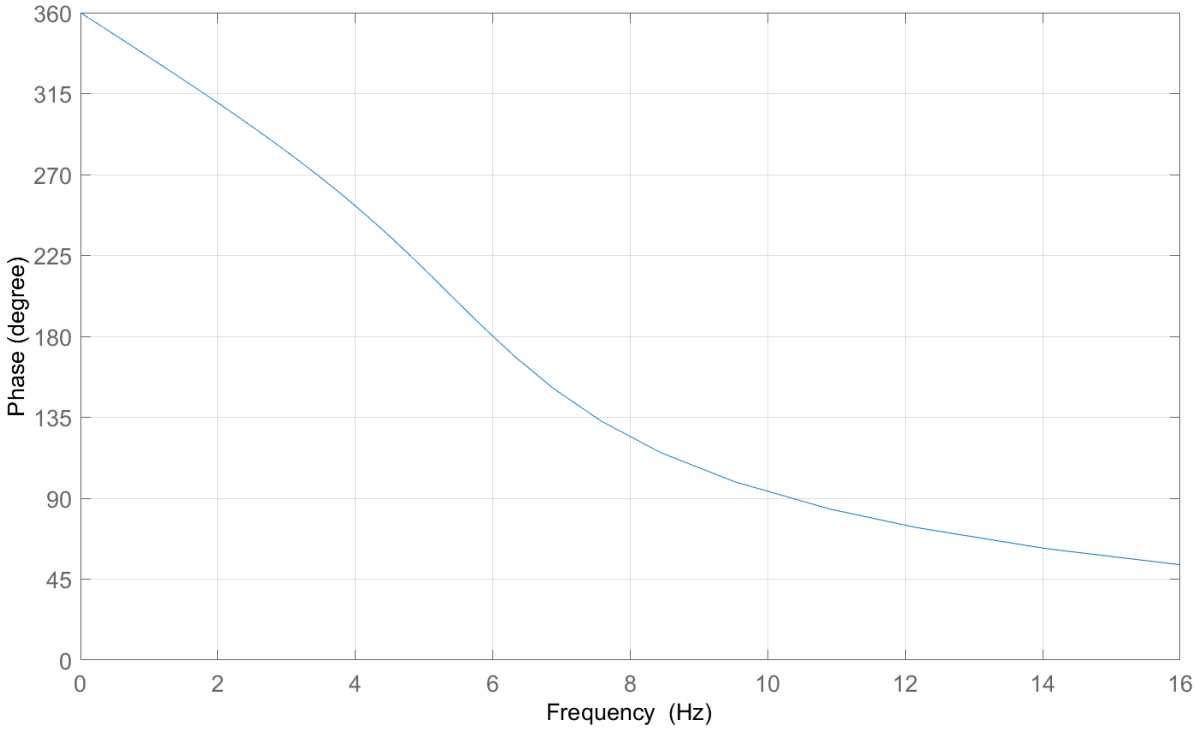

Figure D.4: Phase response of a fourth-order, low-pass Butterworth filter with cut-off frequency of 6 Hz.

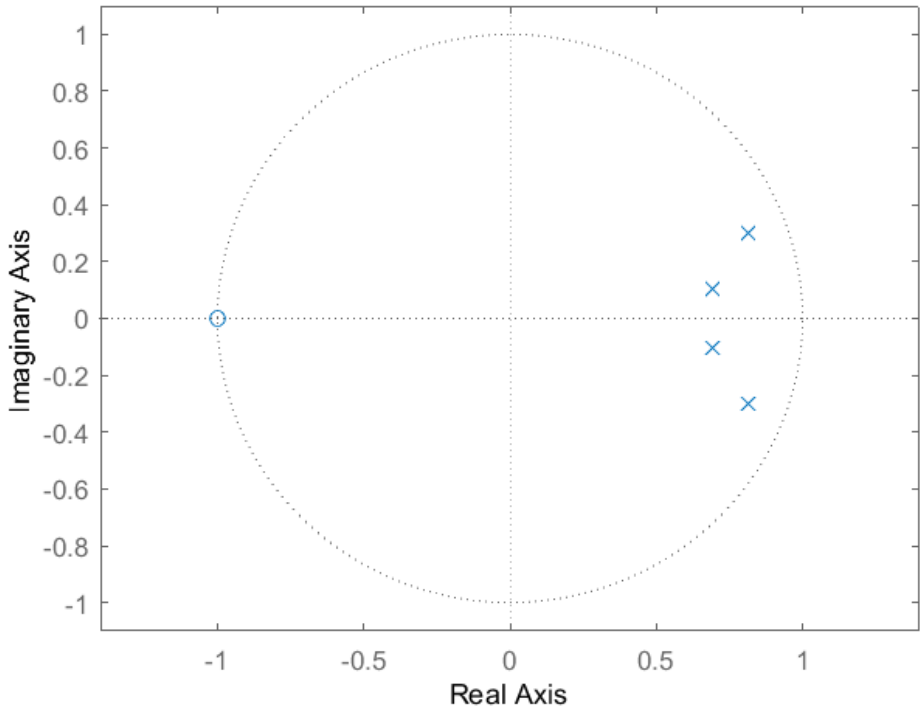

Figure D.5: The poles (x's) and zeroes (o's) corresponding to a fourth-order, low-pass Butterworth filter with cut-off frequency of 6 Hz.

D.2.2 Kinetic Data

The built-in Matlab function *butter* was used to design a fourth order, low-pass Butterworth filter with a cut-off frequency of 10 Hz for kinetic data, as recommended in [128] and used in [66], [106], [108], [261], [262], [290]. The amplitude and phase response of this filter are shown in Figure B6 and Figure B7, respectively. The pole-zero plot is shown in Figure B8. Since all poles are within the unit circle, the filter is stable for any stable input.

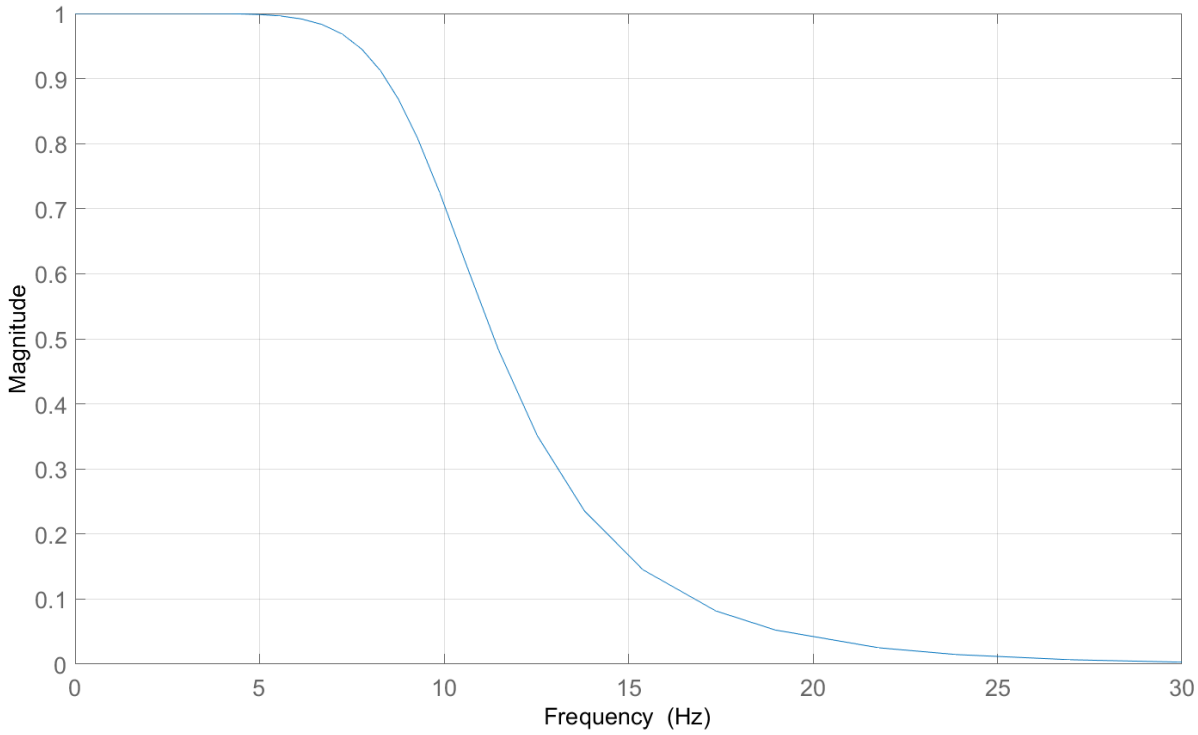

Figure D.6: Magnitude response of a fourth-order, low-pass Butterworth filter with cut-off frequency of 10 Hz.

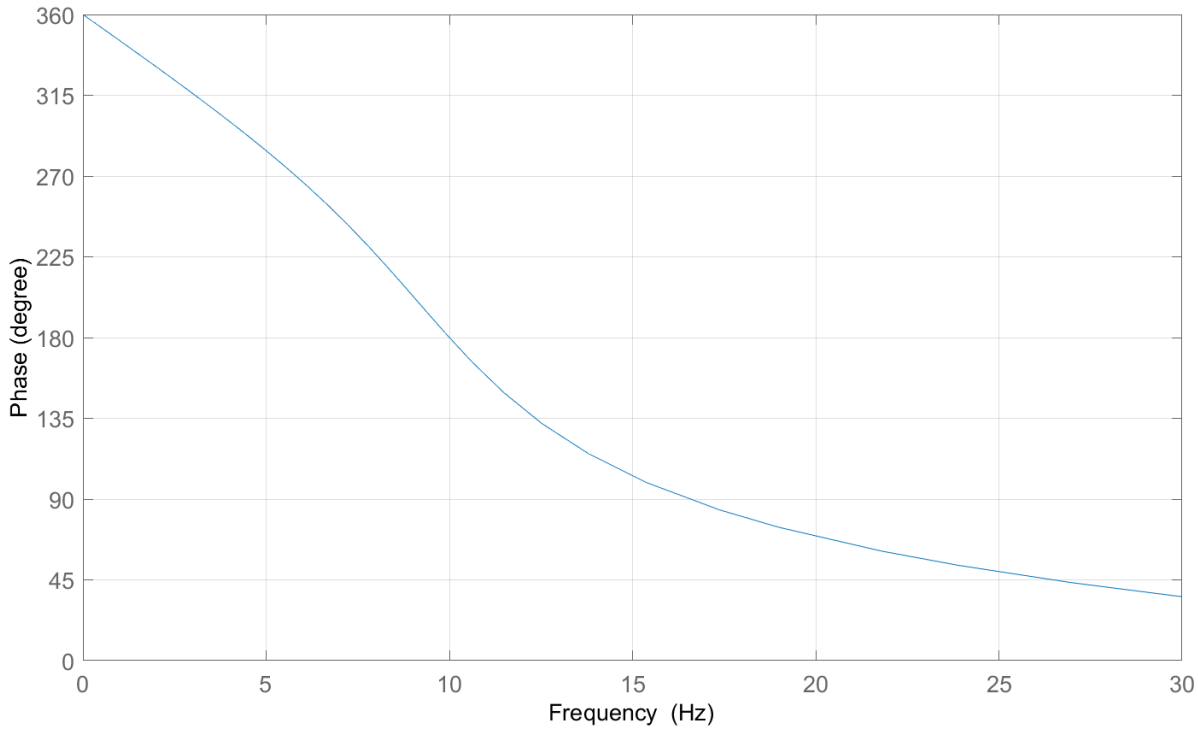

Figure D.7: Phase response of a fourth-order, low-pass Butterworth filter with cut-off frequency of 10 Hz.

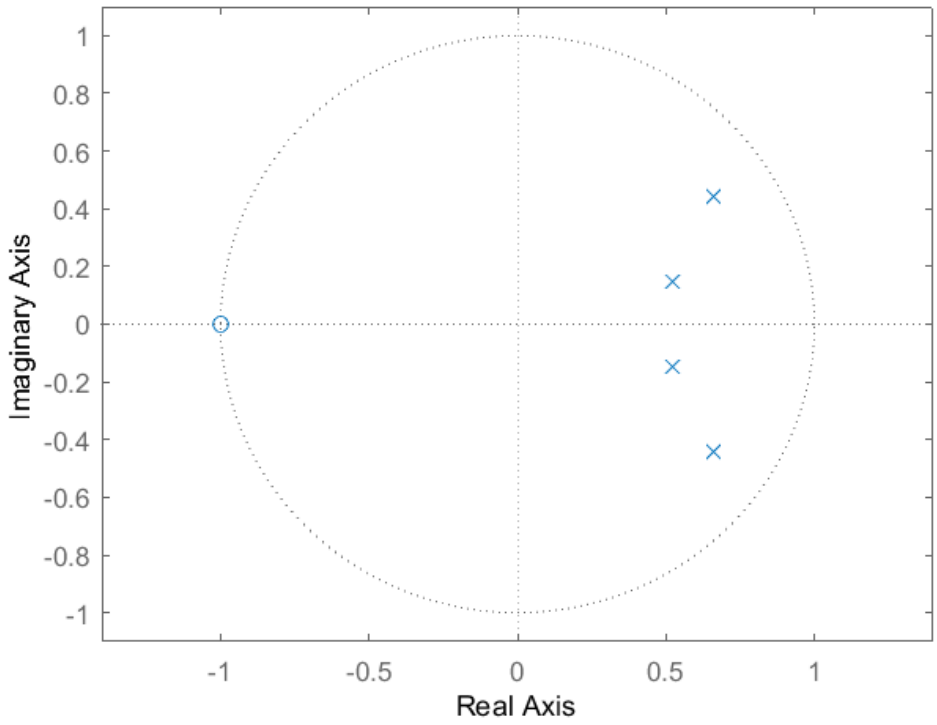

Figure D.8: The poles (x's) and zeroes (o's) corresponding to a fourth-order, low-pass Butterworth filter with cut-off frequency of 10 Hz.

Appendix E: Effect of Mediolateral Ground Reaction Force Fluctuations on Center of Mass Position and Velocity Estimation

Over a typical step in unperturbed gait, the horizontal ground reaction force (GRF) in the mediolateral (ML) direction is zero only once, shortly after heel strike (HS), when the lateral GRFs from both sides are equal in absolute magnitude and opposite in direction. However, it was observed that, for some steps, the resultant ML GRF fluctuated about zero throughout a step, rather than cross only once, as is typical. These fluctuations created multiple zero points which result in added discontinuities through the (zero-point-to-zero-point) ZPZP algorithm. In turn, the added discontinuities created excessive (and sharp) fluctuations in the estimated centre of mass position (CoM) and velocity (v_{CoM}), which are direct inputs into equation (9) used to predict the extrapolated centre of mass (XCoM). Confirmation of the excessive fluctuations was accomplished by a comparison of the CoM acceleration determined through division of the ML force by participant mass (actual CoM acceleration) to the CoM acceleration predicted from finite-difference approximation of the CoM position as determined by the ZPZP algorithm. This can be seen in Figure D1, below. During each of the first two steps (left and right steps 1), the ML GRF crosses the zero axis only once, as expected. Though there is some discrepancy between the actual and predicted CoM acceleration, the curves overlap quite well through the majority of the step. On the other hand, in the last two steps (left and right steps 2), the ML GRF crosses the zero axis multiple times, creating large differences between the two CoM acceleration curves. Whereas the actual CoM acceleration remained relatively low, the predicted CoM acceleration reached in excess of 3 m/s^2 at multiple instances. Based on these observations, steps in which the ML GRF crossed the zero axis more than once should be excluded from analysis to prevent the inclusion of erroneous data.

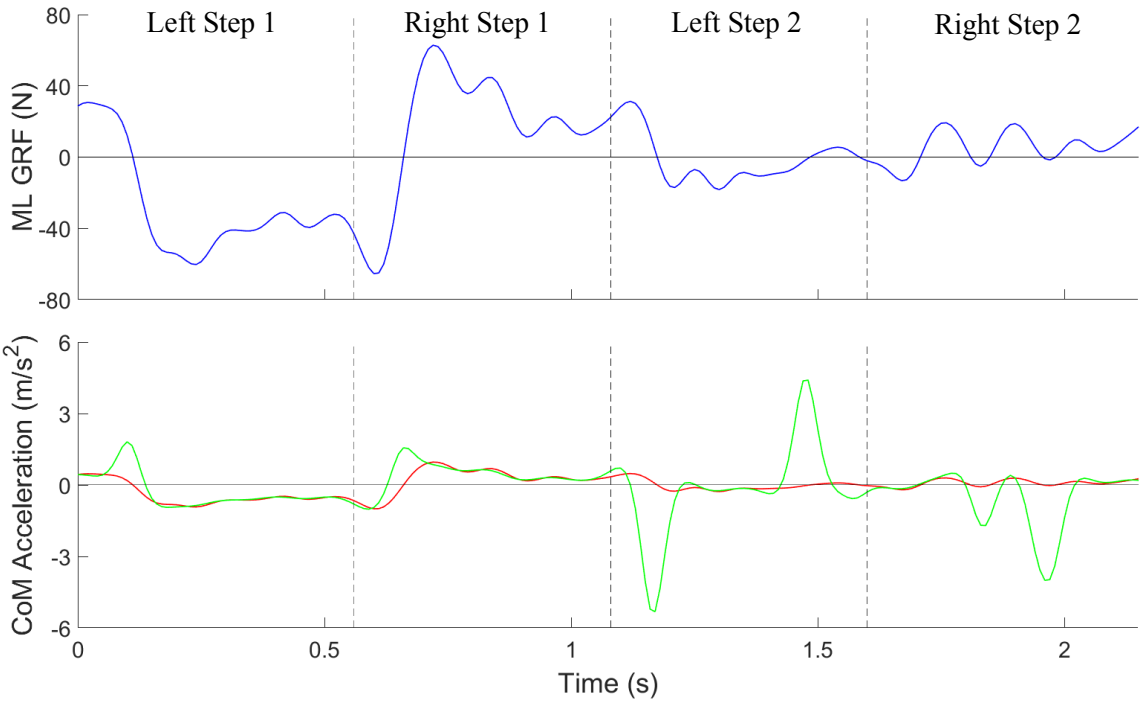

Figure E.1: A plot of the mediolateral (ML) ground reaction force (GRF), and the corresponding CoM acceleration in the ML direction over two complete walking strides (two steps per body side). Top: ML GRF is given by the blue line. Bottom: line color indicates CoM acceleration determined by dividing ML force by participant mass (red) and CoM acceleration predicted by differentiation of CoM displacement as determined by the ZPZP algorithm. Dashed vertical lines indicate heel strike and, thus, separate steps.